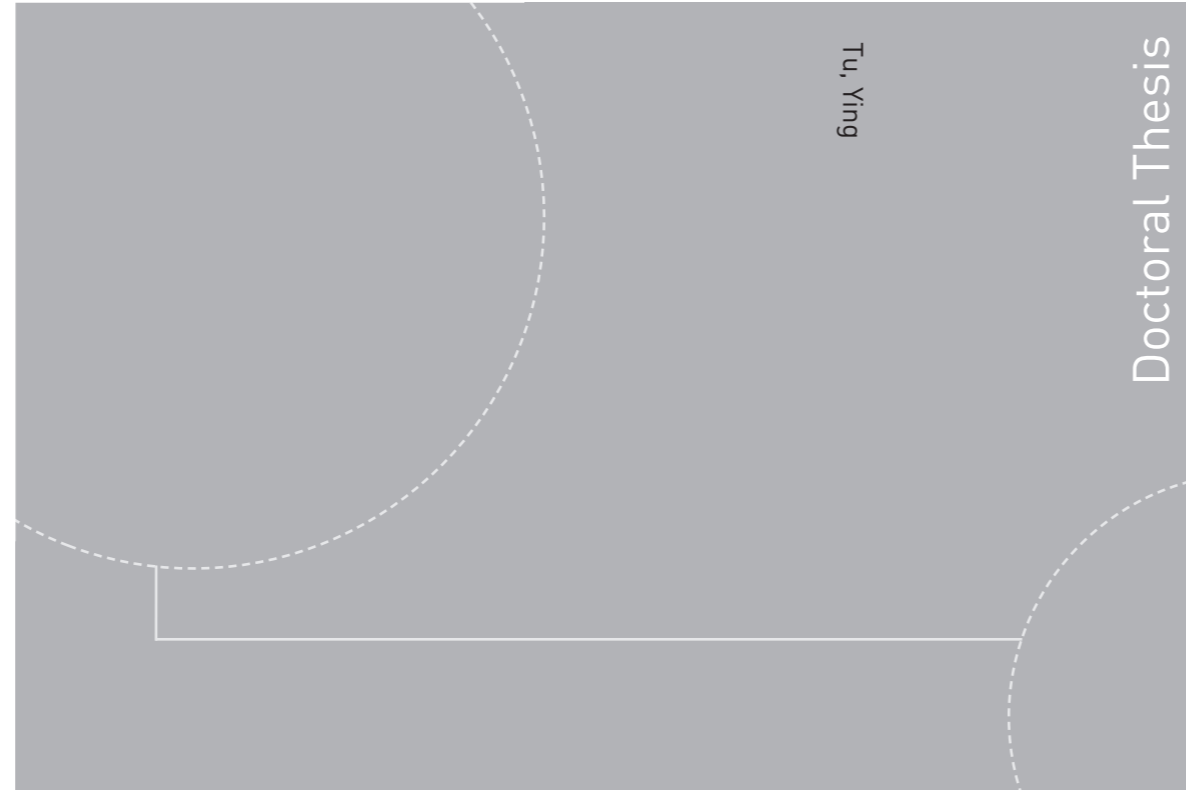


Doctoral theses at NTNU, 2018:237

Tu, Ying

Wave Slamming Forces on Offshore Wind Turbine Jacket Substructures



ISBN 978-82-326-3264-0 (printed version)
ISBN 978-82-326-3265-7 (electronic version)
ISSN 1503-8181

Doctoral theses at NTNU, 2018:237

NTNU
Norwegian University of
Science and Technology
Faculty of Engineering
Department of Civil and Environmental Engineering

 **NTNU**
Norwegian University of
Science and Technology

 NTNU

 **NTNU**
Norwegian University of
Science and Technology

Tu, Ying

Wave Slamming Forces on Offshore Wind Turbine Jacket Substructures

Thesis for the degree of Philosophiae Doctor

Trondheim, July 2018

Norwegian University of Science and Technology
Faculty of Engineering
Department of Civil and Environmental Engineering



Norwegian University of
Science and Technology

NTNU

Norwegian University of Science and Technology

Thesis for the degree of Philosophiae Doctor

Faculty of Engineering

Department of Civil and Environmental Engineering

© Tu, Ying

ISBN 978-82-326-3264-0 (printed version)

ISBN 978-82-326-3265-7 (electronic version)

ISSN 1503-8181

Doctoral theses at NTNU, 2018:237



Printed by Skipnes Kommunikasjon as

For my 18-year-old self, who decided to study something helpful to the environment.

Contents

| | |
|---|-------------|
| Abstract | v |
| Preface | vii |
| Acknowledgment | ix |
| Publication List | xi |
| Glossary | xiii |
| List of Figures | xvii |
| List of Tables | xix |
| 1 Introduction | 1 |
| 1.1 Background | 1 |
| 1.2 Objectives | 6 |
| 1.3 Scope | 7 |
| 1.4 Thesis structure | 7 |
| 2 Inverse Estimation of Slamming Forces | 9 |
| 2.1 Extraction of dynamic force part | 9 |
| 2.2 Force reconstruction methods | 12 |
| 2.2.1 Optimization-based deconvolution | 13 |
| 2.2.2 Horizontal approach | 14 |
| 2.2.3 Vertical approach | 15 |
| 2.2.4 Extended vertical approach | 18 |
| 3 Statistical Characteristics of Slamming Forces | 21 |
| 3.1 Characteristics of local slamming forces | 22 |
| 3.2 Characteristics of global slamming forces | 25 |

| | | |
|----------|---|-----------|
| 4 | Global Slamming Force Model | 31 |
| 4.1 | Development of the model | 31 |
| 4.1.1 | Determination of exponential parameters | 33 |
| 4.1.2 | Determination of wave-dependent parameters | 34 |
| 4.2 | Application of the model | 40 |
| 5 | Slamming Loads in Offshore Wind Turbine Design | 43 |
| 5.1 | Slamming load consideration in offshore wind turbine simu- lations | 43 |
| 5.1.1 | Detection of slamming events | 43 |
| 5.1.2 | Calculation of slamming loads | 44 |
| 5.1.3 | Integration of slamming loads in fully coupled analysis | 45 |
| 5.2 | Plunging breaking wave detection with machine learning | 45 |
| 6 | Conclusions and Recommendations for Future Work | 49 |
| 6.1 | Conclusions | 49 |
| 6.2 | Recommendations for future work | 51 |
| | References | 53 |
| A | Appended Papers | 59 |
| A.1 | Paper 1 | 59 |
| A.2 | Paper 2 | 69 |
| A.3 | Paper 3 | 83 |
| A.4 | Paper 4 | 93 |
| A.5 | Paper 5 | 115 |
| A.6 | Paper 6 | 135 |
| A.7 | Paper 7 | 149 |

Abstract

Currently, the development of offshore wind energy is mainly in shallow or intermediate water, where bottom-fixed substructures (e.g. monopiles and jackets) are mainly used. In harsh environmental conditions at certain locations, these substructures are exposed to plunging breaking waves, which cause slamming forces. A slamming force features a high impact force within a short time. It can affect the structural integrity and the fatigue life of Offshore Wind Turbines (OWTs). Slamming forces on cylindrical structures have been widely studied, while the investigations regarding these forces on OWT jacket substructures are limited.

This study addresses the statistical characteristics of slamming forces on OWT jacket substructures and develops a global slamming force model, based on the large-scale experimental data from the WaveSlam project.

Three methods are developed to reconstruct slamming forces on the jacket model, including the optimization-based deconvolution (ODC), vertical approach and extended vertical approach. The vertical approach, which is based on linear regression, is more robust and easier to use than the state-of-the-art horizontal approach that uses deconvolution techniques. The vertical approach can be applied to reconstruct the time series of both local and global slamming forces.

A plunging breaking wave impacts different locations on the braces of the jacket model at different instants in a more or less random order. Statistical analysis indicates that both local and global slamming forces exhibit high variability for the given wave condition, which is controlled in the laboratory. This variability contributes to the uncertainties of the slamming forces, so it is important and should be considered.

A global slamming force model is proposed based on the statistical analysis of the experimental data. The force model involves five parameters, including two exponential parameters and three dimensionless coefficients for the expressions of wave-dependent parameters. Given a sea state, this force model provides a deterministic and conservative prediction of global

slamming force time series, which inherently have random features.

Three major aspects regarding the application of slamming forces to OWT simulations are discussed, including the detection of slamming events, the calculation of slamming loads and the integration of slamming loads in fully coupled analysis. A supervised machine learning approach is proposed for the detection of plunging breaking waves. A classifier is trained with wave elevation data by using logistic regression algorithm. The classifier has a better performance than the classical McCowan breaking wave criterion.

Preface

This thesis is submitted to the Norwegian University of Science and Technology (NTNU) for partial fulfillment of the requirements for the degree of philosophiae doctor.

This doctoral work has been carried out at the Department of Civil and Environmental Engineering at NTNU, under the supervision of Prof. Michael Muskulus as the main supervisor and Prof. Andrei Metrikine from the Faculty of Civil Engineering and Geosciences at the Delft University of Technology as the co-supervisor.

This work has been supported by the European Community's Seventh Framework Programme through the grant to the budget of the Integrating Activity HYDRALAB IV within the Transnational Access Activities, Contract no. 261520. Additional financial support has been provided by NOWITECH FME (Research Council of Norway, contract no. 193823)

Acknowledgment

I would like to express my deepest gratitude to my supervisor, Prof. Michael Muskulus, for his patient guidance and continuous encouragement throughout my PhD study. I was strongly influenced by his enthusiasm for research and his curiosity of unknowns. I particularly appreciate that he encouraged me to approach the problems in my own way, while offering me valuable suggestions when I needed. I would like to thank Prof. Andrei Metrikine for supporting me as my co-supervisor.

Special thanks to the supervisors of my Master's thesis, Prof. Gerard van Bussel and Fabian Vorpahl, who introduced me into the amazing offshore wind energy field and recommended me to pursue a PhD with Michael. Without them, I would probably not even have started this PhD.

I am thankful for the generous support regarding the experimental data from my colleagues in the WaveSlam project, Assoc. Prof. Øivind Arntsen at NTNU, Stefan Schimmels and Matthias Kudella at University of Hannover.

I am particularly grateful for the enlightening suggestions from my colleagues in the Marine Civil Engineering group. Discussions with Thorvald Grindstad during the coffee breaks were illuminating, and the results turned out to be an important part of the thesis. Torodd Nord gave me many insightful suggestions on inverse methods. Advice and comments given by Mayilvahanan Alagan Chella and Arun Kamath guided me to an in-depth understanding of wave theories.

It was a lot of fun and a great honor to work in a dynamic research group of offshore wind turbine technology with my colleagues Sebastian Schafhirt, Lars Einar Stieng, Helene Seyr, Lisa Ziegler, Gordon Stewart, Wojciech Popko and visiting scholar Chew Kok Hon. Sebastian was like my elder brother in Trondheim, who supported me for almost everything in both work and life. I am sincerely thankful for his care and help during these years. Lars and Helene guided me through many mathematical puzzles that were challenging at the first glance, and we had so many laughs at the

Friday meetings.

Working in a sunny “basement” with warm-hearted people in the Norwegian cold winters is a realistic portrayal of my PhD life. I am thankful to all the amazing “basement people” who made this experience an unforgettable part of my life.

My special thanks to my dearest friends Yang Yueting, Zhang Manping, Li Yan and Holger Schwarze, who have been supportive of my PhD, as well as of my life over the years. There are many friends and colleagues that are not listed, but I am grateful to all of these wonderful people and the experiences we shared.

I would like to express the deepest appreciation to my beloved spouse Cheng Zhengshun, the most brilliant and considerate person in my world. Without Zhengshun, I could never have achieved what I have today. No matter what has happened, Zhengshun has always been firmly on my side and shared the joys and sorrows with me.

I am indebted to my parents for their love and the continuous support for my dreams. Since seven years, I have been living on a continent far away from my homeland. I know how much they have been concerned about me, although they always tried to keep their emotion deep in the heart.

Tu Ying
July 2018
Trondheim, Norway

Publication List

List of Appended Papers

Paper 1:

Tu Y, Muskulus M, Arntsen ØA. Experimental analysis of slamming load characteristics for truss structures in offshore wind applications. *Journal of Ocean and Wind Energy* 2015; **2**(3):138-145.

Paper 2:

Tu Y, Grindstad TC, Muskulus M. Inverse estimation of local slamming loads on a jacket structure. *Journal of Offshore Mechanics and Arctic Engineering* 2017; **139**(6):061601.

Paper 3:

Tu Y, Muskulus M. Statistical properties of local slamming forces on a jacket structure in offshore wind applications. *The 26th International Ocean and Polar Engineering Conference*, International Society of Offshore and Polar Engineers, 2016.

Paper 4:

Tu Y, Cheng Z, Muskulus M. Global slamming forces on jacket structures for offshore wind applications. *Marine Structures* 2018; **58**:53-72.

Paper 5:

Tu Y, Cheng Z, Muskulus M. A global slamming force model for offshore wind jacket structures. *Marine Structures* 2018; **60**:201-217.

Paper 6:

Tu Y, Cheng Z, Muskulus M. A review of slamming load application to offshore wind turbines from an integrated perspective. *Energy Procedia* 2017; **137**:346-357.

Paper 7:

Tu Y, Cheng Z, Muskulus M. Detection of plunging breaking waves based on machine learning. *ASME 2018 37th International Conference on Ocean, Offshore and Arctic Engineering*, American Society of Mechanical Engineers, 2018.

List of Additional Papers**Paper 1:**

Tu Y, Muskulus M, Arntsen ØA. Experimental analysis of slamming load characteristics for truss structures in offshore wind applications. *The 25th International Ocean and Polar Engineering Conference*, International Society of Offshore and Polar Engineers, 2015.

Paper 2:

Tu Y, Muskulus M, Grindstad TC. Two methods for the inverse estimation of local slamming loads on a jacket structure. *ASME 2016 35th International Conference on Ocean, Offshore and Arctic Engineering*, American Society of Mechanical Engineers, 2016; V006T09A041.

Paper 3:

Robertson AN, Wendt FF, Jonkman JM, Popko W, Vorpahl F, Stansberg CT, Bachynski EE, Bayati I, Beyer F, de Vaal JB, et al.. OC5 Project Phase I: Validation of hydrodynamic loading on a fixed cylinder. *The 25th International Ocean and Polar Engineering Conference*, International Society of Offshore and Polar Engineers, 2015.

Paper 4:

Robertson AN, Wendt F, Jonkman JM, Popko W, Borg M, Bredmose H, Schlutter F, Qvist J, Bergua R, Harries R, et al.. OC5 Project Phase Ib: Validation of hydrodynamic loading on a fixed, flexible cylinder for offshore wind applications. *Energy Procedia* 2016; **94**:82-101.

Glossary

List of Abbreviations

| | |
|-------------|--|
| CFD | Computational Fluid Dynamics |
| EMD | Empirical Mode Decomposition |
| EU | European Union |
| FZK | Coastal Research Centre |
| LCoE | Levelized Cost of Energy |
| NTNU | Norwegian University of Science and Technology |
| ODC | Optimization-based deconvolution |
| OWT | Offshore Wind Turbine |
| UiS | University of Stavanger |

Nomenclature

| | |
|----------------------|---|
| α_1, α_2 | exponential parameters of global slamming force model |
| δ | step factor |
| η_b | maximum elevation of breaking wave |
| η_p | elevation at the wave crest |

| | |
|---------------------------------|--------------------------------------|
| $\hat{\mathbf{f}}_{\mathbf{W}}$ | estimated wave slamming force vector |
| $\hat{\boldsymbol{\beta}}$ | estimated parameter vector |
| λ | curling factor |
| \mathbf{e} | error term vector |
| $\mathbf{F}_{\mathbf{H}}$ | hammer impact force matrix |
| $\mathbf{f}_{\mathbf{W}}$ | wave slamming force vector |
| $\mathbf{R}_{\mathbf{H}}$ | hammer response force matrix |
| $\mathbf{r}_{\mathbf{W}}$ | wave response force vector |
| μ | mean |
| μ_L | log location parameter |
| $\boldsymbol{\beta}$ | parameter vector |
| ρ | water density |
| σ | standard deviation |
| σ_L | log scale parameter |
| τ_s | slam duration |
| ζ_1 | duration coefficient |
| ζ_2 | rising time coefficient |
| ζ_3 | peak force coefficient |
| C_b | breaking wave celerity |
| C_s | slamming coefficient |
| C_v | coefficient of variation |

| | |
|--------|---|
| D | diameter |
| d | water depth |
| D_x | equivalent width of structure in wave direction |
| D_y | equivalent width of structure in y-axis direction |
| F | total wave force |
| $f(t)$ | force time series |
| F_D | drag force |
| F_I | inertial force |
| F_p | peak force |
| F_S | slamming force |
| g | gravitational acceleration |
| H | wave height |
| $h(t)$ | impulse response function |
| I | impulse |
| I_L | left impulse |
| I_R | right impulse |
| p | number of hypothetical hammer hits |
| $r(t)$ | response time series |
| R^2 | coefficient of determination |
| T | duration |
| t | time |

| | |
|-------|---|
| T_p | wave period acquired from two neighboring peaks in the wave elevation time series |
| t_p | the moment of the peak in the time series |
| T_r | rising time |

List of Figures

| | | |
|-----|--|----|
| 1.1 | Plunging breaking wave | 2 |
| 1.2 | Sketch of a plunging breaking wave interacting with a cylinder | 3 |
| 1.3 | Illustration of a slamming force time series | 3 |
| 1.4 | Substructures for offshore wind turbines | 5 |
| 1.5 | Experimental setup and global coordinates | 6 |
| 1.6 | Thesis structure and the topics covered by the appended papers | 8 |
| 2.1 | Inverse estimation of local and global slamming forces | 10 |
| 2.2 | Separation of quasi-static and dynamic parts of a measured response force time series, by using robust LOESS smoother method | 11 |
| 2.3 | Illustration of the ODC method | 13 |
| 2.4 | Horizontal and vertical approaches for force reconstruction . . | 15 |
| 2.5 | Illustration of the vertical approach | 16 |
| 2.6 | Comparison of the results from horizontal approach and ver- tical approach, at one location for one wave | 18 |
| 2.7 | Comparison of the results from vertical approach and ex- tended vertical approach | 19 |
| 3.1 | Variation of peak force of local slamming force with regard to wave ID | 22 |
| 3.2 | Variation of impulse of local slamming force with regard to wave ID | 23 |
| 3.3 | Variation of peak force of local slamming force with regard to test run | 24 |
| 3.4 | Variation of impulse of local slamming force with regard to test run | 24 |
| 3.5 | Variation of peak force and impulse of local slamming force with regard to location | 25 |
| 3.6 | Parameters to describe one global slamming force time series | 25 |

| | | |
|-----|--|----|
| 3.7 | Variation of six parameters of global slamming force with regard to wave ID | 27 |
| 3.8 | Variation of six parameters of global slamming force with regard to test run | 28 |
| 4.1 | Representative global slamming force time series and its standard deviation for one wave condition | 32 |
| 4.2 | Representative global slamming force time series for six cases | 33 |
| 4.3 | Fitting of converted representative global slamming force time series of the six cases | 34 |
| 4.4 | Variation of ζ_1 in each case and over different cases | 36 |
| 4.5 | Variation of ζ_2 in each case and over different cases | 37 |
| 4.6 | Variation of ζ_3 in each case and over different cases | 37 |
| 4.7 | Statistical properties of ζ_3 , represented by histogram, distribution fitting by lognormal function, mean and confidence interval of the mean | 39 |
| 4.8 | Cumulative distribution function of ζ_3 based on the original data and the fitted lognormal distribution | 39 |
| 4.9 | Application flow chart of the global slamming force time series model | 41 |
| 5.1 | Three aspects involved in slamming load application to OWT simulations | 44 |
| 5.2 | Work flow of detecting plunging breaking waves based on machine learning | 46 |

List of Tables

| | | |
|-----|--|----|
| 1.1 | Slamming force models for cylindrical structures | 4 |
| 3.1 | Wave case used for statistical analysis | 21 |
| 3.2 | Correlation matrix of six parameters of global slamming force | 29 |
| 4.1 | Four representative quantiles and corresponding ζ_3 values estimated from the lognormal distribution and the original data | 40 |
| 5.1 | Evaluation of the result of plunging breaking wave detection using machine learning | 47 |

Chapter 1

Introduction

1.1 Background

Wind has been an important source of energy since the dawn of human civilization. In the traditional society, wind was a powerful natural alternative to human and animal power for production activities, such as grinding grains or pumping water. The significance of wind power declined after the Industrial Revolution, until the modern wind energy technology entered the attention of the public as an alternative to fossil fuels, during the environmental movements that started in the late 1960s and the oil crisis in mid-1970s [1]. Wind energy technology has been thriving since the 1990s with the developments in many other areas of technology. Today, wind has again become an important source of energy in some regions of the world. In 2016, wind took the place of coal as the 2nd largest form of power generation capacity in Europe [2]. In 2017, the electricity generated by wind was enough to meet 11.6% of the total electricity demand of the European Union (EU) countries [2]. 55% of the newly installed power capacity in the EU in 2017 came from wind, of which 20% was from offshore wind [2].

While onshore wind has become competitive in cost with coal, gas and nuclear during the recent years, offshore wind still has a reputation for the high cost. In 2013, the Levelized Cost of Energy (LCoE) for offshore wind energy was €140/MWh [3]. This cost is aimed to be reduced to €80/MWh by 2025 [4]. In order to achieve the cost reduction goal, developments are required in wind turbine technology, support structure production, supply chain optimization etc. For a bottom-fixed offshore wind power plant project, the cost of substructure and foundation accounts for 13.9% of the capital expenditures [5]. A cost-efficient design of substructure and foundation is essential for the cost reduction of the whole project.

Among various loads on Offshore Wind Turbine (OWT) substructures, the slamming forces due to plunging breaking waves are one of the most dangerous type of loads. It is also challenging to estimate the values of these loads and to consider them in an integrated analysis of OWT. Slamming forces have been identified, for example, for a 2 MW wind turbine mounted on a monopile at the Blyth wind farm off the coast of England based on on-site measurement data [6]. Since slamming forces can affect the performance and the fatigue life of OWT substructures, these forces should be considered in the design of OWTs, if the site is likely to be exposed to plunging breaking waves, as recommended by various standards and guidelines [7, 8, 9].

The slamming forces mentioned in this study are impact forces exerted by breaking waves on offshore structures. A breaking wave is a wave whose amplitude reaches a critical level at which it becomes unstable and dissipates large amounts of wave energy into turbulent kinetic energy. It may occur at certain sites, depending on the local water depth, wave height, wave length, wave steepness, sea bed slope etc. Breaking waves are usually categorized into three types: spilling, plunging and surging [7] (or sometimes four types with an additional collapsing type). The wave profile of each type is different. Among different types of breaking waves, the plunging type, as shown in Fig. 1.1, is the type that causes impulsive slamming forces. Figure 1.2 illustrates the interaction between a plunging breaking wave and a cylinder with a simplified two dimensional sketch. Figure 1.3 demonstrates a typical slamming force time series of such an interaction. Since the wave-structure interaction features a relatively small dissipating area and a very high local pressure, the slamming force has a high impulsive force and a very short duration [10].



Figure 1.1: Plunging breaking wave (Source: NOAA).

Because of the slamming force, it is not suitable to describe the total force due to a plunging breaking wave only by using the Morison's equa-

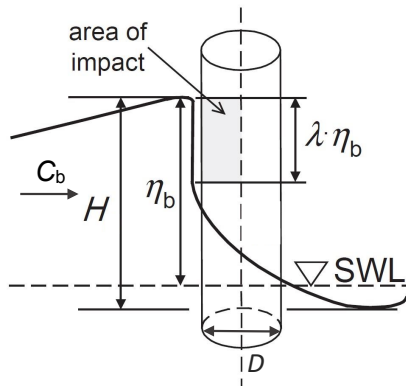


Figure 1.2: Sketch of a plunging breaking wave interacting with a cylinder [11].

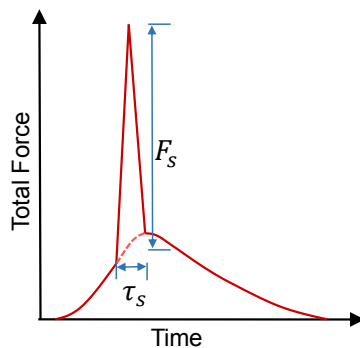


Figure 1.3: Illustration of a slamming force time series [12].

tion [13], which is typically used for calculating quasi-static wave forces. A common engineering practice to take the slamming force into account is to add an extra slamming term F_S in addition to the drag term F_D and the inertia term F_I of the Morison's equation.

$$F = F_D + F_I + F_S \quad (1.1)$$

There are four major approaches to investigate slamming forces: theoretical analyses, numerical simulations, model-scale tests and full-scale field measurements. Theoretical analyses were initially carried out by von Kármán [14] and Wagner [15]. Most of the later theoretical investigations were based on one of their theories. Due to the strong nonlinearities of breaking

Table 1.1: Slamming force models for cylindrical structures (modified from [12]).

| Author | Theory | Maximum C_s | Slam duration, τ_s | Time history of slamming coefficient, $C_s(t)$ |
|----------------------------|--|---------------|-------------------------|--|
| Goda et al. [24] | von Karman | π | $\frac{D}{2C_b}$ | $\pi \left(1 - \frac{2C_b t}{D}\right)$ |
| Campbell and Weynberg [25] | Experimental study | 5.15 | $\frac{D}{C_b}$ | $5.15 \left(\frac{D}{D+19C_b t} + \frac{0.107C_b t}{D}\right)$ |
| Cointe and Armand [26] | Wagner and matched asymptotic expansions | 2π | $\frac{3D}{2C_b}$ | $2\pi - \left(4.72 - \ln\left(\frac{2C_b t}{D}\right)\right) \sqrt{\frac{2C_b t}{D}}$ |
| Wienke and Oumeraci [11] | Wagner | 2π | $\frac{13D}{64C_b}$ | $2\pi - 2\sqrt{\frac{2C_b t}{D}} \left(\tanh^{-1} \sqrt{1 - \frac{C_b t}{2D}}\right)$ (for $0 \leq t \leq \frac{D}{16C_b}$) $\pi \sqrt{\frac{1}{12} \frac{D}{C_b t'} - \left(\frac{16}{3} \frac{C_b t'}{D}\right)^{\frac{1}{2}} \tanh^{-1} \sqrt{1 - \frac{2C_b t'}{D}} \sqrt{\frac{12C_b t'}{D}}}$ $t' = t - \frac{D}{64C_b}$ (for $\frac{D}{16C_b} \leq t \leq \frac{13D}{64C_b}$) |
| WiFi formulation [27] | Wagner | 2π | $\frac{13D}{64C_b}$ | a symmetric load shape |

Note that C_s is the slamming coefficient, D is the diameter of the cylinder, C_b is breaking wave celerity. In the WiFi formulation, the slamming force is assumed to be symmetric in time around the crest when the crest touches the structure surface.

waves, it is difficult to estimate slamming forces accurately by using theoretical analyses only. Numerical simulations of breaking waves commonly employ Computational Fluid Dynamics (CFD) [16]. CFD simulations can predict slamming forces, but the simulations are usually time consuming, since they involve complex two-phase flow and fluid-structure interaction problems, and they require a small time step to accurately resolve the impact peaks that occur in a very short period of time. Model tests and field measurements are more accurate approaches to predict slamming forces. Many model tests of slamming forces on vertical or inclined cylindrical structures have been carried out. The slamming force models proposed in some of these studies are given in Table 1.1. Other experimental studies that are not shown in this table include but are not limited to Chan et al. [17], Irschik et al. [18], Sawaragi and Nochino [19], Sarpkaya [20], Tanimoto et al. [21], Ros [22], Peeringa and Hermans [23].

To be noticed, the available slamming force models were developed for cylindrical structures, so they are applicable to monopiles (see Fig. 1.4). Space frame substructures, such as jacket (see Fig. 1.4), are also promising substructure concepts for OWTs, especially since the turbine size, the water depth and the distance to shore are all increasing for the offshore wind projects in recent years. As the second most popular type of OWT substructures in Europe, jacket accounts for 9.4% of the total installed substructures in 2017 [28]. Due to more complicated geometry of the structure, the slamming scenario of a jacket is expected to be different from that of a monopile. However, researches on slamming forces for jackets were still limited in number to e.g. Aashamar [29] and Loukogeorgaki et al. [30].

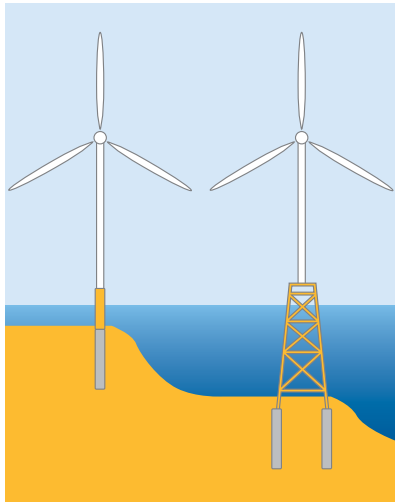


Figure 1.4: Substructures for offshore wind turbines: Monopile (left) and jacket (right) (modified from [31]).

The WaveSlam project [32, 33, 34] was initiated as one of the earliest experimental campaigns for slamming forces on jacket substructures. The project was conducted by a consortium headed by University of Stavanger (UiS) and Norwegian University of Science and Technology (NTNU) in 2012–2013. The experiment was run in 2013 in the Large Wave Flume at Coastal Research Centre (FZK), Hannover, Germany. The jacket model used in the experiment was similar to the jacket designed by Reinertsen Engineering for the Thornton bank wind farm [33]. The scale of the experiment was 1:8.

The experimental setup is shown in Fig. 1.5. The wave flume is approximately 300m long, 5m wide and 7m deep. The waves were generated by the wave board at one end of the flume, went over a slope, and then reached the jacket on a platform. During the wave test, the water depth at the jacket ranged from 1.8m to 2.0m to simulate a water depth of approximately 16m. The legs and braces of the jacket model were 0.14m in diameter.

A global coordinate system is defined as follows: The origin is positioned at the middle position of the wave board ($x = 0$), at the bottom of the channel ($z = 0$) and at the south side of the flume, namely the right side when following the flow ($y = 0$). The x-axis is positive in the wave direction. The z-axis is positive upwards. The y-axis forms a right hand system with the other axes.

Wave gauges were installed at 15 different locations. Three Acoustic Doppler Velocity meters were installed in the plane of the legs. The motion

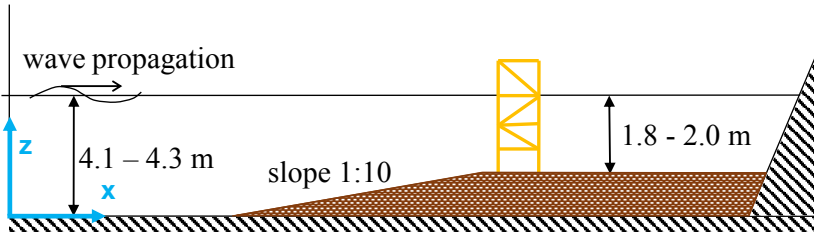


Figure 1.5: *Experimental setup and global coordinates [35]. The wave flume is about 300 m long, and the jacket is located at about 100 m before the end of the flume, with a much gentler slope than illustrated.*

of the wave paddle was recorded. The jacket was equipped with four total force transducers, ten local force transducers on the legs, twelve XY force transducers on the braces, and four one-directional accelerometers.

The WaveSlam project provided many experimental data for detailed analyses of both local and global slamming forces on jacket substructures. However, the measured forces are not the desired slamming forces, since the jacket model is relatively flexible. Therefore, inverse methods are required to estimate the actual slamming forces from the experimental data. Statistical analyses are also essential for understanding the features of the slamming forces, before an engineering force model is proposed.

1.2 Objectives

The main objectives of this study are to reveal the characteristics of slamming forces on OWT jacket substructures and to develop a global slamming force model, based on the large-scale experimental data from the WaveSlam project. The following sub-objectives are defined.

- Develop inverse methods to estimate slamming forces
- Reveal the statistical characteristics of local slamming forces
- Reveal the statistical characteristics of global slamming forces
- Develop a global slamming force model

1.3 Scope

This study focuses on the interaction between breaking waves and structures and, more specifically, on slamming forces. The formation of breaking waves, categorization of breaking waves, energy dissipation due to breaking waves and the probability of occurrence of breaking waves in ocean conditions are out of the scope of this study.

The slamming forces refer to the wave impact forces caused by plunging breaking waves in shallow water. The forces due to other types of breaking waves or in other water depth are out of the scope of this study.

The studied substructure is the jacket type for offshore wind applications. Other types of substructures for offshore wind applications, as well as offshore structures that are used in other industries are out of the scope of this study.

The study focuses on inverse modeling and statistical analyses based on experimental data. Numerical approaches for breaking wave simulations are out of the scope of this study.

1.4 Thesis structure

This thesis is written as a collection of articles. The seven research articles in the appendix are considered to be part of the thesis, while the first six chapters serve as a brief introduction and the summary of main research findings.

Chapter 1 provides the background and motivation of the research topic and introduces the objectives, the scope and the structure of the thesis. Chapters 2 to 5 cover the four major topics of the thesis that are shown in Fig. 1.6.

In Chapter 2, the methods for the inverse estimation of slamming forces are introduced. There are two major challenges in this topic: extraction of dynamic force part and force reconstruction. Papers 1, 2 and 3 provide different solutions to these challenges.

In Chapter 3, the statistical characteristics of the local and global slamming forces under a given wave condition are investigated. Paper 3 focuses on the local forces, while Paper 4 focuses on the global forces.

In Chapter 4, the development and application of a global slamming force model is presented. This chapter covers the main results of Paper 5.

In Chapter 5, various aspects regarding slamming load consideration in OWT simulations are discussed. In addition, machine learning is introduced

as an alternative approach to detect plunging breaking waves. This chapter covers the main results of Paper 6 and Paper 7.

In Chapter 6, conclusions and recommendations for future study are presented.

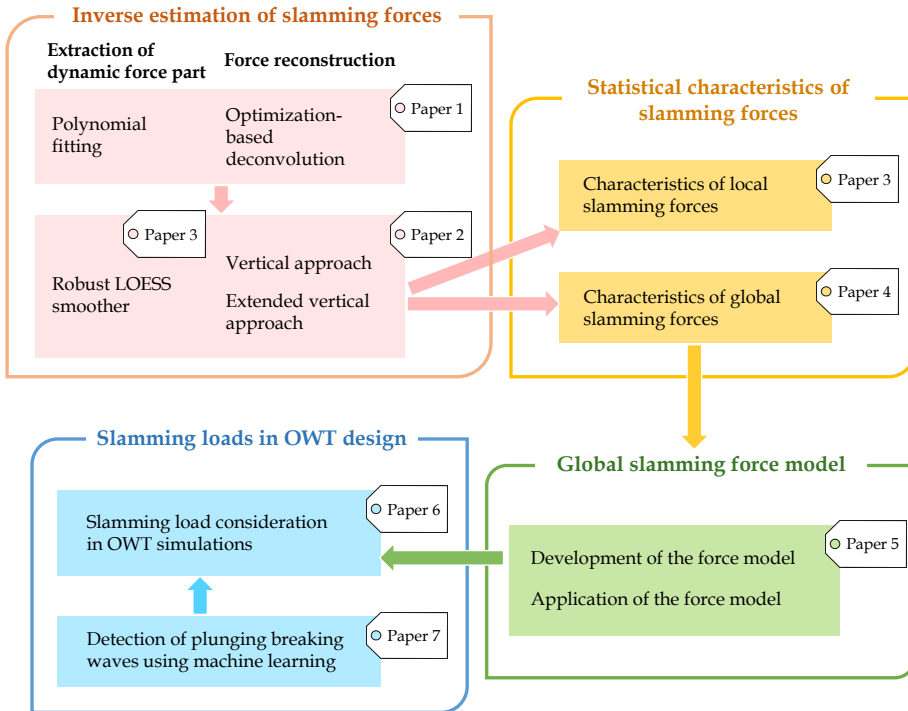


Figure 1.6: Thesis structure and the topics covered by the appended papers.

Chapter 2

Inverse Estimation of Slamming Forces

Although both local and global forces were measured by various transducers in the WaveSlam project as mentioned in Section 1.1, these measurements are not slamming forces, but the response forces of the jacket model due to the wave impacts. Since the jacket model is relatively flexible, the response forces have different values from the exerted slamming forces by the waves. Therefore, the slamming forces should be inversely estimated from the available experimental data, before they can be used for further analysis.

The approaches for estimating local and global slamming forces are summarized in Fig. 2.1. In both approaches, the response force measurements from the wave test are used together with the hammer test data for the slamming force estimation, and both approaches are composed of three stages: preprocessing, force reconstruction and post-processing. However, the used measurements and the detailed steps are different.

In preprocessing stage, the extraction of dynamic part from the measured response force is an important step, which is elaborated below in Section 2.1. Force reconstruction is the most crucial one among the three stages for an accurate estimation of the slamming forces, so the methods used in this stage are explained in detail in Section 2.2.

2.1 Extraction of dynamic force part

The force exerted by a breaking wave on a structure is composed of two parts: a quasi-static force and an impact force by the breaker, namely the slamming force. Therefore, a measured response force includes both a slowly varying part caused by the quasi-static force and a dynamic part

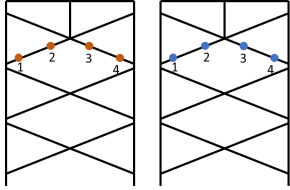
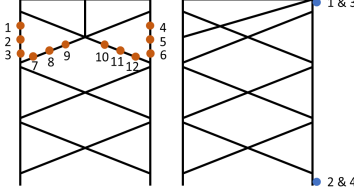
| | | Local force | Global force |
|-------------------------------|--|--|--|
| | |  Front view Front view |  Front view Side view |
| Used data | Exerted hammer impacts | At locations 1-4 in red | At locations 1-12 in red |
| | Response forces from hammer test and wave test | From local force transducers in wave direction at locations 1-4 in blue, same as the hammer impact locations | From total force transducers in wave direction at locations 1-4 in blue |
| Slamming force representation | | Local slamming forces on the two braces are represented by effective local slamming forces at locations 1-4 in red. | Total slamming forces on the whole wave impact region at the jacket model are represented by effective total slamming forces at locations 1-12 in red or their mean value. |
| Preprocessing | | For measured response force: <ul style="list-style-type: none"> • Filtering, zero-shifting • Extraction of dynamic part For measured hammer impact forces: <ul style="list-style-type: none"> • Resampling | For measured response force: <ul style="list-style-type: none"> • Filtering, zero-shifting • Summation of four measurements • Extraction of dynamic part For measured hammer impact forces: <ul style="list-style-type: none"> • Resampling |
| Force reconstruction | | Treat transducers independently: <ul style="list-style-type: none"> • Horizontal approach • Vertical approach Treat transducers interactively: <ul style="list-style-type: none"> • ODC method • Extended vertical approach | <ul style="list-style-type: none"> • Horizontal approach • Vertical approach |
| Post-processing | | <ul style="list-style-type: none"> • Calculating peak forces and impulses | <ul style="list-style-type: none"> • Averaging force time series • Calculating six parameters |

Figure 2.1: Inverse estimation of local and global slamming forces.

due to the slamming force. In order to reconstruct the slamming force, only the dynamic part should be used. The quasi-static contribution should be eliminated from the measured force signals. Common methods to achieve this goal are frequency domain filtering or Empirical Mode Decomposition (EMD) combined with filtering [18]. However, these methods overestimate the quasi-static part in the region of the maximum load [18], leading, therefore, to an underestimated dynamic part. Therefore, two approaches are

proposed to extract the dynamic part more accurately.

In Paper 1, a 10-degree polynomial curve is used to fit the time series of the measured response force in order to estimate the quasi-static part. The curve fitting is applied to a short range of the time series at the beginning and another range of the time series at the end, with an interval in the middle to avoid taking out part of the slamming contribution. The ranges are manually selected based on many tests to ensure (1) that the positive and negative amplitudes of the dynamic part are more or less equal after the first few peaks; (2) that the peak of the quasi-static curve is not close to the highest peak of the measured response force; (3) that the dip before the first peak in the dynamic part should be as small as possible. This method avoids eliminating part of the slamming contribution around the main peaks, while having a smooth transition for the quasi-static curve over this time range, although it might introduce some uncertainties due to the manual data range selection.

In Paper 3, a time domain robust LOESS smoother [37] is used to estimate the quasi-static part by smoothing the total response force. It is realized by local regression using weighted linear least squares and a second degree polynomial model. The method assigns zero weight to the data outside six mean absolute deviations. The smoothing span is set to be 5% of the total number of data points. Fig. 2.2 shows an example of the method application. According to the figure, the quasi-static force is well estimated in general. There is no significant overestimation around the peak of the

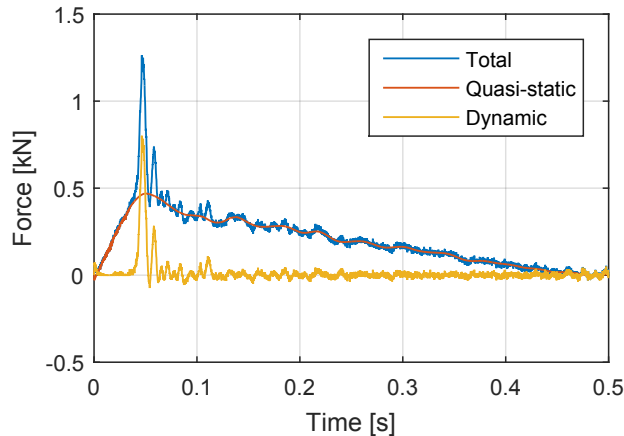


Figure 2.2: Separation of quasi-static and dynamic parts of a measured response force time series, by using robust LOESS smoother method [36].

quasi-static force, since the data points around the peak of the response force are considered as outliers in the smoothing, and zero weight is assigned to them. Therefore, the dynamic part is not underestimated. For some measurements, when the quasi-static part and the dynamic part are merged together in the beginning of the time series, the separation is more challenging. Using this method, the estimated quasi-static part is higher than the measured force before the wave impact. This leads to a deep dip in the resulting dynamic part. This dip can also be observed when other methods (e.g. frequency domain filtering) are used. In order to avoid this unrealistic dip, the negative values before the wave impact in the estimated dynamic part are set to be zero. Due to this adjustment, the method is not considered to be perfect, but it is still an effective tool to process the measured data and to acquire the desired dynamic forces. This method is more convenient to use compared to the one used in Paper 1, so it is applied to Papers 2, 4 and 5 as well.

2.2 Force reconstruction methods

The idea of reconstructing wave slamming forces is to use the available response forces measured in the wave tests, and both the impact forces and response forces measured in the hammer tests to calculate the wave impact forces. This is an inverse problem and in general ill-defined. Compared to forward problems, inverse problems are more significantly influenced by noise, and the solutions of the inverse problems are more susceptible to indeterminacies. Therefore, more sophisticated methods are required for solving inverse problems than for solving forward problems. Common methods of force reconstruction fall into three categories: direct methods, regularized methods and probabilistic/statistical methods [38]. The aforementioned data used for the force reconstruction problem in this study are deterministic, so the direct methods and regularized methods are more applicable to this problem. The force reconstruction methods proposed here are therefore inspired by these two categories of methods.

Ideally, a reference impact test that covers the whole wave slamming area would be most helpful for the reconstruction. In practice, the hammer tests could only be done for discrete locations. The reconstructed forces are “effective forces”, which means that the wave slam is assumed to occur only on the locations of the corresponding hammer impacts used for the reconstruction.

The impulse and response of the jacket model exhibit linear relationship, as shown in Paper 1. Therefore, the force reconstruction methods described

in this section are all based on this linear behavior of the structure.

Four approaches of force reconstruction are summarized in this section: optimization-based deconvolution (ODC), horizontal approach, vertical approach and extended vertical approach. The first approach is proposed in Paper 1, and the other three are proposed in Paper 2.

2.2.1 Optimization-based deconvolution

The optimization-based deconvolution (ODC) method is proposed for estimating the local slamming loads on the two front braces of the jacket model as shown in Fig. 2.1. The load at each of the four locations is described by two parameters: the impulse of the load and its starting time. All together eight parameters can be calculated to represent the local slamming loads.

With the help of Fig. 2.3, the ODC method is explained. For a hammer impact at each location, the time series of the response forces at all of the four locations are normalized by dividing the impulse exerted by the hammer. The normalized local force time series from the hammer test are essentially the impulse response functions [40], and there are 16 of them (four hammer impact locations times four response locations). The eight parameters (the impulse of the load and its starting time for four hammer impact locations) are used to shift and to scale the impulse response func-

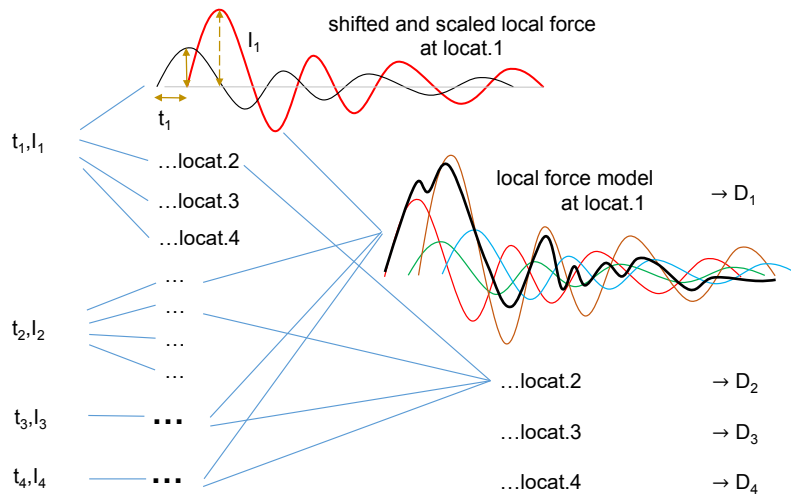


Figure 2.3: Illustration of the ODC method [39]. The symbols in this figure, t_i , I_i and D_i ($i = 1, 2, 3, 4$) are starting times, impulses and Euclidean distances for the four locations.

tions, to get 16 response force time series at the four locations. The response force time series at each of the four locations are summed up, to get four calculated response force time series due to the wave slam. The Euclidean distance between the calculated response forces and the measured response forces in the wave test is then calculated. By minimizing the Euclidean distance, the eight parameters are estimated.

In the ODC method, the measurements from the four local force transducers are treated interactively. The loads caused by the wave impacts on the other locations at the braces are taken into account during the force reconstruction. The slamming loads are only represented by effective impulses. The time series of the slamming forces cannot be acquired.

2.2.2 Horizontal approach

The horizontal approach is a state-of-the-art approach for reconstructing the external forces of a linear system. The response of a linear system $r(t)$ can be expressed by a Duhamel's integral, namely a convolution of an external force time series $f(t)$ with an impulse response function $h(t)$, as shown in Equation 2.1.

$$r(t) = \int_0^t f(t - \tau)h(\tau) d\tau \quad (2.1)$$

As shown in Fig. 2.4, the approach is composed of two steps:

1. The hammer test impact force and the hammer test response force are used to deconvolve $h(t)$.
2. The calculated $h(t)$ is used together with the measured wave test response force to estimate the effective wave impact force.

Since the data are used horizontally in pairs, the approach is named ‘‘horizontal’’.

Numerical deconvolution is an ill-posed problem [42, 43, 38]. Small error or noise in the input data can lead to large variations in the output, which makes the results unstable. Therefore, a conjugate gradient technique [42] is applied in step one, and a weighted eigenvector expansion technique [44] is applied in step two, in order to acquire useful results.

The horizontal approach can be applied to both global and local slamming force reconstructions. When used for local force reconstruction, the transducers are treated independently, which means only the wave impact force exerted at the same location as the response measurement used for the reconstruction is considered. The time series of the slamming forces can be

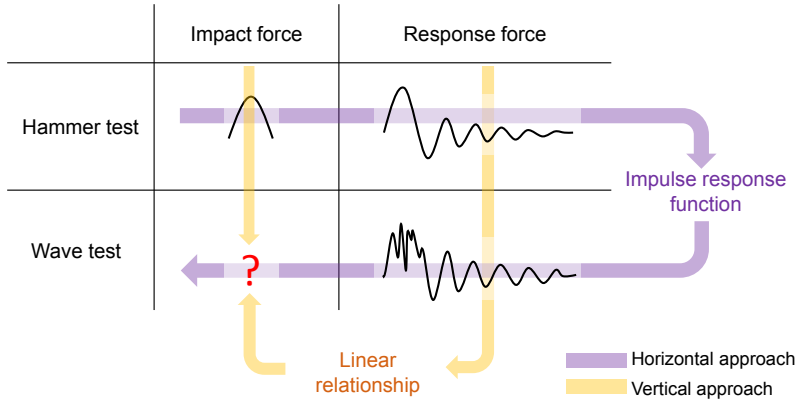


Figure 2.4: Horizontal and vertical approaches for force reconstruction [41].

resolved. The approach involves two numerical factors, which need to be selected during the application.

2.2.3 Vertical approach

In this approach, the data are used vertically in pairs, as shown in Fig. 2.4, so the approach is named “vertical”. The basic principle of the approach is demonstrated in Fig. 2.5. A wave slam on the structure is imagined as a hammer hitting one location on the structure with different amplitudes for multiple times. Here are the three main steps of the approach:

1. Knowing the response forces from one wave slam and from one hammer impact, the wave response force is decomposed into multiple hammer response forces scaled by corresponding coefficients.
2. Each hammer response force corresponds to one hammer impact force. So, the hammer impact forces, corresponding to the hammer response forces obtained from Step 1, are determined by using the same coefficients.
3. Summing up the multiple hammer impact forces, the impact force from one wave slam is acquired.

The mathematical expression of the approach is illustrated below:
The wave slamming force is written as an $n \times 1$ vector

$$\mathbf{f}_w = (f_{w_1} \ f_{w_2} \ f_{w_3} \ \cdots \ f_{w_n})^T \quad (2.2)$$

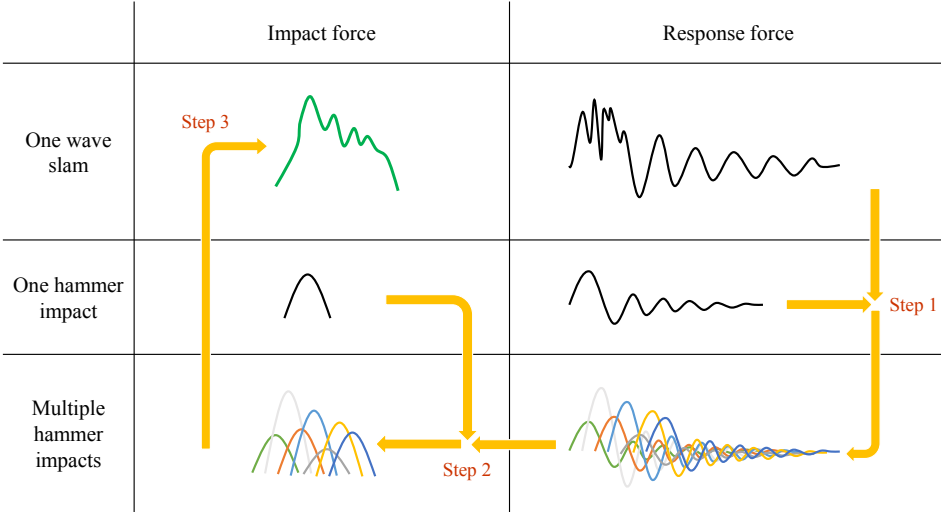


Figure 2.5: Illustration of the vertical approach [45].

It can be expressed as

$$\mathbf{f}_W = \mathbf{F}_H \boldsymbol{\beta} \quad (2.3)$$

where

$$\mathbf{F}_H = \begin{pmatrix} f_{H_1} & 0 & \cdots & 0 \\ \vdots & \vdots & \ddots & \vdots \\ f_{H_\delta} & 0 & \ddots & 0 \\ f_{H_{\delta+1}} & f_{H_1} & \ddots & 0 \\ \vdots & \vdots & \ddots & \vdots \\ f_{H_{(p-1)\delta}} & f_{H_{(p-2)\delta}} & \ddots & 0 \\ f_{H_{(p-1)\delta+1}} & f_{H_{(p-2)\delta+1}} & \ddots & f_{H_1} \\ \vdots & \vdots & \ddots & \vdots \\ f_{H_n} & f_{H_{n-\delta}} & \cdots & f_{H_{n-(p-1)\delta}} \end{pmatrix} \quad (2.4)$$

is an $n \times p$ matrix composed of column vectors representing repeated and shifted hammer impact forces. The symbol p denotes the total number of hypothetical hammer hits. The symbol δ denotes the interval between every two hammer hits, and is named *step factor*. The step factor should be selected during the application.

The coefficients

$$\boldsymbol{\beta} = (\beta_1 \quad \beta_2 \quad \beta_3 \quad \cdots \quad \beta_p)^T \quad (2.5)$$

are given as a $p \times 1$ parameter vector for scaling the hammer hits.

The wave response force is written as an $n \times 1$ vector

$$\mathbf{r}_W = (r_{W_1} \quad r_{W_2} \quad r_{W_3} \quad \cdots \quad r_{W_n})^T \quad (2.6)$$

It can be expressed as

$$\mathbf{r}_W = \mathbf{R}_H \boldsymbol{\beta} + \mathbf{e} \quad (2.7)$$

where

$$\mathbf{R}_H = \begin{pmatrix} r_{H_1} & 0 & \cdots & 0 \\ \vdots & \vdots & \ddots & \vdots \\ r_{H_\delta} & 0 & \ddots & 0 \\ r_{H_{\delta+1}} & r_{H_1} & \ddots & 0 \\ \vdots & \vdots & \ddots & \vdots \\ r_{H_{(p-1)\delta}} & r_{H_{(p-2)\delta}} & \ddots & 0 \\ r_{H_{(p-1)\delta+1}} & r_{H_{(p-2)\delta+1}} & \ddots & r_{H_1} \\ \vdots & \vdots & \ddots & \vdots \\ r_{H_n} & r_{H_{n-\delta}} & \cdots & r_{H_{n-(p-1)\delta}} \end{pmatrix} \quad (2.8)$$

is an $n \times p$ matrix composed of column vectors representing repeated and shifted hammer response forces, and

$$\mathbf{e} = (e_1 \quad e_2 \quad e_3 \quad \cdots \quad e_n)^T \quad (2.9)$$

is an $n \times 1$ error term due to the noise in the measurements.

An ordinary least squares regression technique is used to solve for the parameter vector $\boldsymbol{\beta}$ based on Equation 2.7, so the estimated parameter vector is

$$\hat{\boldsymbol{\beta}} = (\mathbf{R}_H^T \mathbf{R}_H)^{-1} \mathbf{R}_H^T \mathbf{r}_W \quad (2.10)$$

Applying $\hat{\boldsymbol{\beta}}$ to Equation 2.3, the wave slamming force is estimated as

$$\hat{\mathbf{f}}_W = \mathbf{F}_H \hat{\boldsymbol{\beta}} \quad (2.11)$$

The results obtained from horizontal approach and vertical approach agree well, as shown in Fig. 2.6. Compared to the horizontal approach,

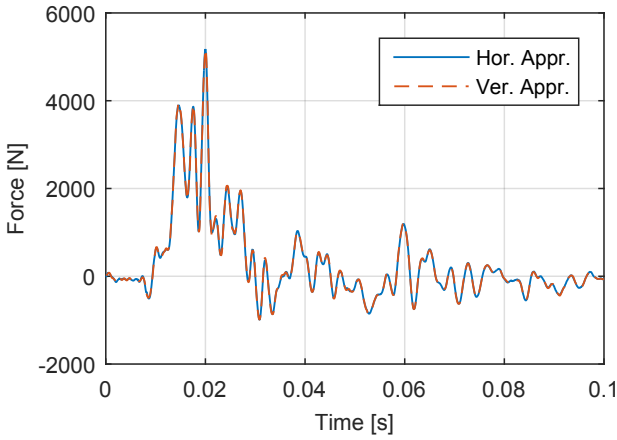


Figure 2.6: Comparison of the results from horizontal approach and vertical approach, at one location for one wave [41].

the proposed vertical approach is numerically more stable and involves only one numerical factor that needs to be selected. This approach is used for the reconstruction of global slamming forces in Paper 4 and Paper 5 and for the reconstruction of local slamming forces in Paper 3. The local force transducers are also treated independently in this approach.

2.2.4 Extended vertical approach

The aforementioned vertical approach can be extended to estimate the local slamming forces more accurately. Similar to the ODC method, the extended vertical approach accounts for the contribution of the impacts at other locations at the braces to the measured response forces. The detailed mathematical expression of this approach can be found in Paper 2.

Compared to the results of the vertical approach, the forces reconstructed by using the extended vertical approach exhibit a similar trend in time, but the values are different. The peak forces and impulses from the vertical approach and the extended vertical approach are compared in Fig. 2.7. The values estimated by the extended vertical approach are in general lower than the ones estimated by the vertical approach, except at locations 3 and 4, where the peak forces estimated by the extended vertical approach are slightly higher. The total impulse exerted by the wave is estimated 22% lower by using the extended approach. This difference is reasonable, because in the vertical approach, the wave response forces due to the impacts at four locations are used as if they are due to the impacts

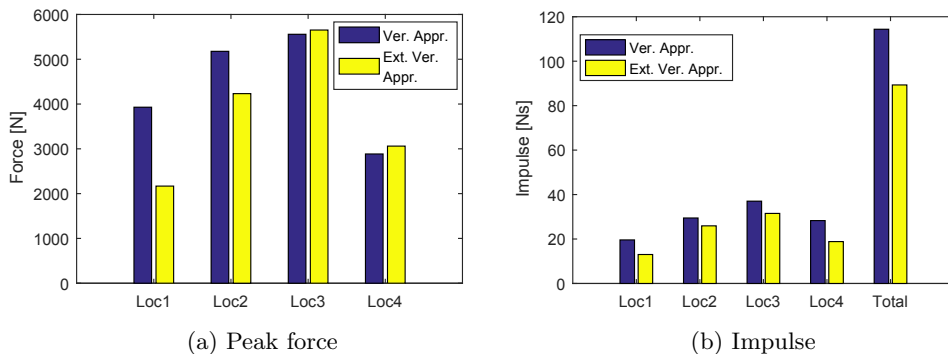


Figure 2.7: Comparison of the results from vertical approach and extended vertical approach [41].

at one location. The wave impact forces are therefore somewhat overestimated. The extended vertical approach, however, eliminates the double counting effect, so the result from it should be more reliable.

Chapter 3

Statistical Characteristics of Slamming Forces

In Chapter 2, the methods for the inverse estimation of slamming forces were described. The inversely estimated wave slamming forces are further studied in this chapter to reveal the statistical characteristics of the slamming forces, under one controlled wave condition in laboratory.

The wave case used for the statistical analysis is illustrated in Table 3.1. There are five test runs with plunging breaking waves under one preset wave condition. In each test run, there are 20 waves. The wave height, wave period and water depth given in the table are nominal values at the wave board. The statistical characteristics of both local slamming forces and global slamming forces are summarized here, and more details can be found in the appended Papers 3 and 4. The vertical approach, as described in Section 2.2.3, was used for the force reconstruction.

Table 3.1: Wave case used for statistical analysis (modified from [36]).

| Condition | Value |
|----------------------|----------------|
| ID of the test runs | 20130617.15~19 |
| No. of runs | 5 |
| No. of waves per run | 20 |
| Wave height | 1.50 m |
| Wave period | 4.9 s |
| Depth | 4.3 m |
| Depth at structure | 2.0 m |
| Run type | Regular |
| Breaking location | At front legs |

3.1 Characteristics of local slamming forces

The local slamming force time series at four locations on the braces of the jacket model (see Fig. 2.1) were reconstructed for each wave in each test run. Two parameters are extracted from each force time series and analyzed further: peak force and impulse.

In Paper 3, the variations of the peak force and the impulse with regard to wave ID, test run and location are mainly discussed.

The variations of the peak force and the impulse under different wave IDs (“positions” in Paper 3) are illustrated by Figs. 3.1 and 3.2. The peak forces and the impulses at each wave ID are averaged over five test runs, and the standard deviations are calculated. Both the peak force and the impulse are strongly dependent on the Wave ID. For waves 2, 18 and 19, the results have much larger standard deviations and distinct means compared to those of other wave IDs. This can be explained by the uncertain behavior of the waves at the beginning and at the end of the test runs. The mean values at the investigated locations 2 and 3 (upper locations) are larger than the ones at locations 1 and 4 (lower locations) in general. This indicates

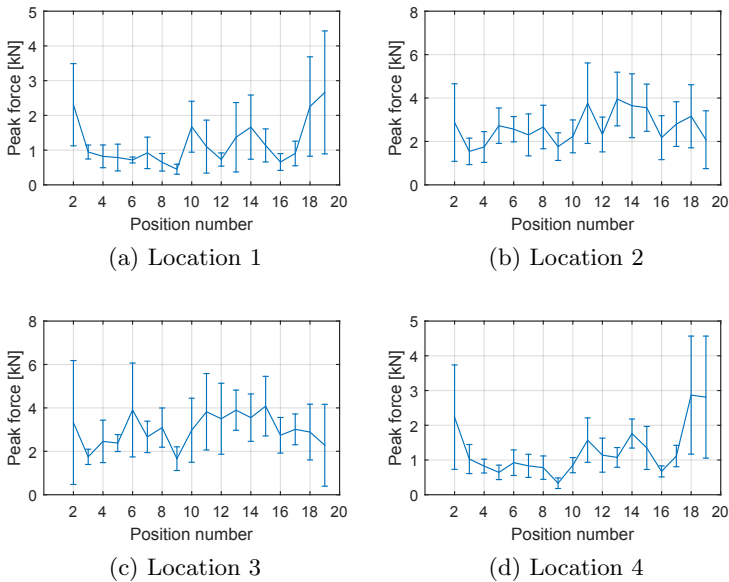


Figure 3.1: Variation of peak force of local slamming force with regard to wave ID [36]. The position number in the x-axis label indicates the wave ID.

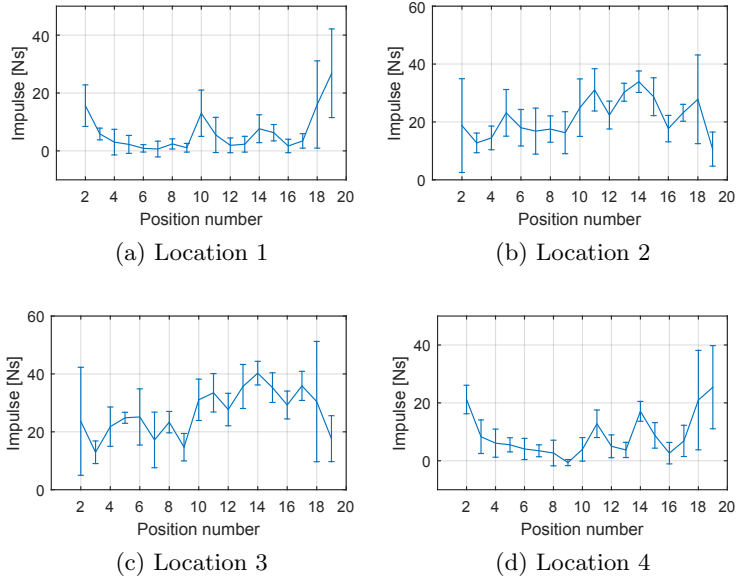


Figure 3.2: Variation of impulse of local slamming force with regard to wave ID [36]. The position number in the x-axis label indicates the wave ID.

that the upper locations are influenced by the breakers more directly.

The variations of the peak force and the impulse under different test runs (“cases” in Paper 3) are illustrated by Figs. 3.3 and 3.4. The peak forces and the impulses of waves 3 to 9 in each run are averaged, and the standard deviations are calculated. The mean values and the standard deviations of the results do not have large variations depending on the test run. No test run stands out with distinct values compared to the others.

The variations of the peak force and the impulse at different locations are illustrated by Fig. 3.5. The peak forces and the impulses of waves 3 to 9 in all five test runs are averaged for each location, and the standard deviations are calculated. From the figure, we can see more clearly that the slamming loads are much larger on the upper locations than on the lower locations. Both the mean values and the standard deviations are higher at the upper locations. The forces on the left locations and on the right locations are slightly asymmetric, which might be caused by the asymmetry of the waves or the uncertainties of the measurement in both the hammer test and the wave test.

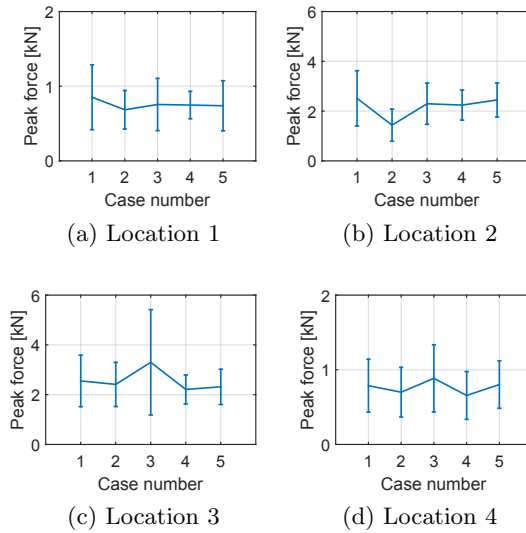


Figure 3.3: Variation of peak force of local slamming force with regard to test run [36]. The case number in the x-axis label indicates the test run.

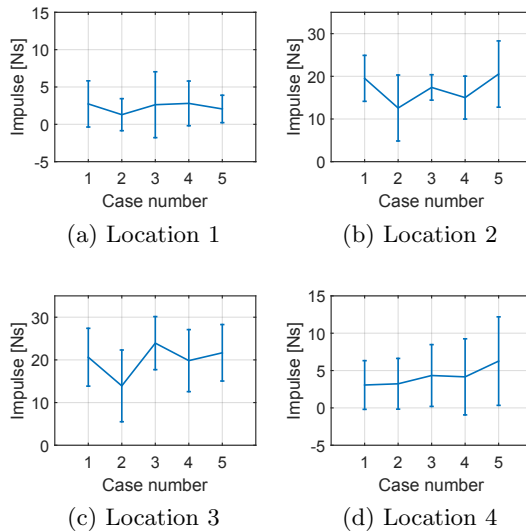


Figure 3.4: Variation of impulse of local slamming force with regard to test run [36]. The case number in the x-axis label indicates the test run.

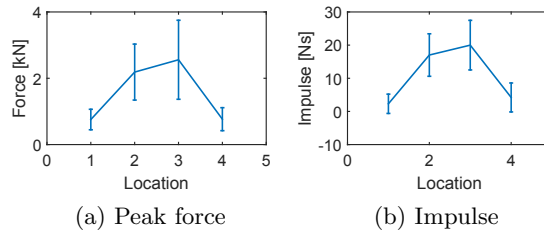


Figure 3.5: Variation of peak force and impulse of local slamming force with regard to location [36].

3.2 Characteristics of global slamming forces

A global slamming force time series was reconstructed by using the hammer test data of each hammer hit at each hammer impact location and for each wave in each test run. By using different combinations of wave test data and hammer test data, many global slamming force time series were thus acquired for statistical analysis. The details about the hammer test data used for the force reconstruction can be found in Paper 4. Only the first peak of each global slamming force time series, which corresponds to the wave impact at the plane of the front legs of the jacket model, was reconstructed, since the waves broke at the front legs of the jacket model in the studied wave case.

Six parameters are extracted from each time series to describe the cor-

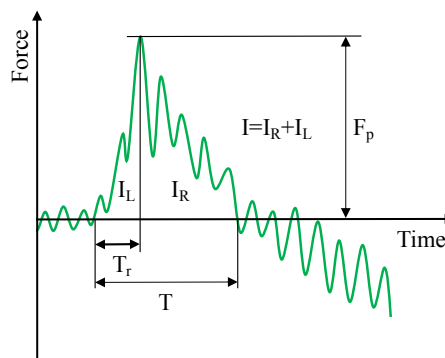


Figure 3.6: Parameters to describe one global slamming force time series [45]. The variation of the time series has been exaggerated for visualization purposes.

responding slamming force, as illustrated in Fig. 3.6.

- F_p : Peak force, the maximum force in the time series.
- T : Duration, the time between the last zero-up-crossing before the peak and the first zero-down-crossing after the peak.
- T_r : Rising time, the time between the last zero-up-crossing before the peak and the peak itself.
- I : Impulse, the integral of the force over the duration.
- I_L : Left impulse, the integral of the force over the rising time.
- I_R : Right impulse, the integral of the force over the time between the peak and the first zero-down-crossing after the peak.

In Paper 4, the variations of the six parameters with regard to the hit ID and the location of the used hammer test data, wave ID and test run are discussed. The correlations among the six parameters are also checked.

The variation with regard to hit ID and the location of the used hammer test data do not have systematic biases, such as dependence on hammer hit location or significant asymmetry.

The force times series reconstructed by using different hammer test data are then averaged for each wave in each test run, and the six parameters extracted from the averaged force time series are analyzed.

The variations of the six parameters under different wave IDs are illustrated by Fig. 3.7. The parameters of the waves of the same wave ID are averaged over five test runs, and the standard errors of the means are calculated. As shown in the figure, the peak force, impulse and right impulse increase as the wave ID increases, i.e. for the later waves in each run. In contrary, the duration and rising time decrease slightly. The left impulse is almost constant. The difference among the waves may be caused by the accumulated diffraction and refraction in each run, which is observed in the video record of the experiment. As these effects, including also a potentially shifting breaking point, cannot be quantified easily, these unknown effects are considered as part of the uncertainties reported.

The variations of the six parameters under different test runs are illustrated by Fig. 3.8. The parameters of waves 3 to 19 in each run are averaged, and the standard errors of the means are calculated. As shown the figure, the result only varies slightly among different runs, which means the test runs have a good repeatability.

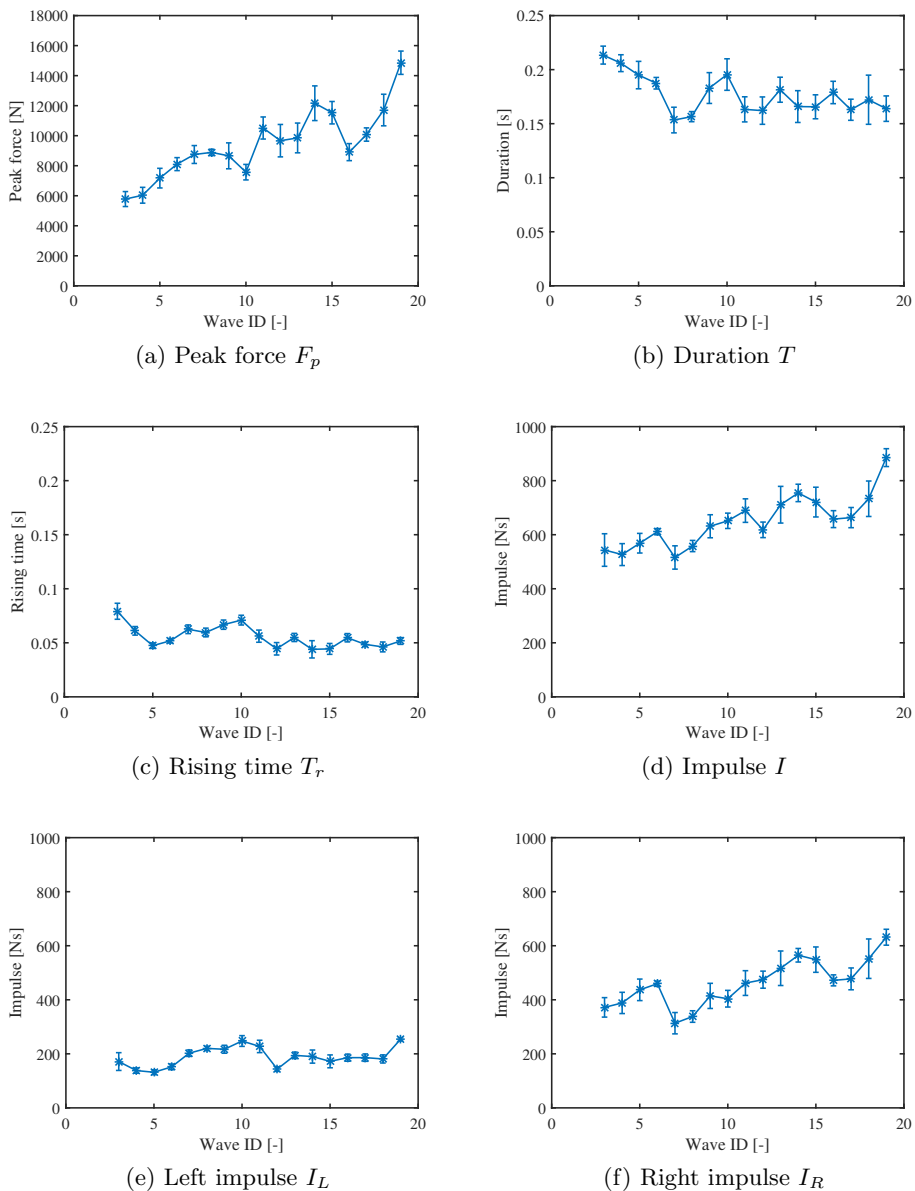


Figure 3.7: Variation of six parameters of global slamming force with regard to wave ID [45].

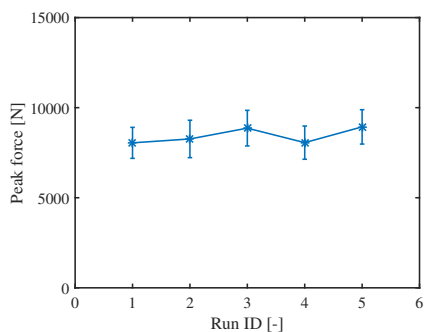
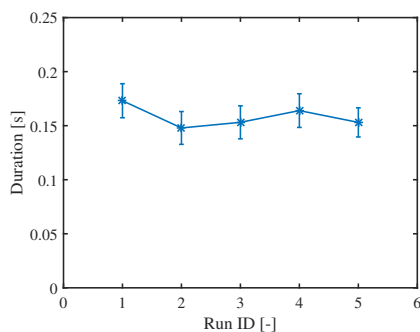
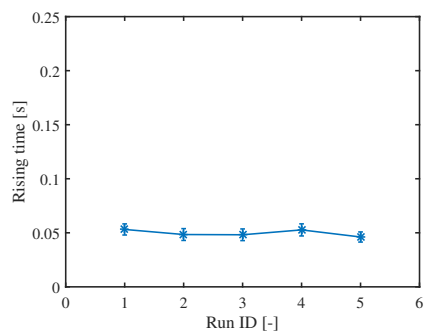
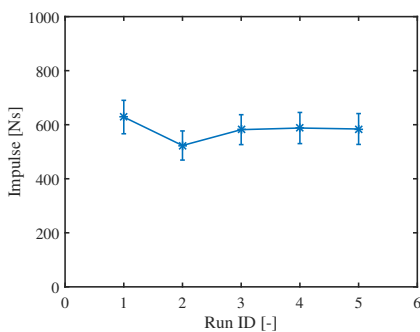
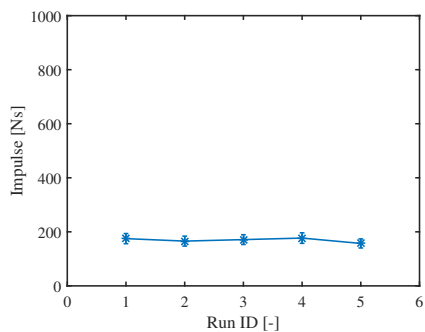
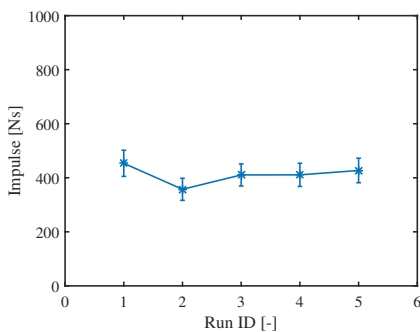
(a) Peak force F_p (b) Duration T (c) Rising time T_r (d) Impulse I (e) Left impulse I_L (f) Right impulse I_R

Figure 3.8: Variation of six parameters of global slamming force with regard to test run [45].

The correlation matrix of the six parameters is calculated, as shown in Table 3.2, in order to investigate the interdependencies among the parameters. For the purpose here, we assume correlations above 0.8 to be strong, and correlations between 0.4 and 0.8 to be moderate. According to the correlation matrix, the peak force F_p has negative linear relationships with the duration T and with the rising time T_r . This is in accordance with the trend observed for example in Fig. 3.7. The impulse I has moderate positive linear relationships both with F_p and with T . The rising time T_r has a stronger linear relationship with the left impulse I_L than with I . The left impulse I_L and the right impulse I_R have very low correlation, which suggests that these two parts of the impulse are independent and can be treated separately. In summary, these results indicate that the chosen parameters are not independent, which could lead to identification issues. However, the only strong correlation is between I and I_R . Therefore, they should not be used together in a proposed force model.

Table 3.2: Correlation matrix of six parameters of global slamming force [45].

| | F_p | T | T_r | I | I_L | I_R |
|-------|-------|-------|-------|------|-------|-------|
| F_p | 1.00 | -0.42 | -0.42 | 0.40 | 0.18 | 0.36 |
| T | -0.42 | 1.00 | 0.53 | 0.53 | 0.10 | 0.55 |
| T_r | -0.42 | 0.53 | 1.00 | 0.23 | 0.64 | -0.07 |
| I | 0.40 | 0.53 | 0.23 | 1.00 | 0.46 | 0.89 |
| I_L | 0.18 | 0.10 | 0.64 | 0.46 | 1.00 | 0.01 |
| I_R | 0.36 | 0.55 | -0.07 | 0.89 | 0.01 | 1.00 |

Chapter 4

Global Slamming Force Model

In the design and certification of Offshore Wind Turbines (OWTs), it is essential to conduct load simulations. A practical force model is therefore desired, should slamming forces be considered in the load simulations. However, a simple but reliable slamming force model specifically for OWTs with jacket substructures is currently in absence. This chapter summarizes the development and application of a global slamming force model for jacket substructure, the details of which are presented in Paper 5.

4.1 Development of the model

The statistical characteristics of the global slamming forces under a given wave condition were discussed in section 3.2 through the analysis of six representative parameters. However, a representative time series of the global slamming forces is still in need, in order to describe the force development in time for the given wave condition. A mean force time series is calculated for this purpose and shown in Fig. 4.1, and the standard deviation of the data points at each time instant is also shown in the figure.

Two models were proposed in Paper 4 to fit this representative force time series. According to the comparisons in the paper, the model with two exponentially decreasing curves from the peak of the time series, as

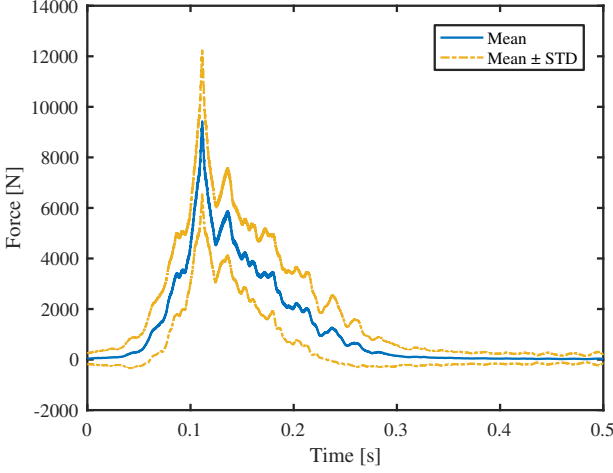


Figure 4.1: Representative global slamming force time series and its standard deviation for one wave condition [45].

expressed in Equation 4.1, has a good fit of the force time series.

$$f(t) = \begin{cases} F_p \exp\left(\alpha_1 \frac{t-t_p}{T_r}\right) & t_p - T_r < t \leq t_p \\ F_p \exp\left(\alpha_2 \frac{t-t_p}{T-T_r}\right) & t_p < t \leq t_p - T_r + T \\ 0 & \text{Otherwise} \end{cases} \quad (4.1)$$

where $f(t)$ is the time series of global slamming force; t_p denotes the moment of the peak in the time series; α_1 and α_2 are two parameters that determine the rate of exponential decay on both sides of the peak; F_p , T and T_r are peak force, duration and rising time, respectively. The three wave related parameters F_p , T and T_r do not have strong linear correlation, according to Section 3.2.

In order to generalize the model to different wave conditions, five more cases in addition to the case shown in Table 3.1 are introduced. The averaged force time series for the available six cases are plotted in Fig. 4.2. The peaks of the time series are aligned in the figure. For all the six cases, the force seems to decay exponentially on both sides of the peak, which is in accordance with the proposed model.

Equation 4.1 can be transformed into

$$\ln\left(\frac{f(t)}{F_p}\right) = \begin{cases} \alpha_1 \frac{t-t_p}{T_r} & t_p - T_r < t \leq t_p \\ \alpha_2 \frac{t-t_p}{T-T_r} & t_p < t \leq t_p - T_r + T \\ 0 & \text{Otherwise} \end{cases} \quad (4.2)$$

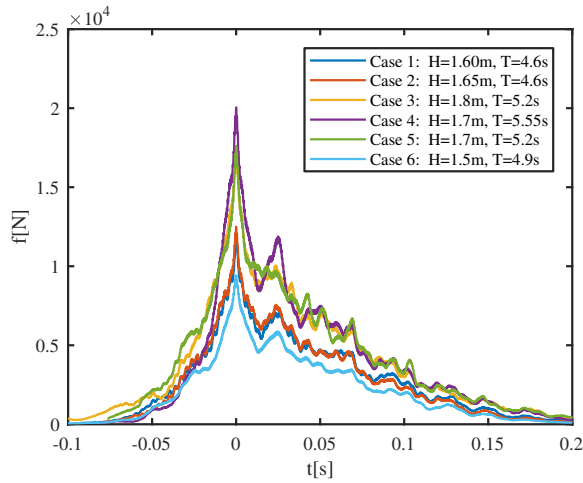


Figure 4.2: Representative global slamming force time series for six cases [35]. The peaks of the time series are aligned at $t = 0$. H denotes wave height, and T denotes wave period in this figure. The values of both parameters are nominal values at the wave board.

The moment of peak t_p can be set to any arbitrary value. For simplification, it is set to zero, so Equation 4.2 becomes

$$\ln \left(\frac{f(t)}{F_p} \right) = \begin{cases} \alpha_1 \frac{t}{T_r} & -T_r < t \leq 0 \\ \alpha_2 \frac{t}{T-T_r} & 0 < t \leq T - T_r \\ 0 & \text{Otherwise} \end{cases} \quad (4.3)$$

In order to apply the model in engineering practice, the five unknown parameters in the model have to be decided. They are discussed separately in two groups below, according to their features.

4.1.1 Determination of exponential parameters

The time series in Fig. 4.2 are converted according to Equation 4.3 using the corresponding parameters F_p , T and T_r of each case. The mean $\mu(t)$ and standard deviation $\sigma(t)$ of the six converted time series are estimated, as depicted in Fig. 4.3. The standard deviation represents the variation of $\ln\left(\frac{f(t)}{F_p}\right)$ with regard to wave condition, and its value varies with the horizontal axis value $\frac{t}{T_r}$ or $\frac{t}{T-T_r}$.

The coefficient of variation (or relative standard deviation, $C_v(t) = \frac{\sigma(t)}{|\mu(t)|}$) varies only slightly with the horizontal axis value and has a low value

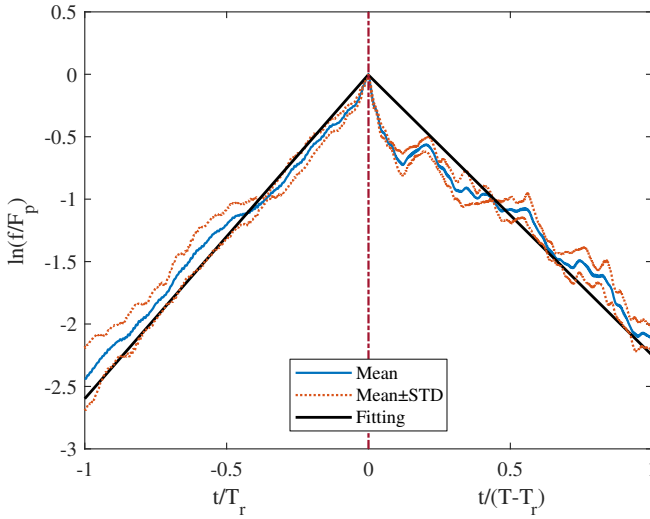


Figure 4.3: Fitting of converted representative global slamming force time series of the six cases [35].

of 0.08 on average. This implies that the variation among the time series is small, and it is plausible to use the mean curve to represent the six time series. It is found that the standard deviation in the vicinity of the peak is smaller than that far away from the peak. Since the force around the peak contributes the most to the impulse caused by a wave impact, it is important to estimate the force around the peak more accurately than the rest of the time series. Therefore, weighted linear regression [46] is applied to fit the mean time series on both sides of the peak. In weighted linear regression, the weighting coefficients are assumed to be inversely proportional to the variance (square of standard deviation), so a smaller standard deviation results in a larger weighting coefficient. This leads to higher weighting around the peak, where the standard deviation is lower. By using the fitting, the exponential parameters are determined: $\alpha_1 = 2.60$ and $\alpha_2 = -2.24$. The coefficients of determination, i.e. R^2 values, of the fitting are calculated using the same weighting scheme to be 0.9999 and 0.9992, respectively. This indicates that the exponential parameters α_1 and α_2 are determined with high confidence.

4.1.2 Determination of wave-dependent parameters

Given an arbitrary regular breaking wave condition, the other three parameters required by the model: duration T , rising time T_r and peak force F_p ,

are not known directly. However, they are wave-dependent parameters due to the physics, and can be determined by the given wave condition. In order to investigate the dependence of these parameters on the wave condition, three dimensionless coefficients are introduced.

The *duration coefficient* ζ_1 is defined as

$$\zeta_1 = \frac{T}{\frac{D_x}{C_b}} \quad (4.4)$$

where D_x is the equivalent width of the structure in the wave direction, the value of which depends on the structure geometry relative to the wave impact. Since the front legs and braces are all in a plane perpendicular to the wave direction and have the same diameter 0.14m, this value is used for D_x . The breaking wave celerity C_b can be approximated by Equation 4.5 , for shallow water waves with high steepness [21, 47].

$$C_b = \sqrt{g(d + \eta_b)} \quad (4.5)$$

where g is the gravitational acceleration; d is the water depth; and η_b is the maximum elevation of the breaking wave, which can be obtained from the wave elevation measurement.

The *rising time coefficient* ζ_2 is defined as the ratio of rising time to duration.

$$\zeta_2 = \frac{T_r}{T} \quad (4.6)$$

The *peak force coefficient* ζ_3 is defined as

$$\zeta_3 = \frac{F_p}{\frac{1}{2}\rho D_y \eta_b C_b^2} = C_s \lambda \quad (4.7)$$

where ρ is the water density; D_y is the equivalent width of the structure in y-axis direction, the value of which depends on the structure geometry relative to the wave impact. For the investigated jacket, $D_y = 2 \times (1 + 2.15) \times 0.14 \text{ m} = 0.88 \text{ m}$. Two inclined braces contribute 2.15 times their diameter 0.14 m each to D_y , due to an inclined angle of 62° with respect to the vertical, while two vertical legs contribute one diameter each to D_y .

A typical formulation of three dimensional slamming force includes two coefficients: slamming coefficient C_s and curling factor λ . In some other studies, e.g. Wienke and Oumeraci [11], C_s was first determined theoretically, then λ was calculated empirically based on the determined C_s . In this study, C_s and λ are treated together as one coefficient ζ_3 instead, since they are not independent.

The values of ζ_1 , ζ_2 and ζ_3 are calculated for each wave of the cases. The η_b acquired from each single wave is the only essential wave parameter for the calculation. The variation of the calculated ζ_1 , ζ_2 and ζ_3 are demonstrated in Figs. 4.4 to 4.6. In the figures, the result variation over different waves in each case is illustrated by the blue bars representing means and standard deviations. The result variation over different cases is illustrated by the red lines. The continuous red line represents the mean value calculated by averaging the means of each case. The dashed red lines represent the standard deviation of the means of each case.

From Fig. 4.4 and Fig. 4.5, it can be noticed that the variation of ζ_1 and ζ_2 over different cases is much smaller than the variation over different waves inside each case. The coefficients of variation of ζ_1 for the six cases range from 0.17 to 0.31, while the value over the six cases is only 0.06. Similarly, the coefficients of variation of ζ_2 for the six cases range from 0.20 to 0.34, while the value over the six cases is only 0.09. Although there is variability of ζ_1 and ζ_2 within each case, the means of all the cases are similar. This implies that ζ_1 and ζ_2 are insensitive to wave condition, so they are treated as constants because their mean values can be assumed to be the same for different wave conditions.

The means and bootstrap 95% confidence intervals of ζ_1 and ζ_2 for each case are calculated. The confidence intervals are narrow compared to the mean values in general, so the means are representative for the cases. The duration coefficient and the rising time coefficient are therefore determined

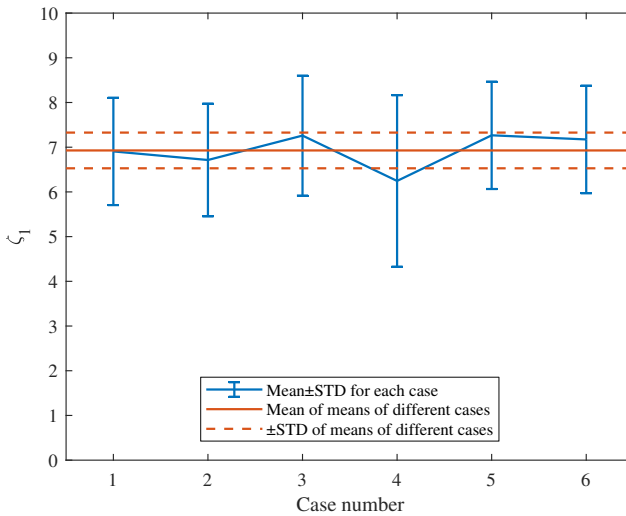


Figure 4.4: Variation of ζ_1 in each case and over different cases [35].

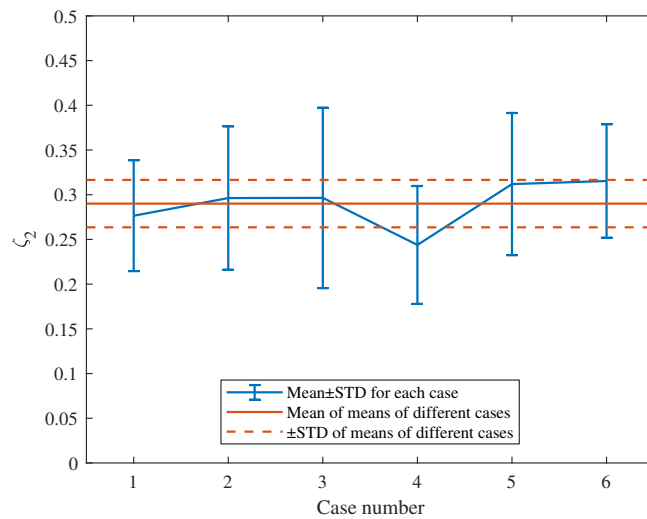


Figure 4.5: Variation of ζ_2 in each case and over different cases [35].

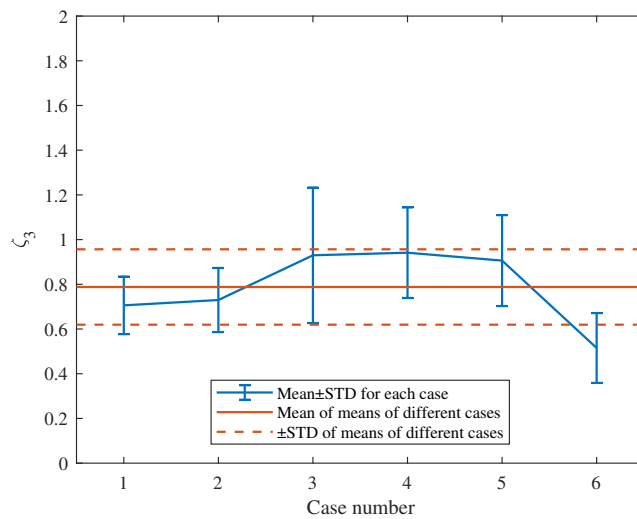


Figure 4.6: Variation of ζ_3 in each case and over different cases [35].

by averaging the means of each case, which leads to $\zeta_1 = 6.93$ with a 95% confidence interval of ± 0.32 and $\zeta_2 = 0.29$ with a 95% confidence interval of ± 0.02 .

From Fig. 4.6, it can be noticed that the variation of ζ_3 over different cases is comparable to the variation over different waves inside each case. The coefficients of variation of ζ_3 for the six cases range from 0.18 to 0.33, and the coefficient over the six cases is 0.21. So a constant value might not be representative enough for the peak force coefficient ζ_3 . Attempts have been made to figure out the relationship between ζ_3 and the wave parameters, such as wave height, wave elevation and deep water wave length, and their ratios. However, the values of ζ_3 are much more widely spread than the values of those parameters and ratios, which does not support an expression of ζ_3 in terms of the wave parameters. The reason for such widely spread ζ_3 values could be explained by the slightly shifted breaking point relative to the jacket model at each wave impact. Although the location of breaking is given for each test run, it is based on the visual estimation for the whole run, and it is not strictly controlled for each wave in such a shallow water breaking wave test with many nonlinearities involved. Even if a wave breaks just slightly before or after the plane of the front legs, the peak force reduces significantly, thus changing the value of ζ_3 also significantly.

Since peak force is a decisive parameter for an accurate estimation of the slamming force time series and the total impulse exerted by a wave on the structure, the peak force coefficient ζ_3 should be determined with a more reliable approach. The ζ_3 values of all the waves in all the test runs are sorted in a histogram in Fig. 4.7. The data are then fitted by various distributions, and a lognormal distribution function is found to give the best goodness of fit among the commonly used distribution functions. The fitted values for the two parameters are log location parameter $\mu_L = -0.4497$ and log scale parameter $\sigma_L = 0.3727$.

The cumulative distribution function of ζ_3 based on the original data is plotted together with the fitted lognormal distribution in Fig. 4.8. From this figure, we can see more clearly that the lognormal distribution fits the data very well in general, although slight overestimation and underestimation exist locally. Four representative quantiles of the cumulative distribution function and their corresponding ζ_3 values are marked in Fig. 4.8, and the ζ_3 values from the fitted distribution are compared to those from the original data in Table 4.1. Since the cumulative distribution function based on the original data is discrete, the smallest available value that is larger than the given quantile is used for the calculation of ζ_3 . In this way, ζ_3 can be well approximated when the number of data points at the quantile considered

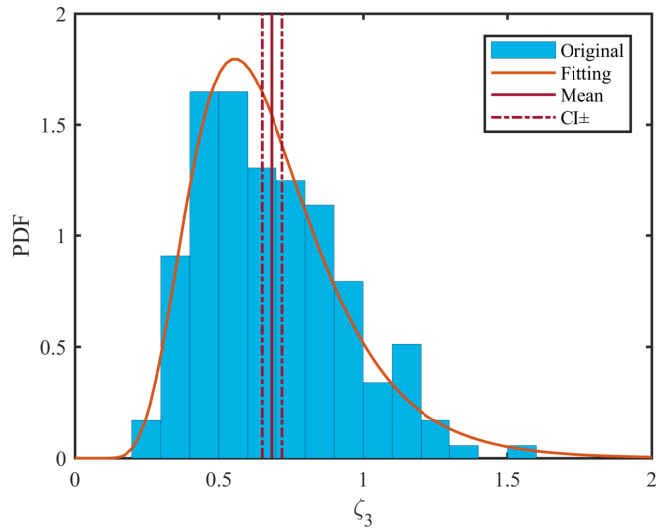


Figure 4.7: Statistical properties of ζ_3 , represented by histogram, distribution fitting by lognormal function, mean and confidence interval of the mean. The log location and log scale parameters of the lognormal distribution are -0.4497 and 0.3727 , respectively [35].

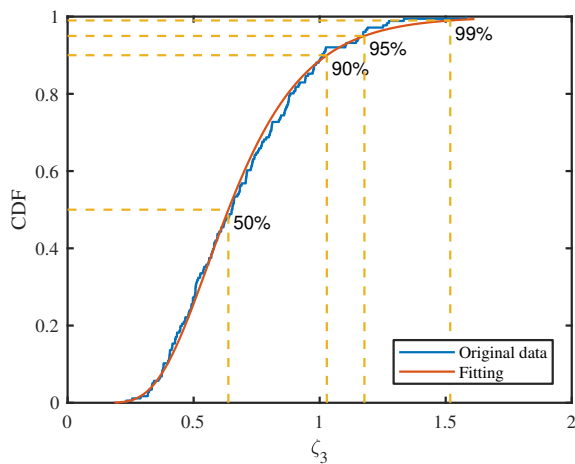


Figure 4.8: Cumulative distribution function of ζ_3 based on the original data and the fitted lognormal distribution. Four representative quantiles and corresponding ζ_3 values are marked for the fitted distribution by the yellow lines [35].

Table 4.1: Four representative quantiles and corresponding ζ_3 values estimated from the lognormal distribution and the original data [35].

| Quantile [%] | ζ_3 from fitted CDF | ζ_3 from original CDF | Relative difference [%] |
|--------------|---------------------------|-----------------------------|-------------------------|
| 50 | 0.638 | 0.651 | -2.00 |
| 90 | 1.028 | 1.009 | 1.88 |
| 95 | 1.178 | 1.172 | 0.51 |
| 99 | 1.518 | 1.334 | 13.79 |

is very large; while for large quantile (e.g. 99%) where less data points are available, the approximated ζ_3 is likely to have a large uncertainty. Therefore, the relative difference between the two cumulative distribution functions is larger for the quantile of 99% than for the rest in the table. In this study, we use $\zeta_3 = 1.178$, which corresponds to the quantile of 95%, as a representative value for the peak force coefficient, because the quantile is relatively large, and the difference between the fitted distribution and the original data is relatively small for this quantile. In the application of the model, the peak force coefficient ζ_3 can be calculated from the lognormal distribution, according to the quantile needed for the design. Now that ζ_1 , ζ_2 and ζ_3 have been determined, the wave-dependent parameters T , T_r and F_p of the force model can be calculated with Equations 4.4, 4.6 and 4.7, for a given structure and wave conditions. The global slamming force model is thus completely defined.

The developed model is then verified through comparisons between its predications and the representative force time series. The details of the verification is described in Paper 5.

4.2 Application of the model

Knowing the five parameters determined in Sections 4.1.1 and 4.1.2, the model of the global slamming force time series is completely defined. Once the site conditions and the structure properties are known, the force time series can be calculated. A flow chart as shown in Fig. 4.9 summarizes the procedure to get the global force time series by applying the model. Knowing site conditions, the wave parameters for the potential breaking waves are determined. Knowing both site conditions and structural properties, water depth d at the structure and the equivalent widths of the structure D_x and D_y are determined. The wave parameters and water depth are then used with suitable wave theories and breaking criteria to derive breaking wave celerity C_b and the maximum elevation of the breaking wave η_b . The determination of wave parameters and η_b for a given site condition and its

challenges are further addressed in Paper 5. Then, the parameters D_x , D_y , C_b and η_b are used together with the coefficients ζ_1 , ζ_2 and ζ_3 to calculate the wave-dependent parameters T , T_r and F_p . Finally, the wave-dependent parameters are used in the force model together with exponential parameters α_1 , α_2 to obtain the time series of the global slamming force $f(t)$.

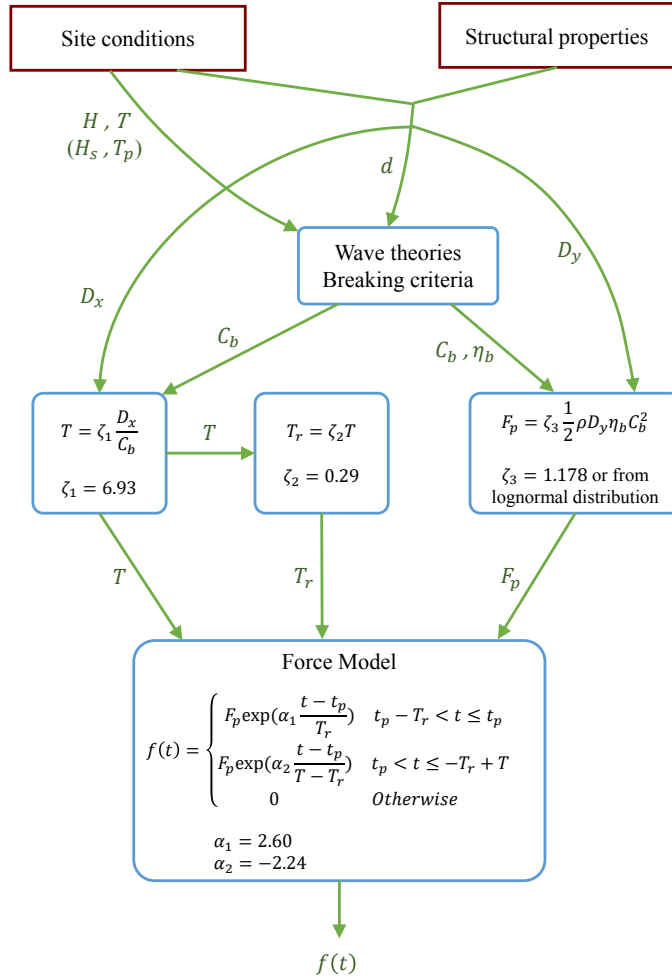


Figure 4.9: Application flow chart of the global slamming force time series model [35]. The parameters H , T (H_s , T_p) from the site conditions in this figure refer to (significant) wave height and (peak) period of a sea state.

Chapter 5

Slamming Loads in Offshore Wind Turbine Design

Knowing the slamming force model, such as the one proposed in Chapter 4, is an important prerequisite for applying slamming forces due to plunging breaking waves to the simulations of Offshore Wind Turbines (OWTs). However, this is only one part of the whole picture.

In this chapter, the major aspects regarding the application of slamming forces to OWT simulations are discussed. This topic is addressed in more detail in Paper 6. In addition, a machine learning approach is introduced to facilitate one of these important aspects: the detection of slamming events. The details of this topic are addressed in Paper 7.

5.1 Slamming load consideration in offshore wind turbine simulations

Three indispensable aspects should be considered for slamming load application to OWT simulations, i.e. how to detect a slamming event, how to calculate the slamming load and how to integrate it into fully coupled analysis. In each of these aspects, there are various issues that should be considered in more detail as shown in Fig. 5.1.

5.1.1 Detection of slamming events

The slamming load should only be considered when a slamming event occurs in the vicinity of OWT support structure. The slamming event here refers to the one caused by a plunging breaking wave. Therefore, for a given wave condition, a suitable breaking criterion should first be applied to judge

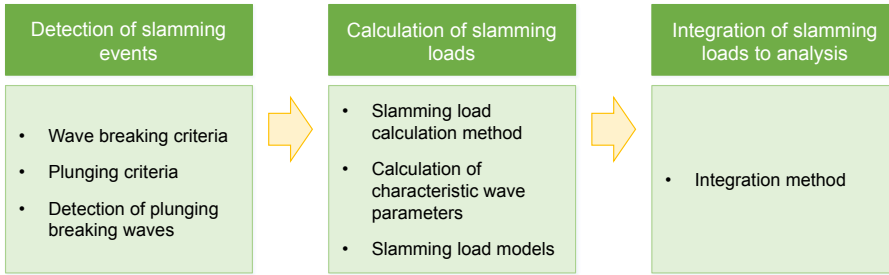


Figure 5.1: Three aspects involved in slamming load application to OWT simulations [12].

whether a wave breaks or not. If the wave indeed breaks, a suitable criterion to distinguish a plunging breaking wave from the other types should be applied. These criteria are commonly developed for regular waves, however, OWTs are usually exposed to irregular waves. Therefore, a suitable approach is required to detect the incidence of plunging breaking waves from large amounts of irregular waves.

5.1.2 Calculation of slamming loads

In order to calculate and to include the slamming loads in the general wave loads, both an engineering approach and a numerical approach can be used.

Based on Computational Fluid Dynamics (CFD), the numerical approach is able to model the interaction of the breaking waves with the structure [48, 49, 50, 51, 52, 53]. This approach costs tremendous simulation time. Therefore, it is not suitable to use this approach in the preliminary design phase of OWTs.

In an engineering approach, the slamming loads are calculated by employing a wave slamming force model. Some available slamming force models for cylindrical structures are listed in Table 1.1. The slamming force models typically feature a slamming coefficient and a certain force distribution pattern in space and in time. They also require certain characteristic wave parameters, for instance the wave celerity in the model by Wienke and Oumeraci [11]. It is very fast to estimate the slamming loads with the help of the force models, hence the engineering approach is a desirable way to integrate slamming loads into fully coupled analyses, which are typically conducted in the preliminary design phase of OWTs.

To estimate the characteristic wave parameters used in the slamming

force models, zero-crossing analysis of wave elevation time series is usually conducted [6, 54, 55]. It is also possible to improve the accuracy of the estimation by using advanced methods to further simulate the evolution of the likely breaking waves that are detected by the zero-crossing analysis [54, 55].

5.1.3 Integration of slamming loads in fully coupled analysis

In the design practice of OWTs, the effect of slamming loads should be assessed by integrated dynamic analysis, which is commonly based on the engineering approach. However, most fully coupled simulation tools for OWTs, such as FAST [56], HAWC2 [57], SIMO-RIFLEX-AeroDyn [58], BLADED [59], do not have the option to directly include the slamming loads. A possible way to consider the slamming loads in the existing tools without modifying the codes is to add the slamming load as an additional inertial or drag term in the Morison's equation [6, 60].

5.2 Plunging breaking wave detection with machine learning

As discussed in Section 5.1, detection of slamming events is an important aspect in the framework to apply slamming loads to OWT design. Only a specific type of breaking waves, the plunging type, leads to slamming forces. Therefore, a slamming event must fulfill both the breaking and plunging criteria. In practice, these criteria are limited to specific bathymetry, water depth and some other conditions, which makes it difficult to apply these criteria in general. For example, the most common way to detect plunging type breaking waves is through surf similarity parameters [61], in which the sea floor slope is an important parameter. This criterion is therefore not suitable for the detection of slamming events at a structure that is located on a flat sea bottom. Using an unsuitable plunging criterion or only breaking criterion may lead to an incorrect detection result.

Machine learning can be an alternative approach to attack the problem of plunging breaking wave detection at a specific site, since wave tests usually provide a large number of data that can be used for the training of a machine learning algorithm. Plunging breaking waves have an on/off feature, so plunging breaking wave detection is a typical binary classification problem in supervised machine learning.

The work flow of the machine learning approach for this problem is illustrated in Fig. 5.2. From the WaveSlam experimental data, 66 cases with

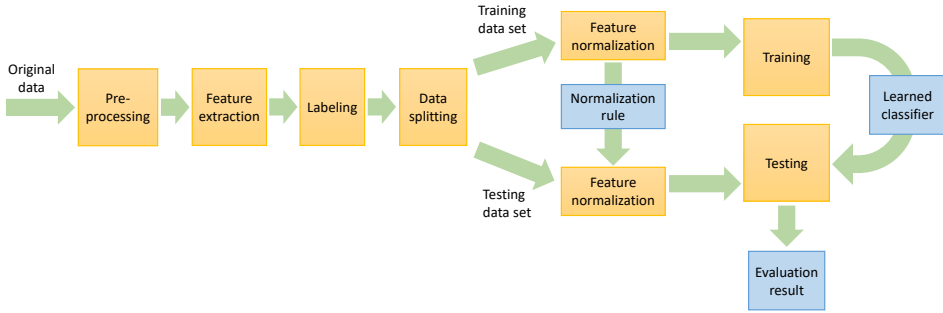


Figure 5.2: Work flow of detecting plunging breaking waves based on machine learning [62].

breaking or non-breaking waves were obtained. These data are divided into a training set (70%) and a testing set (30%). Features are extracted from the elevation time series of each wave, and each wave is labeled breaking (1) or non-breaking (0). A classifier is trained by using linear regression algorithm with the training data set.

The trained criterion for detecting plunging breaking waves is written as

$$1.337 \frac{\eta_p}{H} + \frac{H}{d} - 0.025 \sqrt{\frac{gT_p^2}{H}} - 1.227 \geq 0 \quad (5.1)$$

The parameter η_p denotes the wave elevation at the crest. The parameter T_p denotes wave period. This parameter is written as T_p , because the wave period is acquired from two neighboring peaks in the wave elevation time series. It is NOT the peak period of a wave spectrum. The parameter d denotes water depth; H denotes wave height; g denotes gravitational acceleration.

The performance of the trained classifier is compared to that of the classical McCowan breaking criterion [63] (i.e. $H/d \geq 0.78$) with respect to the testing data set. The comparison is given in Table 5.1. The precision of the breaking criterion is slightly higher than that of the trained classifier. However, the recall of the breaking criterion is lower by about 8%, which implies that a significant amount of breaking waves are not detected by the breaking criterion. The trained classifier has also a higher F_1 score (harmonic average of precision and recall) [64], a higher accuracy and thus a better performance than the McCowan breaking criterion in general.

Table 5.1: Evaluation of the result of plunging breaking wave detection using machine learning [62]. The result of McCowan breaking criterion [63] is acquired from the testing data set.

| | Training | Testing | McCowan criterion |
|----------------|----------|---------|-------------------|
| True positive | 1048 | 454 | 416 |
| False positive | 6 | 2 | 0 |
| False negative | 7 | 5 | 43 |
| True negative | 185 | 73 | 75 |
| Accuracy | 99.0% | 98.7% | 91.9% |
| Precision | 99.4% | 99.6% | 100.0% |
| Recall | 99.3% | 98.9% | 90.6% |
| F_1 score | 99.4% | 99.2% | 95.1% |

Chapter 6

Conclusions and Recommendations for Future Work

6.1 Conclusions

This study addresses the statistical characteristics of slamming forces on Offshore Wind Turbine (OWT) jacket substructures and develops a global slamming force model, based on the large-scale experimental data from the WaveSlam project.

The main contributions of the thesis are summarized as follows:

- **Inverse methods for slamming force estimation**

Three methods are developed to reconstruct slamming forces on the jacket model, including the optimization-based deconvolution (ODC), vertical approach and extended vertical approach. The vertical approach is based on linear regression, and it is verified by a comparison against the state-of-the-art horizontal approach that uses deconvolution techniques. The vertical approach is more robust and easier to use than the horizontal approach. The vertical approach can be applied to reconstruct the time series of both local and global slamming forces. The extended vertical approach can take the loads transferred among the transducers into account and reconstruct the local forces more accurately than the vertical approach.

- **Statistical characteristics of local slamming forces**

A plunging breaking wave impacts different locations on the braces

of the jacket model at different instants in a more or less random order. The time series of the local slamming forces on the braces are represented by two parameters: peak force and impulse. The variations of both parameters are significant for different waves in the same test run. However, the variations are not significant for different test runs under the same wave condition. The magnitude of the force is strongly dependent on the location. The upper locations on the braces bear higher slamming forces than the lower locations, and the variations of peak force and impulse are also higher at the upper locations, for the given wave condition.

- **Statistical characteristics of global slamming forces**

The time series of the global slamming forces are represented by six parameters: peak force, duration, impulse, rising time, left impulse and right impulse. Strong correlation is only found between impulse and right impulse. High variability of these parameters is observed for the given wave condition, which is controlled in the laboratory. The contribution of this variability to the uncertainties of the slamming forces has been mostly neglected in the literature. Yet, it is important according to the result of this statistical analysis.

- **Global slamming force model**

A global slamming force model is proposed based on the statistical analysis of the experimental data. The force model involves five parameters, including two exponential parameters (i.e. α_1 and α_2) and three dimensionless coefficients for the expressions of wave-dependent parameters (i.e. duration coefficient ζ_1 , rising time coefficient ζ_2 and peak force coefficient ζ_3). Statistical analysis reveals that α_1 , α_2 , ζ_1 and ζ_2 are approximately constant, while ζ_3 follows a lognormal distribution. Given a sea state, this force model provides a deterministic and conservative prediction of global slamming force time series, which inherently have random features.

- **Detection of plunging breaking waves**

A supervised machine learning approach is proposed as an alternative to breaking criteria for the detection of plunging breaking waves. A classifier is trained with wave elevation data by using logistic regression algorithm. The classifier consists of four parameters, i.e. water depth, wave height, crest height and wave period. Compared to the classical McCowan breaking wave criterion, the classifier has a better performance in detecting plunging breaking waves from the testing data set.

6.2 Recommendations for future work

The following topics are recommended for future work:

- The global slamming force model is developed in shallow water by using a jacket model with four legs and with waves coming from 0° . The application of the model to other jacket types or for waves coming from other directions or in intermediate water is not studied yet. Further studies are required to extend the applicability of this force model.
- Further investigations on the local slamming forces and potentially the development of a local slamming force model based on the proposed inverse methods and the force measurements by different transducers are suggested.
- The application of slamming forces to OWT simulations has been reviewed from an integrated perspective. Further investigations on the practical details are needed for the implementation of slamming forces in the integrated dynamic analysis of OWTs.
- It is worthy of studying how to employ the global slamming force model in probability-based design of OWT jacket substructures.
- The machine learning approach is only applied to regular waves for the detection of plunging breaking waves. It is more challenging but also more helpful to investigate how to apply the approach under irregular wave conditions.

References

- [1] Manwell JF, McGowan JG, Rogers AL. *Wind energy explained: theory, design and application*. John Wiley & Sons, 2010.
- [2] WindEurope Business Intelligence. Wind in power 2017, Annual combined onshore and offshore wind energy statistics. *Technical Report*, WindEurope 2018.
- [3] LEANWIND consortium. Driving cost reductions in offshore wind, the LEANWIND project final publication. *Technical Report* 2017.
- [4] Nghiem A, Pineda I. Wind energy in Europe: Scenarios for 2030. *Technical Report*, WindEurope 2017.
- [5] Stehly TJ, Heimiller DM, Scott GN. 2016 cost of wind energy review. *Technical Report*, National Renewable Energy Laboratory (NREL), Golden, CO (United States) 2017.
- [6] Hallowell S, Myers A, Arwade S. Variability of breaking wave characteristics and impact loads on offshore wind turbines supported by monopiles. *Wind Energy* 2016; **19**(2):301–312.
- [7] International Electrotechnical Commission (IEC). International standard 61400-3, wind turbines, part 3: Design requirements for offshore wind turbines 2009.
- [8] Det Norske Veritas (DNV). DNV-OS-J101, Offshore standard: Design of offshore wind turbine structures 2014.
- [9] GL Renewables Certification. Guideline for the certification of offshore wind turbines 2012.
- [10] Alagan Chella M, Tørum A, Myrhaug D. An overview of wave impact forces on offshore wind turbine substructures. *Energy Procedia* 2012; **20**:217–226.

-
- [11] Wienke J, Oumeraci H. Breaking wave impact force on a vertical and inclined slender pile - theoretical and large-scale model investigation. *Coastal Engineering* 2005; **52**:435–462.
- [12] Tu Y, Cheng Z, Muskulus M. A review of slamming load application to offshore wind turbines from an integrated perspective. *Energy Procedia* 2017; **137**:346–357.
- [13] Morison J, Johnson J, Schaaf S, *et al.*. The force exerted by surface waves on piles. *Journal of Petroleum Technology* 1950; **2**(05):149–154.
- [14] Von Karman T. The impact on seaplane floats during landing. *National Advisory Committee on Aeronautics* 1929; .
- [15] Wagner H. Über die entstehung des dynamischen auftriebes von tragflügeln. *ZAMM-Journal of Applied Mathematics and Mechanics/Zeitschrift für Angewandte Mathematik und Mechanik* 1925; **5**(1):17–35.
- [16] Perlin M, Choi W, Tian Z. Breaking waves in deep and intermediate waters. *Annual review of fluid mechanics* 2013; **45**:115–145.
- [17] Chan ES, Cheong HF, Tan BC. Laboratory study of plunging wave impacts on vertical cylinders. *Coastal Engineering* 1995; **25**(1-2):87–107.
- [18] Irschik K, Sparboom U, Oumeraci H. Breaking wave loads on a slender pile in shallow water. *Coastal Engineering 2004*, vol. 1, World Scientific, 2005; 568–580.
- [19] Sawaragi T, Nochino M. Impact forces of nearly breaking waves on a vertical circular cylinder. *Coastal Engineering in Japan* 1984; **27**(1):249–263.
- [20] Sarpkaya T, *et al.*. Wave impact loads on cylinders. *Society of Petroleum Engineers Journal* 1979; **19**(01):29–36.
- [21] Tanimoto K, Takahashi S, Kaneko T, Shiota K. Impulsive breaking wave forces on an inclined pile exerted by random waves. *Coastal Engineering Proceedings* 1986; **1**(20):2288–2302.
- [22] Ros Collados X. Impact forces on a vertical pile from plunging breaking waves. Master's Thesis, Norwegian University of Science and Technology, Trondheim, Norway 2011.

- [23] Peeringa JM, Hermans KW. Impact of new slamming wave design method on the structural dynamics of a classic, modern and future offshore wind turbine. *ASME 2017 36th International Conference on Ocean, Offshore and Arctic Engineering*, American Society of Mechanical Engineers, 2017.
- [24] Goda Y, Haranaka S, Kitahata M. Study on impulsive breaking wave forces on piles. *Report Port and Harbour Technical Research Institute* 1966; **6**(5):1–30.
- [25] Campbell I, Weynberg P. *Measurement of parameters affecting slamming*. University of Southampton, Department of Aeronautics and Astronautics, 1980.
- [26] Cointe R, Armand JL. Hydrodynamic impact analysis of a cylinder. *Journal of offshore mechanics and Arctic engineering* 1987; **109**(3):237–243.
- [27] Burmester S, de Ridder EJ, Wehmeyer C, Asp E, Gujer P. Comparing different approaches for calculating wave impacts on a monopile turbine foundation. *ASME 2017 36th International Conference on Ocean, Offshore and Arctic Engineering*, American Society of Mechanical Engineers, 2017.
- [28] WindEurope Business Intelligence. Offshore wind in Europe, Key trends and statistics 2017. *Technical Report*, WindEurope 2018.
- [29] Aashamar MZ. Wave slamming forces on truss support structures for wind turbines. Master's Thesis, Norwegian University of Science and Technology, Trondheim, Norway 2012.
- [30] Loukogeorgaki E, Lentsiou EN, Chatjigeorgiou IK, *et al.*. Experimental investigation of slamming loading on a three-legged jacket support structure of offshore wind turbines. *Proceedings of 26th International Ocean and Polar Engineering Conference*, International Society of Offshore and Polar Engineers: (Vol. 1, pp.192-198) Rhodes, Greece, 2016.
- [31] Arapogianni A, Genachte A, Ochagavia RM, Vergara J, Castell D, Tsouroukdissian AR, Korbijn J, Bolleman N, Huera-Huarte F, Schuon F, *et al.*. Deep water: The next step for offshore wind energy. *Report*, European Wind Energy Association (EWEA), Brussels, Belgium 2013.
- [32] Arntsen Ø, Obhrai C, Gudmestad O. Data storage report: wave slamming forces on truss structures in shallow water. *Technical Report*,

- WaveSlam (HylV-FZK-05)*, Norwegian University of Science and Technology 2013.
- [33] Tørum A. Wave slamming forces on truss structures in shallow water. *Technical report, version 2011-10-03*, Department of Civil and Transport Engineering, Norwegian University of Science and Technology 2011.
- [34] Rausa IE, Muskulus M, Arntsen ØA, Wåsjør K. Characterization of wave slamming forces for a truss structure within the framework of the WaveSlam project. *Energy Procedia* 2015; **80**:276–283.
- [35] Tu Y, Cheng Z, Muskulus M. A global slamming force model for offshore wind jacket structures. *Marine Structures* 2018; **60**:201 – 217.
- [36] Tu Y, Muskulus M. Statistical properties of local slamming forces on a jacket structure in offshore wind applications. *The 26th International Ocean and Polar Engineering Conference*, International Society of Offshore and Polar Engineers, 2016.
- [37] Cleveland WS. Robust locally weighted regression and smoothing scatterplots. *Journal of the American Statistical Association* 1979; **74**(368):829–836.
- [38] Sanchez J, Benaroya H. Review of Force Reconstruction Techniques. *Journal of Sound and Vibration* March 2014; **333**(14):2999–3018.
- [39] Tu Y, Muskulus M, Arntsen ØA. Experimental analysis of slamming load characteristics for truss structures in offshore wind applications. *Journal of Ocean and Wind Energy* 2015; **2**(3):138–145.
- [40] Clough RW, Penzien J. *Dynamics of structures*. McGraw-Hill, 1975.
- [41] Tu Y, Grindstad TC, Muskulus M. Inverse estimation of local slamming loads on a jacket structure. *Journal of Offshore Mechanics and Arctic Engineering* 2017; **139**(6):061601.
- [42] Sarkar T, Tseng F, Rao S, Dianat S, Hollmann B. Deconvolution of Impulse Response from Time-Limited Input and Output: Theory and Experiment. *Instrumentation and Measurement, IEEE Transactions on* December 1985; **IM-34**(4):541–546.
- [43] Jacquelin E, Bennani a, Hamelin P. Force Reconstruction: Analysis and Regularization of a Deconvolution Problem. *Journal of Sound and Vibration* May 2003; **265**:81–107.

- [44] Ekstrom M, Rhoads R. On the Application of Eigenvector Expansions to Numerical Deconvolution. *Journal of Computational Physics* March 1974; **14**(4):319–340.
- [45] Tu Y, Cheng Z, Muskulus M. Global slamming forces on jacket structures for offshore wind applications. *Marine Structures* 2018; **58**:53–72.
- [46] Bevington PR, Robinson DK. *Data reduction and error analysis for the physical sciences*. McGraw-Hill, 2003.
- [47] Mei CC, Stiassnie M, Yue DK. *Theory and applications of ocean surface waves: nonlinear aspects*. World Scientific, 2005.
- [48] Corte C, Grilli ST, *et al.*. Numerical modeling of extreme wave slamming on cylindrical offshore support structures. *The Sixteenth International Offshore and Polar Engineering Conference*, International Society of Offshore and Polar Engineers, 2006.
- [49] Alagan Chella M, Collados XR, Bihs H, Myrhaug D, Arntsen ØA. Numerical and experimental investigation of breaking wave interaction with a vertical slender cylinder. *Energy Procedia* 2016; **94**:443–451.
- [50] Bredmose H, Jacobsen NG. Vertical wave impacts on offshore wind turbine inspection platforms. *ASME 2011 30th International Conference on Ocean, Offshore and Arctic Engineering*, American Society of Mechanical Engineers, 2011; 645–654.
- [51] Christensen ED, Bredmose H, Hansen EA. Extreme wave forces and wave run-up on offshore wind turbine foundations. *Proceedings of Copenhagen Offshore Wind* 2005; :1–10.
- [52] Nielsen AW, Mortensen SB, Jacobsen V, Christensen ED. Numerical modelling of wave run-up on a wind turbine foundation. *ASME 2008 27th International Conference on Offshore Mechanics and Arctic Engineering*, American Society of Mechanical Engineers, 2008; 597–603.
- [53] Jose J, Choi SJ, Lee KH, Gudmestad OT, *et al.*. Breaking wave forces on an offshore wind turbine foundation (jacket type) in the shallow water. *The 26th International Ocean and Polar Engineering Conference*, International Society of Offshore and Polar Engineers, 2016.
- [54] Marino E, Borri C, Peil U. A fully nonlinear wave model to account for breaking wave impact loads on offshore wind turbines. *Journal of Wind Engineering and Industrial Aerodynamics* 2011; **99**(4):483–490.

-
- [55] Marino E, Borri C, Peil U. Offshore wind turbines: a wind-fully non-linear waves integrated model. *The Fifth International Symposium on Computational Wind Engineering (CWE2010)*, 2010.
- [56] Jonkman JM, Buhl Jr ML. FAST user's guide. *Technical Report*, National Renewable Energy Laboratory (NREL), Golden, CO (United States) 2005.
- [57] Larsen JT, Hansen MA. How 2 HAWC2, the user's manual. *Technical Report*, Risø National Laboratory, Technical University of Denmark, Roskilde, Denmark 2015.
- [58] Ormberg H, Bachynski EE. Global analysis of floating wind turbines: Code development, model sensitivity and benchmark study. *The 22nd International Offshore and Polar Engineering Conference*, International Society of Offshore and Polar Engineers, 2012.
- [59] Garrad Hassan. Bladed user manual. *Technical Report*, Garrad Hassan and Partners Limited Document 2013.
- [60] Marino E. An integrated nonlinear wind-waves model for offshore wind turbines. PhD Thesis, University of Florence, Firenze, Italy 2011.
- [61] Iribarren Cavanilles R, Casto Nogales M. Protection des ports. *17th Int. Navigation Congress* 1949; **2**:31–80.
- [62] Tu Y, Cheng Z, Muskulus M. Detection of plunging breaking waves based on machine learning. *ASME 2018 37th International Conference on Ocean, Offshore and Arctic Engineering*, American Society of Mechanical Engineers, 2018.
- [63] McCowan J. On the highest wave of permanent type. *Philosophical Magazine Series 5* 1894; **38**(233):351–358.
- [64] Powers DM. Evaluation: from precision, recall and F-measure to ROC, informedness, markedness and correlation. *Journal of machine learning technologies* 2011; **2**(1):37–63.

Appendix A

Appended Papers

A.1 Paper 1

Paper 1:

Tu Y, Muskulus M, Arntsen ØA. Experimental analysis of slamming load characteristics for truss structures in offshore wind applications. *Journal of Ocean and Wind Energy* 2015; **2**(3):138-145. <http://dx.doi.org/10.17736/jowe.2015.jcr32>

Is not included due to copyright

A.2 Paper 2

Paper 2:

Tu Y, Grindstad TC, Muskulus M. Inverse estimation of local slamming loads on a jacket structure. *Journal of Offshore Mechanics and Arctic Engineering* 2017; **139**(6):061601. <http://dx.doi.org/10.1115/1.4037175>

Is not included due to copyright

A.3 Paper 3

Paper 3:

Tu Y, Muskulus M. Statistical properties of local slamming forces on a jacket structure in offshore wind applications. *The 26th International Ocean and Polar Engineering Conference*, International Society of Offshore and Polar Engineers, 2016.

Is not included due to copyright

A.4 Paper 4

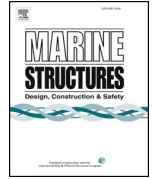
Paper 4:

Tu Y, Cheng Z, Muskulus M. Global slamming forces on jacket structures for offshore wind applications. *Marine Structures* 2018; **58**:53-72. <https://doi.org/10.1016/j.marstruc.2017.11.001>



Contents lists available at ScienceDirect

Marine Structures

journal homepage: www.elsevier.com/locate/marstruc

Global slamming forces on jacket structures for offshore wind applications

Ying Tu^a, Zhengshun Cheng^{b,*}, Michael Muskulus^a

^a Department of Civil and Environmental Engineering, Norwegian University of Science and Technology, Høgskoleringen 7A, 7491 Trondheim, Norway

^b Department of Marine Technology, Centre for Autonomous Marine Operations and Systems, Norwegian University of Science and Technology, Otto Nielsens veg 10, 7491 Trondheim, Norway

ARTICLE INFO

Keywords:

Wave slamming force
Jacket structure
Experimental study
Statistical analysis
Slamming coefficient
Force model
Plunging breaking wave

ABSTRACT

This study investigates the global slamming forces due to plunging breaking waves on a jacket structure, based on the statistical analysis of the experimental data from the WaveSlam project. Hammer tests and wave tests were conducted in the project, and the data are used to reconstruct the time series of the global slamming force by employing a method based on linear regression. The used wave test data were acquired under one wave condition. A total of 3910 force time series are reconstructed and analyzed statistically to reveal the characteristics of the slamming force. For each force time series, six parameters are introduced to describe it, including the peak force, duration, impulse and rising time, etc. The variability and correlation of these parameters are investigated. The distribution of these parameters is modeled with various probability distributions. The results show the high variability of the slamming force and the importance of statistical analyses. Based on these statistical analyses, the slamming coefficient is estimated from the peak force. For a curling factor of 0.4, the mean slamming coefficient is about 1.29. When considering one standard deviation around the mean, the slamming coefficient varies from 0.70 to 6.78 for a curling factor ranging from 0.1 to 0.5. A representative time series of wave slamming force is obtained by averaging the individual force time series. Accordingly, a 3-parameter triangular force model and a 5-parameter exponential force model are proposed to describe the development of the slamming force in time.

1. Introduction

Currently, the substructures supporting offshore wind turbines are usually bottom-fixed structures, such as monopiles, tripods, jackets, gravity based structures, etc. In certain sea environments, they are exposed to plunging breaking waves at some locations, which leads to slamming forces. Such kind of slamming forces have been identified based on the recorded sea state conditions and associated structural responses for a 2 MW wind turbine mounted on a monopile at the Blyth wind farm off the coast of England [1]. Slamming forces can affect the performance and fatigue life of the substructures for offshore wind turbines. They should therefore be considered in the design of offshore wind turbines, as recommended by various standards and guidelines [2–4].

Slamming is a strongly nonlinear phenomenon that usually causes an extremely high impact force within a very short time [5,6]. In the past decades, a large amount of efforts have been devoted to investigate slamming forces theoretically, numerically and experimentally. Theoretical analysis is usually based on the von Karman or the Wagner impact model together with several reasonable assumptions [5,7], and numerical studies on slamming forces use Computational Fluid Dynamics (CFD), considering either

* Corresponding author.

E-mail address: zhengshun.cheng@ntnu.no (Z. Cheng).

inviscid or viscid flows [6,8]. Due to the strong nonlinearities of slamming forces, small-scale experiments or full-scale field measurements seem to be the most reliable method to quantify them. To date, several experimental studies of slamming forces on vertical or inclined slender cylindrical structures have been carried out [9–11]. An on-site measurement regarding the slamming loads has also been conducted for a monopile wind turbine at the Blyth wind farm [1].

Most of the aforementioned studies on slamming forces are with respect to slender cylindrical structures, and the results can be used for the design of monopiles. Truss structures, such as jackets, are also a promising support structure concept for offshore wind turbines, especially in intermediate water. Because of the presence of several legs and braces, the waves approaching the hind legs and braces are affected by the front ones. This will result in a more complicated slamming scenario than that of the monopiles. Nevertheless, investigations of the slamming forces on jacket structures are still limited in number to date. The WaveSlam project¹ was initiated to bridge this knowledge gap. Using a 1:8 model of a jacket structure typical for offshore wind applications, the project is the first one at this scale and for this kind of structures.

Several other studies have been conducted to investigate the slamming forces on jacket structures based on the experimental data from the WaveSlam project. Rausa et al. [12] studied breaking wave forces on the front bracings of the jacket structure with a finite element model by assuming a triangular time history of wave slamming forces. A fitting procedure was then applied to match the result from the finite element model with the experimental data. Tu et al. [13] investigated the slamming loads on the bracings of the jacket structure based on local force data. An optimization-based deconvolution (ODC) method, which used the linearity of the structure, was proposed for the estimation. However, the methods used in these studies are only able to calculate the peak forces based on additional assumptions (e.g. assuming a triangular shape force model, which is not validated) or the impulses of the loads. The time series of the forces, which are necessary for the force analysis, were not resolved.

To obtain the time series of wave slamming forces, Jose et al. [14] applied Empirical Mode Decomposition (EMD) to analyze the total slamming force and the Frequency Response Function method to analyze the local slamming force on the jacket structure. Tu et al. [15] employed the regularization method, which is a classical inverse method, to develop two approaches for the reconstruction of the local slamming force time series. The method by Tu et al. [15] takes the structure property into consideration and can provide an easily applicable solution for the inverse estimation of slamming loads.

In this study, the slamming force estimation method proposed by Tu et al. [15] was further applied to reconstruct the global slamming force time series using the data set from the WaveSlam project. Six parameters were introduced to describe the global slamming force time series, such as the peak force, duration, total impulse, etc. The variation, correlation and distribution features of these parameters were investigated to reveal the characteristics of the global slamming force under one wave condition. A representative slamming force time history and the slamming coefficient were then estimated. Based on the representative time history, two slamming force models are proposed, which provide potential means to properly account for slamming forces in the future design of jacket structures.

2. Experiment and data

WaveSlam is a research project that aims to improve the method for calculating forces from plunging breaking waves on jacket structures through model tests on a large scale [16]. The project was conducted by a consortium headed by the University of Stavanger (UiS) and the Norwegian University of Science and Technology (NTNU) in 2012–2013. The jacket model used in the experiment was similar to the structure designed by Reinertsen AS for the Thornton Bank offshore wind farm [17]. Following the earlier small scale (1:50) model tests at NTNU [18], a 1:8 scale model of the jacket structure was constructed, and the experiment was carried out in summer 2013 using the Large Wave Flume facilities at the Coastal Research Centre (Forschungszentrum Küste, FZK)², Hannover, Germany. The data is now publicly available.

2.1. Experimental setup

The setup of the experiment is demonstrated in Fig. 1. The wave flume is approximately 300 m long, 5 m wide and 7 m deep. The waves were generated by the wave board at the left end of the flume, went over a 1:10 slope, then reached the jacket model on a 2.3 m high plateau. A water depth of 16 m was simulated, but the water depth at the jacket model was adjusted slightly to be 1.8 m (instead of 2.0 m) for some test cases. The legs and braces of the jacket model were both 0.14 m in diameter.

A global coordinate system is defined as following: The origin is at the center of the wave board and at the bottom of the wave flume. The x-axis is positive in the wave direction. The z-axis is positive upwards. The y-axis forms a right hand system with the other axes.

Wave gauges were installed at 15 different locations. Three Acoustic Doppler Velocity meters (ADV) were installed in the plane of the legs. The motion of the wave paddle was also recorded. The jacket was equipped with four total force transducers, ten local force transducers on the legs, twelve XY force transducers on the braces, and four one-directional accelerometers.

The measurements taken by the total force transducers are essential in this study to investigate the global slamming forces. As shown in Fig. 2, there were two total force transducers installed at the top of the jacket model and two installed at the bottom of the jacket model. The structure was hung from the top and did not touch the ground during the tests. The measured forces are in global x

¹ <http://hydralab.eu/research-results/ta-projects/project/19/>; December 2016.

² <https://www.fzk.uni-hannover.de/>; December 2016.

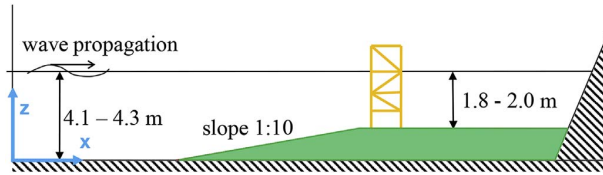


Fig. 1. Experimental setup and global coordinates.

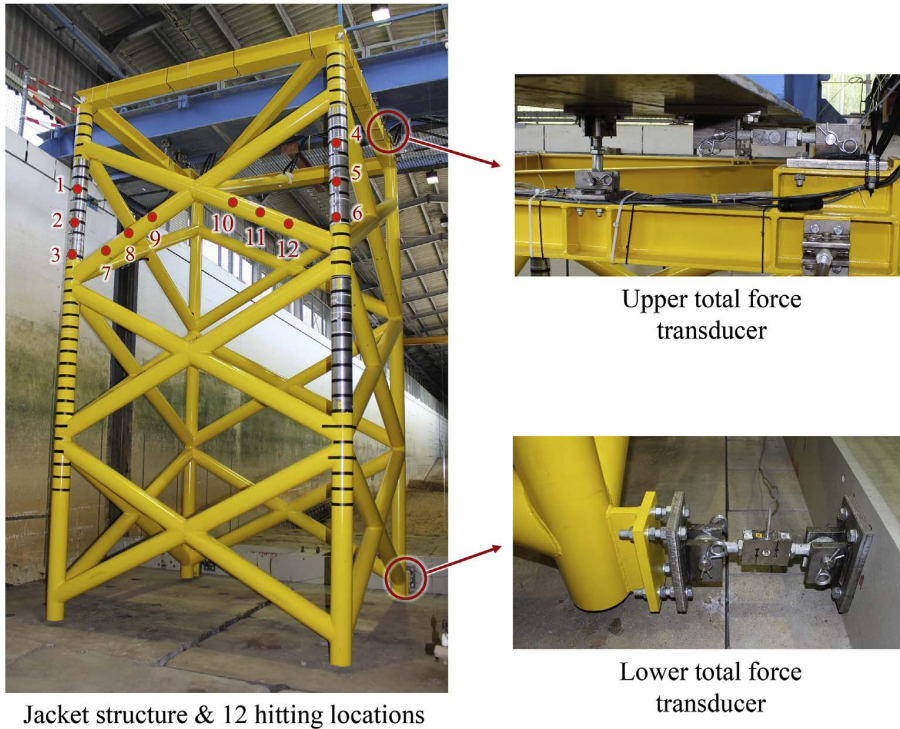


Fig. 2. Jacket structure, hammer hitting locations and total force transducers. Figures reprinted with permission from the WaveSlam project.

direction (wave direction) and have a sampling frequency of 10 kHz. The details of the transducers are illustrated in the figure as well. The names and locations of the transducers are introduced in Table 1. The local force measurements are not used in this study, so the locations of those transducers are not shown in the figure.

2.2. Wave test cases

Five wave cases repeated with exactly the same preset condition were selected for the investigation. The cases and the test condition are shown in Table 2. The waves are regular shallow water plunging breaking waves. The break points of the waves are approximately in the plane of the front legs of the jacket. The wave heights at the structure were taken from the measurement, so the values are slightly different from case to case.

Table 1
Total force transducers and their locations in global coordinates.

| Transducer | Description | x [m] | y [m] | z [m] |
|------------|--------------------------|---------|-------|-------|
| FTTF01 | Total force bottom south | 200.961 | 1.405 | 2.465 |
| FTTF02 | Total force top south | 200.265 | 1.405 | 6.935 |
| FTTF03 | Total force bottom north | 200.961 | 3.655 | 2.465 |
| FTTF04 | Total force top north | 200.265 | 3.655 | 6.935 |

Table 2
Wave test cases.

| Condition | Value |
|--------------------------|------------------|
| ID of test run | 20130617.15 ~ 19 |
| Number of runs | 5 |
| Number of waves per run | 20 |
| Wave height | 1.5 m |
| Wave height at structure | 1.809 ~ 1.833 m |
| Wave period | 4.9 s |
| Depth | 4.3 m |
| Depth at structure | 2.0 m |
| Run type | Regular |
| Breaking location | At front legs |

2.3. Hammer test cases

Apart from the wave test data, hammer test data are also essential to reconstruct the slamming forces. During the hammer tests, the structure was hit by a 1.5 kg impulse hammer in the wave direction. The impulse hammer recorded the time series of the forces exerted on the structure with a sampling frequency of 9600Hz, in addition to the measurements mentioned in Section 2.1. The selected hammer test cases shown in Table 3 were all carried out in water. The water depth was 2 m to match the wave cases. The hammer hit at twelve locations in the front side of the structure, both on the braces and on the legs. These locations (see Fig. 2) are in or close to the expected wave slamming zone for the wave tests. Since the hammer impacts were exerted manually, the locations shown in the figure are approximate. Data for different number of hits are available for different locations as shown in Table 3.

3. Calculation of wave slamming forces

3.1. Pre-processing of the data

Given the raw measurement data, some pre-processing is necessary before they can be used to calculate the slamming forces. A bandpass filter was used to eliminate the high frequency noise in the measurements and to only preserve the signal from 0 to 300Hz. The effect of the filtering is shown in Fig. 3. Since the transducers were not always precisely calibrated to zero before each test, the measured forces were subtracted by the mean values of the measurement over some seconds at calm status in the same run. The forces measured by the four transducers were summed up to obtain the total forces as shown in Fig. 4. The first natural frequency of the jacket structure in water is determined by spectral analysis of the hammer response data, the value of which is 25.2 Hz. The impulse hammer measurements were resampled to 10 kHz to match the total force measurements.

The force exerted by a breaking wave on a structure is composed of two parts: a quasi-static force $f_{qs}(t)$ and an impact force by the breaker, namely the slamming force $f_s(t)$. Therefore, a measured response force due to this wave also has two parts: a quasi-static part caused by $f_{qs}(t)$ and a dynamic part caused by $f_s(t)$. The dynamic part should be extracted, so that it can be used to reconstruct the slamming force.

Two common methods to achieve this goal are frequency domain filtering and Empirical Mode Decomposition (EMD) combined with filtering [10]. However, these methods overestimate the quasi-static part in the region of the maximum load [10], thus leading to underestimation of the dynamic part.

A time domain robust LOESS smoother [19] is used in this study to estimate the quasi-static part. The dynamic part equals the total response force minus the quasi-static part. The smoothing method is realized by local regression using weighted linear least squares and a 2nd degree polynomial model. The method assigns zero weight to the data outside six mean absolute deviations. The

Table 3
Hammer test cases.

| Hit location number | Total hammer hits | ID of test run |
|---------------------|-------------------|------------------|
| 1 | 6 | 24062013.14 ~ 16 |
| 2 | 4 | 24062013.17 ~ 18 |
| 3 | 4 | 24062013.22 ~ 23 |
| 4 | 6 | 24062013.31 ~ 33 |
| 5 | 8 | 24062013.34 ~ 37 |
| 6 | 6 | 24062013.38 ~ 40 |
| 7 | 2 | 24062013.24 |
| 8 | 2 | 24062013.25 |
| 9 | 2 | 24062013.26 |
| 10 | 2 | 24062013.27 |
| 11 | 2 | 24062013.28 |
| 12 | 2 | 24062013.30 |

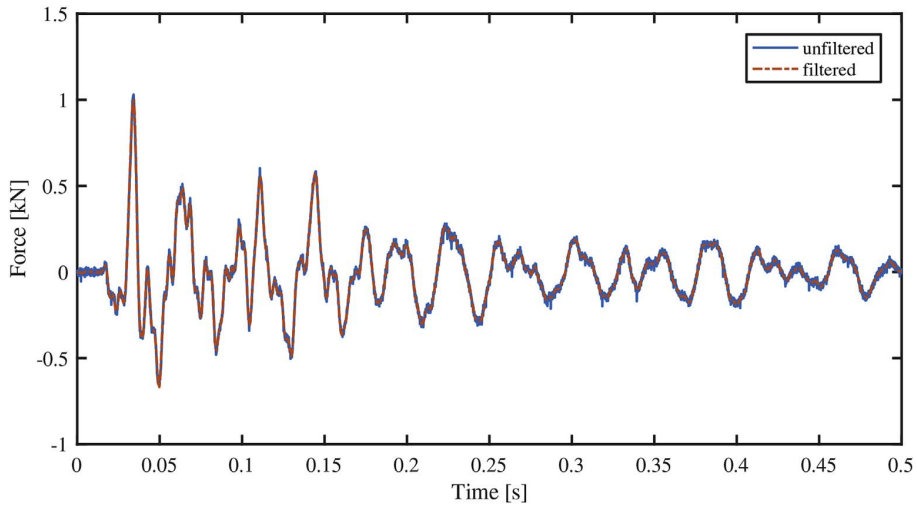


Fig. 3. Comparison of unfiltered and filtered forces measured by one transducer.

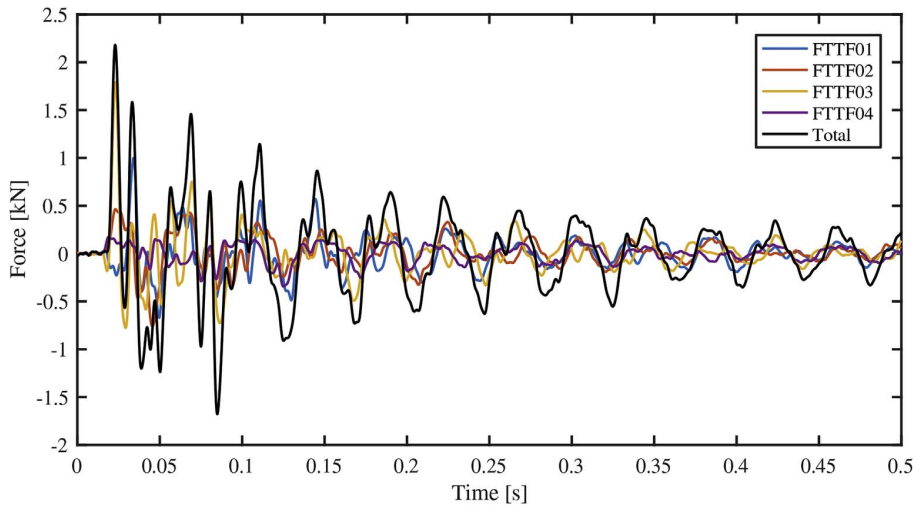


Fig. 4. Summation of the forces measured by four transducers.

smoothing span is set to be 5% of the total number of data points.

Fig. 5 shows one example where the method is applied. The response force has two peaks, because the wave hit the structure first on the front side and then again on the back side in the experiment. Only the first peak is used in this study, since the waves broke at the front legs. The general trend of the quasi-static part is captured very well by the method. There is no significant overestimation of the quasi-static part around the first peak, because the data points in this region are considered as outliers, and zero weight is assigned to them. For the second peak, the response force is caused by a mixture of two impacts and the separation may be inaccurate, but since we only focus on the first peak, it is not very important to have a precise separation after that.

3.2. Reconstruction of wave slamming forces

The idea of reconstructing wave slamming forces is to use the available response forces of the structure measured in the wave tests, and both the impact forces and response forces measured in the hammer tests to calculate the wave impact forces. This is an inverse problem and in general ill-defined. Therefore, additional assumptions must be made.

Ideally, a reference impact test that covers the whole wave slamming area would be most helpful for the reconstruction. In practice, the hammer tests could only be done for twelve discrete locations. Therefore, each response force from the wave test is combined with hammer test data from different hits at different locations for the reconstruction. The reconstructed forces are

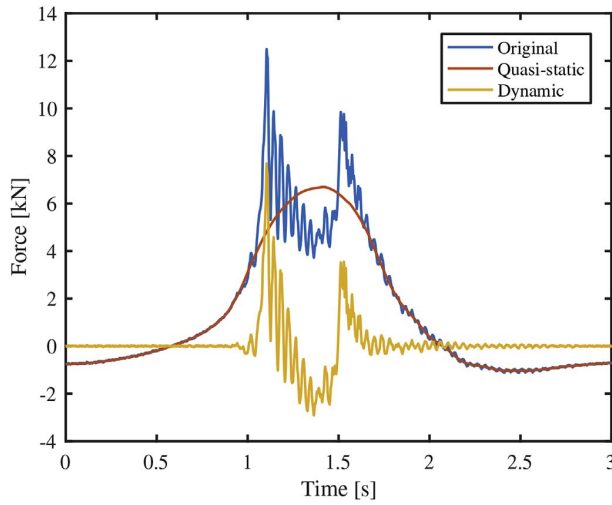


Fig. 5. Separation of quasi-static and dynamic parts in a total response force.

“effective forces”, which means that the wave slam is assumed to occur only on the corresponding hammer impact location. The result obtained by using all such “wave-hammer data pairs” is analyzed further in later sections.

The hammer test data used for force reconstruction were acquired from the experiment with the structure in water. However, the change of water depth due to the existence of waves is not taken into account, due to the limitation of the data. The reconstruction inherently includes hydroelastic effects, since it employs experimental data that includes such effects. Loads on an ideal, rigid jacket structure are expected to be somewhat different. The structure model in the experiment has a high first eigenfrequency, which is not far from the frequency of typical slamming excitations. The hydroelastic effect caused thereby is expected to be stronger than that for a normal full-scale wind turbine jacket under slamming loads.

The wave test and hammer test data used for reconstruction have all been pre-processed according to Section 3.1. The reconstructed slamming forces are only in the wave direction due to the data properties.

For each wave-hammer data pair, the force reconstruction method proposed in Tu et al. [15] is used. It makes use of the linearity of the structure as discussed in Tu et al. [13].

The basic principle of the method is demonstrated in Fig. 6.

A wave slam on the structure is imagined as a hammer hitting one location on the structure with different amplitudes for multiple times.

Step 1 Knowing the response forces from one wave slam and from one hammer impact, the wave response force is decomposed into multiple hammer response forces scaled by corresponding coefficients.

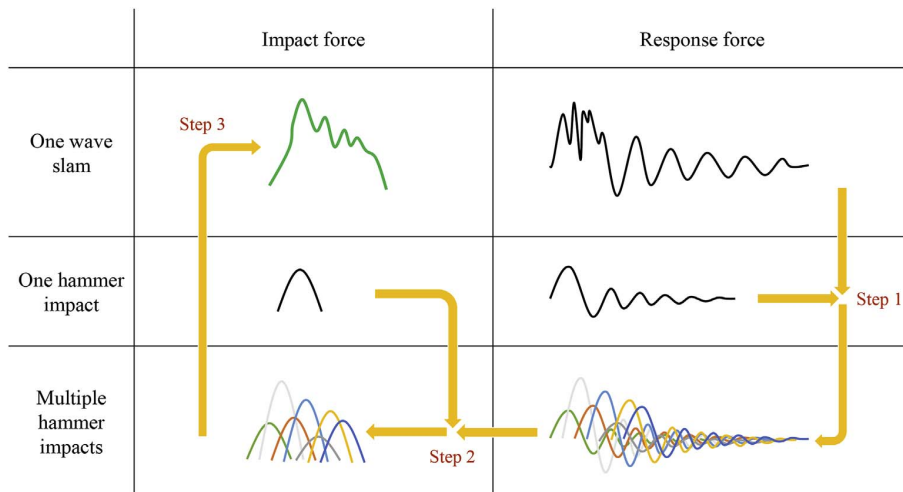


Fig. 6. Illustration of the force reconstruction method.

Step 2 Each hammer response force corresponds to one hammer impact force. So, the hammer impact forces, corresponding to the hammer response forces obtained from Step 1, are determined by using the same coefficients.

Step 3 Summing up the multiple hammer impact forces, the impact force from one wave slam is acquired.

For more detailed explanation, the wave slamming force is written as a vector

$$\mathbf{f}_W = (f_{W_1} \ f_{W_2} \ f_{W_3} \ \cdots \ f_{W_n})^T \tag{1}$$

It can be expressed as

$$\mathbf{f}_W = \mathbf{F}_H \boldsymbol{\beta} \tag{2}$$

where

$$\mathbf{F}_H = \begin{pmatrix} f_{H_1} & 0 & \cdots & 0 \\ \vdots & \vdots & \ddots & \vdots \\ f_{H_\delta} & 0 & \ddots & 0 \\ f_{H_{\delta+1}} & f_{H_1} & \ddots & 0 \\ \vdots & \vdots & \ddots & \vdots \\ f_{H_{(p-1)\delta}} & f_{H_{(p-2)\delta}} & \ddots & 0 \\ f_{H_{(p-1)\delta+1}} & f_{H_{(p-2)\delta+1}} & \ddots & f_{H_1} \\ \vdots & \vdots & \ddots & \vdots \\ f_{H_n} & f_{H_{n-\delta}} & \cdots & f_{H_{n-(p-1)\delta}} \end{pmatrix} \tag{3}$$

is composed of column vectors representing repeated and shifted hammer impact forces. The symbol p denotes the total number of hypothetical hammer hits. The symbol δ denotes the interval between every two hammer hits, and is named *step factor*. The step factor is set to be 5 for most cases, according to Tu et al. [15].

The coefficients

$$\boldsymbol{\beta} = (\beta_1 \ \beta_2 \ \beta_3 \ \cdots \ \beta_p)^T \tag{4}$$

are given as a parameter vector for scaling the hammer hits.

The wave response force is written as

$$\mathbf{r}_W = (r_{W_1} \ r_{W_2} \ r_{W_3} \ \cdots \ r_{W_n})^T \tag{5}$$

It can be expressed as

$$\mathbf{r}_W = \mathbf{R}_H \boldsymbol{\beta} + \mathbf{e} \tag{6}$$

where

$$\mathbf{R}_H = \begin{pmatrix} r_{H_1} & 0 & \cdots & 0 \\ \vdots & \vdots & \ddots & \vdots \\ r_{H_\delta} & 0 & \ddots & 0 \\ r_{H_{\delta+1}} & r_{H_1} & \ddots & 0 \\ \vdots & \vdots & \ddots & \vdots \\ r_{H_{(p-1)\delta}} & r_{H_{(p-2)\delta}} & \ddots & 0 \\ r_{H_{(p-1)\delta+1}} & r_{H_{(p-2)\delta+1}} & \ddots & r_{H_1} \\ \vdots & \vdots & \ddots & \vdots \\ r_{H_n} & r_{H_{n-\delta}} & \cdots & r_{H_{n-(p-1)\delta}} \end{pmatrix} \tag{7}$$

is composed of column vectors representing repeated and shifted hammer response forces, and

$$\mathbf{e} = (e_1 \ e_2 \ e_3 \ \cdots \ e_n)^T \tag{8}$$

is an error term due to the noise in the measurements.

An ordinary least squares regression technique is used to solve for the parameter vector $\boldsymbol{\beta}$ based on Eq. (6), so the estimated parameter vector is

$$\hat{\boldsymbol{\beta}} = (\mathbf{R}_H^T \mathbf{R}_H)^{-1} \mathbf{R}_H^T \mathbf{r}_W \tag{9}$$

Applying $\hat{\boldsymbol{\beta}}$ to Eq. (2), the wave slamming force is estimated as

$$\hat{\mathbf{f}}_W = \mathbf{F}_H \hat{\boldsymbol{\beta}} \tag{10}$$

Applying $\hat{\boldsymbol{\beta}}$ to Eq. (6), the wave response force can be recalculated as

$$\hat{\mathbf{r}}_W = \mathbf{R}_H \hat{\boldsymbol{\beta}} \tag{11}$$

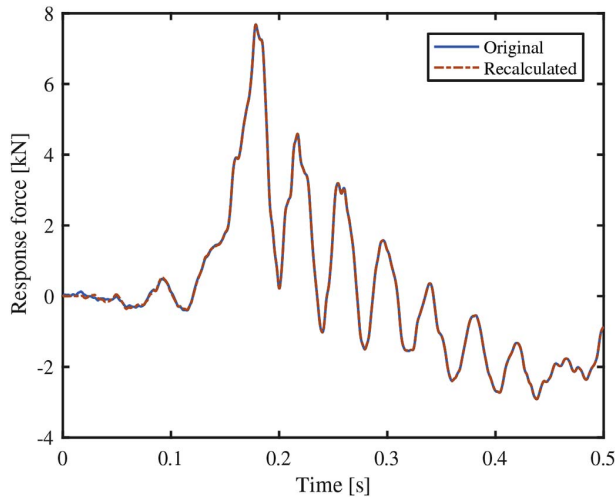


Fig. 7. Comparison of original and recalculated response forces.

A exemplary comparison between an original wave response force and the corresponding recalculated wave response force is shown in Fig. 7. Since the response forces match well, the estimated $\hat{\beta}$ is deemed to be an appropriate representation of the slamming event. Using this $\hat{\beta}$, the corresponding wave slamming force is estimated and shown in Fig. 8.

4. Statistical analysis of wave slamming forces

Using different combinations of the wave test data and the hammer test data described in Section 2, the wave slamming forces were reconstructed following the methods described in Section 3.

As stated in Section 2.2, the used wave test data were acquired from 5 runs with 20 waves in each run under the same preset conditions. Even under the same conditions, the waves in the tests were not exactly the same. Fig. 9 and Fig. 10 illustrate how the wave height and the wave period vary in the tests. The difference in the slamming forces is expected to be partially caused by the difference in the waves, as shown in the figures.

The difference in the waves is also reflected in the measured response forces. The 1st waves in each run led to very low dynamic response forces, which implies that the waves were not broken at the structure as expected. The 2nd and 20th waves led to very unstable results due to the transient status of the starting and the ending of the test runs. Although the wave periods of the 18th wave and the 19th wave are higher than those of the other waves, there is no obvious effect on the response forces.

As long as the wave response forces are valid, more data points lead to a more informative statistical analysis, so the response forces from the 3rd to 19th waves in each run were used for the slamming force reconstruction. The data from each of the 46 hammer

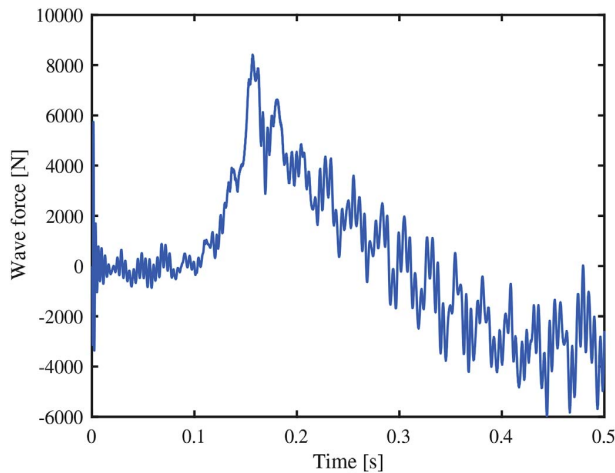


Fig. 8. Estimated wave slamming force.

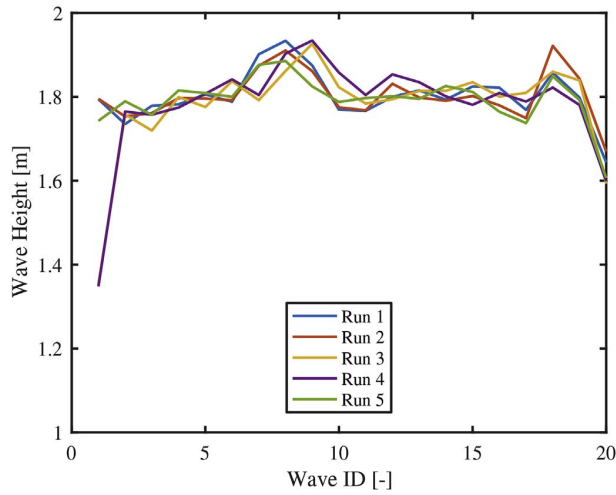


Fig. 9. Wave height variation over different runs and waves.

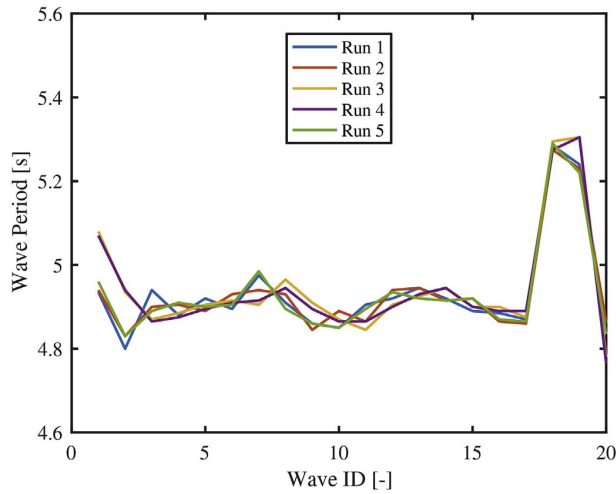


Fig. 10. Wave period variation over different runs and waves.

hits (see Table 3) were combined with the response force from each used wave for reconstructing the slamming force independently – the resulting forces are then averaged, as explained in Section 4.1.2. All together $46 \text{ (hits)} \times 5 \text{ (runs)} \times 17 \text{ (waves)} = 3910$ time series of the slamming forces were reconstructed. Statistical analysis is conducted for these slamming forces in this section, to better understand the variability of the estimated forces.

4.1. Analysis methods

Two basic methods used for the analysis are introduced, namely parametrization and multi-level analysis. Parametrization enables a statistical analysis of the slamming forces by using representative parameters that describe the main features of the force time series. Multi-level analysis is then used to average the results at various steps in the analysis, depending on which source of variability is investigated.

4.1.1. Parametrization

Since a large number of time series cannot be compared and analyzed directly, six parameters are assigned to each time series to describe the slamming forces, as illustrated in Fig. 11.

- F_p : Peak force, the maximum force in the time series.

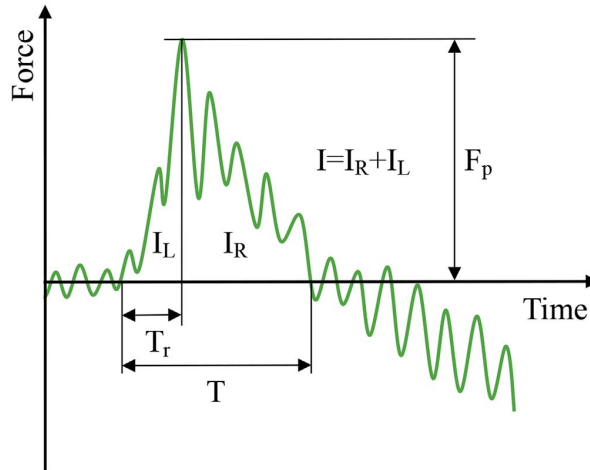


Fig. 11. Parameters to describe one wave slamming force time series. The variation of the time series has been exaggerated for visualization purposes.

- T : Duration, the time between the last zero-up-crossing before the peak and the first zero-down-crossing after the peak.
- T_r : Rising time, the time between the last zero-up-crossing before the peak and the peak itself.
- I : Impulse, the integral of the force over the duration.
- I_L : Left impulse, the integral of the force over the rising time.
- I_R : Right impulse, the integral of the force over the time between the peak and the first zero-down-crossing after the peak.

4.1.2. Multi-level analysis

The reconstructed slamming forces are organized according to the data hierarchy, as shown in Fig. 12. The total result is composed of the result calculated from 5×17 wave response forces. The result from each wave response force is composed of the results from hammer test data at 12 locations. The result from each hammer test location is composed of the results from different hits.

For the analysis in Section 4.2, averaging at three levels is introduced. The symbol X represents an arbitrary parameter describing the slamming force. The subscripts h, l, w, r , represent the indices of hit, location, wave and run, respectively.

- Average 1: Averaging the result from different hits for one location.

$$X_{r,w,l} = \frac{1}{N_h(l)} \sum_{h=1}^{N_h(l)} X_{r,w,l,h} \tag{12}$$

The number of hits $N_h(l)$ depends on the location (see Table 3).

- Average 2: Averaging the result from different locations for one wave.

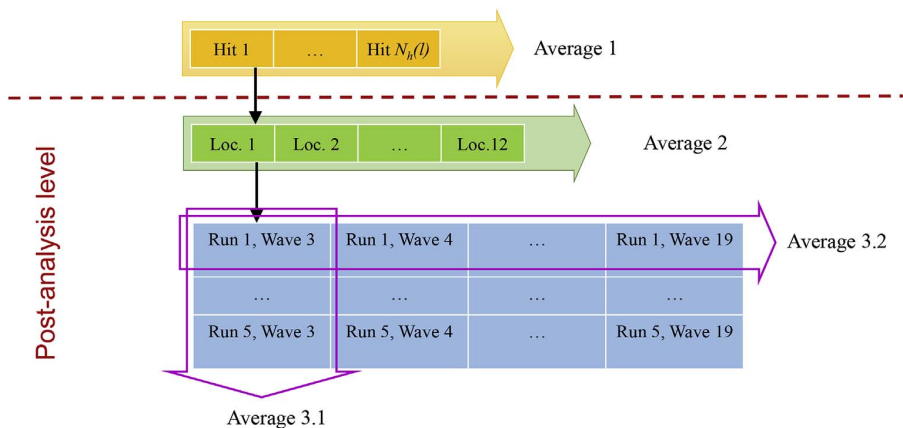


Fig. 12. Illustration of multi-level analysis.

$$X_{r,w} = \frac{1}{12} \sum_{l=1}^{12} X_{r,w,l} \quad (13)$$

- Average 3.1: Averaging the result from the same waves but over different runs.

$$X_w = \frac{1}{5} \sum_{r=1}^5 X_{r,w} \quad (14)$$

- Average 3.2: Averaging the result from the same runs but for different waves.

$$X_r = \frac{1}{17} \sum_{w=3}^{19} X_{r,w} \quad (15)$$

Since the number of hammer hits is different depending on the location, a post-analysis level (see Fig. 12) is further defined to eliminate the difference due to unequal weights. The time series of the reconstructed force are averaged over different hits at each location. The peaks of the time series are aligned for the averaging. In the post-analysis level, these averaged time series are used, so that the forces at different locations carry the same statistical weight. A total of $12 \times 17 \times 5 = 1020$ averaged time series are available for analysis in this level. The discussions in Section 4.3 onward are all based on the results in the post-analysis level.

4.2. Variation features

Ideally, the slamming forces under the same wave condition should be identical. However, each wave in the experiment is different even under the same preset condition. Also, each group of hammer test data used for the force reconstruction is different, from hit to hit, and from location to location. Therefore, the variation features of the reconstructed slamming forces at different levels need to be checked.

The variation at the hit level is represented by the mean calculated using Average 1 (see Section 4.1.2) and the corresponding standard error of the mean. The values are calculated for the six representative parameters (see Section 4.1.1), and for all locations and all waves. In Fig. 13, an exemplary result, which shows the hit variation for twelve locations using the 16th wave of the 4th run, is demonstrated by the blue error bars. The hit variation shows no signs of systematic biases (such as dependence on hammer hit location or significant asymmetry), and the results from Average 1 are considered to be appropriate estimates of the slamming forces at this level. In addition, no special pattern among the locations is observed if all the waves are checked.

The variation at the location level is represented by the mean calculated using Average 2 and the corresponding standard error of the mean. The location variation for the same wave is demonstrated by the red and orange lines in Fig. 13.

The variation at the wave level is represented by the mean calculated using Average 3.1 and the corresponding standard error of the mean. As shown in Fig. 14, the peak force, impulse and right impulse increase as the wave ID increases, i.e. for the later waves in each run. In contrary, the duration and rising time decrease slightly. The left impulse is almost constant. The difference among the waves may be caused by the accumulated diffraction and refraction in each run, which is observed in the video record of the experiment. As these effects, including also a potentially shifting breaking point, cannot be quantified easily, we consider these unknown effects as part of the uncertainties reported.

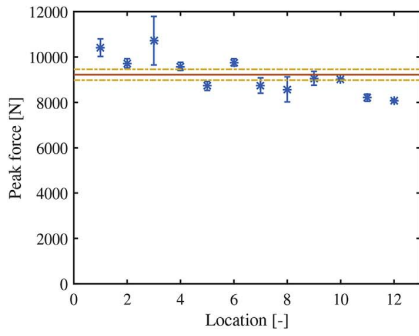
The variation at the run level is represented by the mean calculated using Average 3.2 and the corresponding standard error of the mean. As shown in Fig. 15, the result only varies slight among different runs, which means the test runs have a good repeatability.

4.3. Correlation features

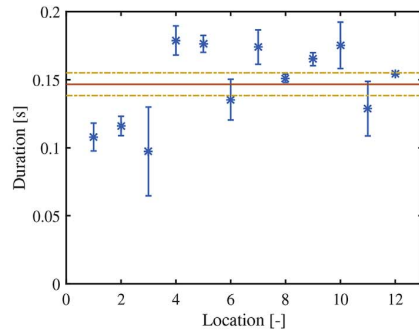
The correlation matrix of the six parameters is calculated and shown in Table 4. For the purposes here, we assume correlations above 0.8 to be strong, and correlations between 0.4 and 0.8 to be moderate. According to the correlation matrix, the peak force F_p has negative linear relationships with the duration T and with the rising time T_r . This is in accordance with the trend observed for example in Fig. 14. The impulse I has moderate positive linear relationships both with F_p and with T . The rising time T_r has a stronger linear relationship with the left impulse I_L than with I . The left impulse I_L and the right impulse I_R have very low correlation, which suggests that these two parts of the impulse are independent and can be treated separately. In summary, these results indicate that the chosen parameters are not independent, which could lead to identification issues. However, the only strong correlation is between I and I_R . Therefore, they will not be used together in the proposed force models (see Section 6).

4.4. Distribution features

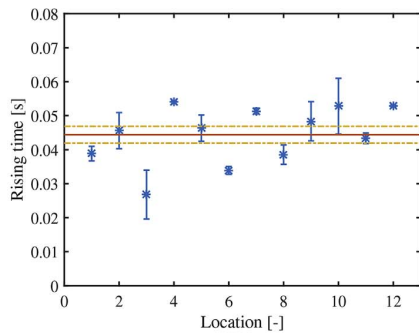
To illustrate the data distribution features of the six parameters, histograms are plotted in Fig. 16. The number of bins is set as 30 for all histograms. The data are further fit by various distributions. The names and parameters of the distributions that seem to result in the best match, as well as the log-likelihood of the fitting are shown in Table 5. The means and 95% bootstrap confidence intervals



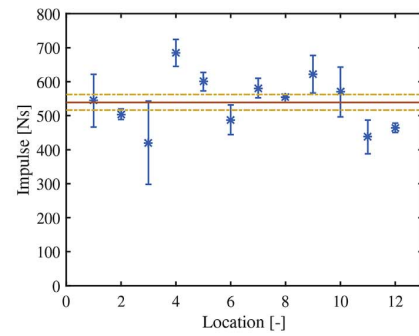
(a) Peak force F_p



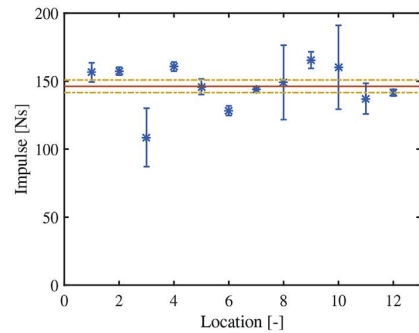
(b) Duration T



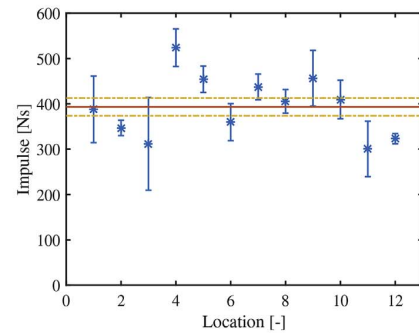
(c) Rising time T_r



(d) Impulse I



(e) Left impulse I_L



(f) Right impulse I_R

Fig. 13. Hit variation of the six parameters representing the slamming force (blue error bars indicate the standard error of the mean), and location variation of the six parameters representing the slamming force (red line indicates the mean, and orange lines indicate the standard error of the mean). The result shown is for the 16th wave of the 4th run, as a typical example. (For interpretation of the references to colour in this figure legend, the reader is referred to the web version of this article.)

[20] of the means based on 2000 bootstrap samples are marked in Fig. 16 and listed in Table 5.

4.5. Representative wave slamming force time series

Although the statistical properties of the representative parameters have been discussed thoroughly in the previous sections, a representative time series of the slamming force is still necessary to describe the force development in time. Therefore, a mean force time series is calculated according to Eq. (16) and shown in Fig. 17. The standard deviation of the data points at each time instance is

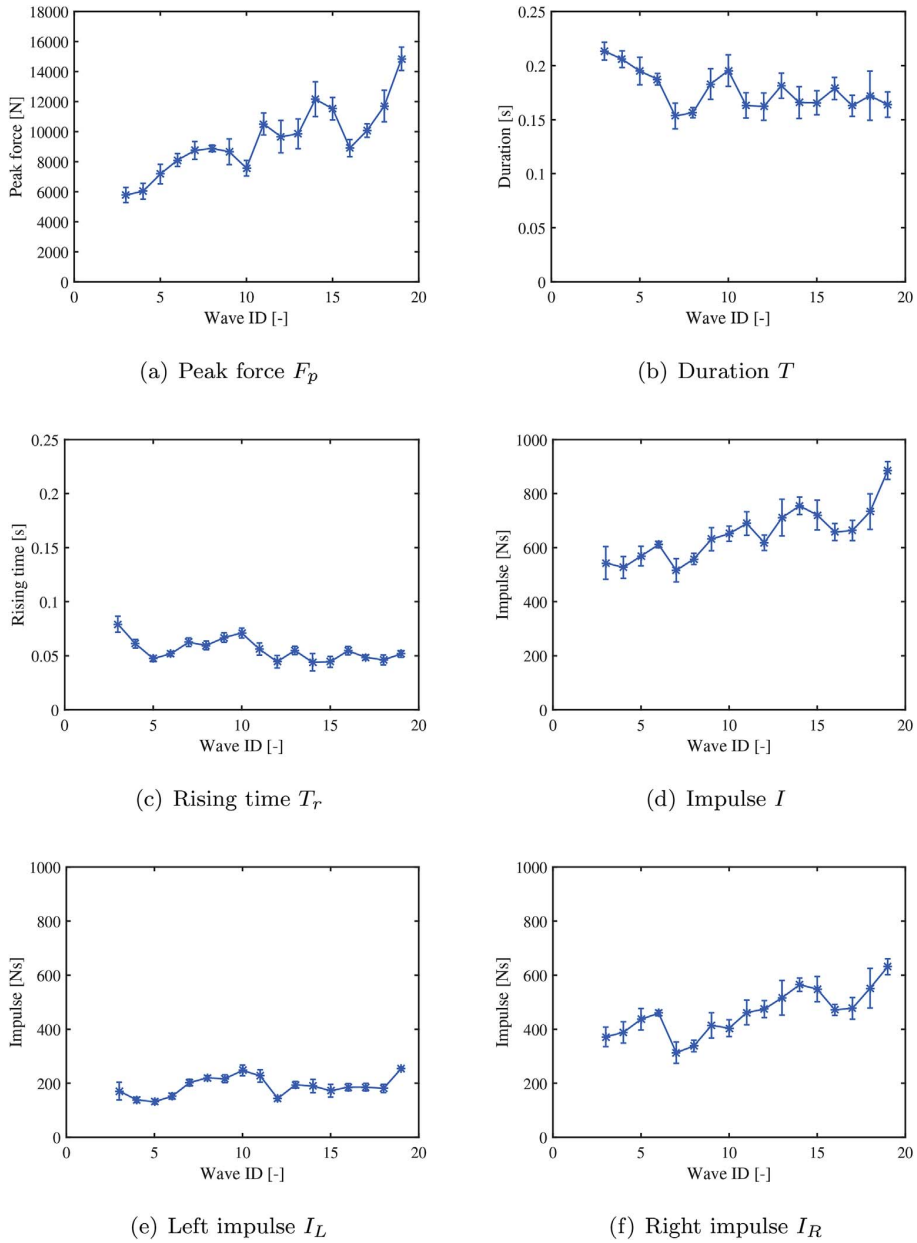


Fig. 14. Wave variation of the six parameters representing the slamming force.

also shown in the figure.

$$f_{rep}(t) = \frac{1}{12 \times 17 \times 5} \sum_{r=1}^5 \sum_{w=3}^{19} \sum_{l=1}^{12} f_{r,w,l}(t) \tag{16}$$

5. Estimation of slamming coefficient

The slamming coefficient is an important factor to connect wave kinematics and slamming forces in engineering practice. It is essential for the calculation of the maximum slamming forces on a structure, given a certain wave condition. According to Goda et al.

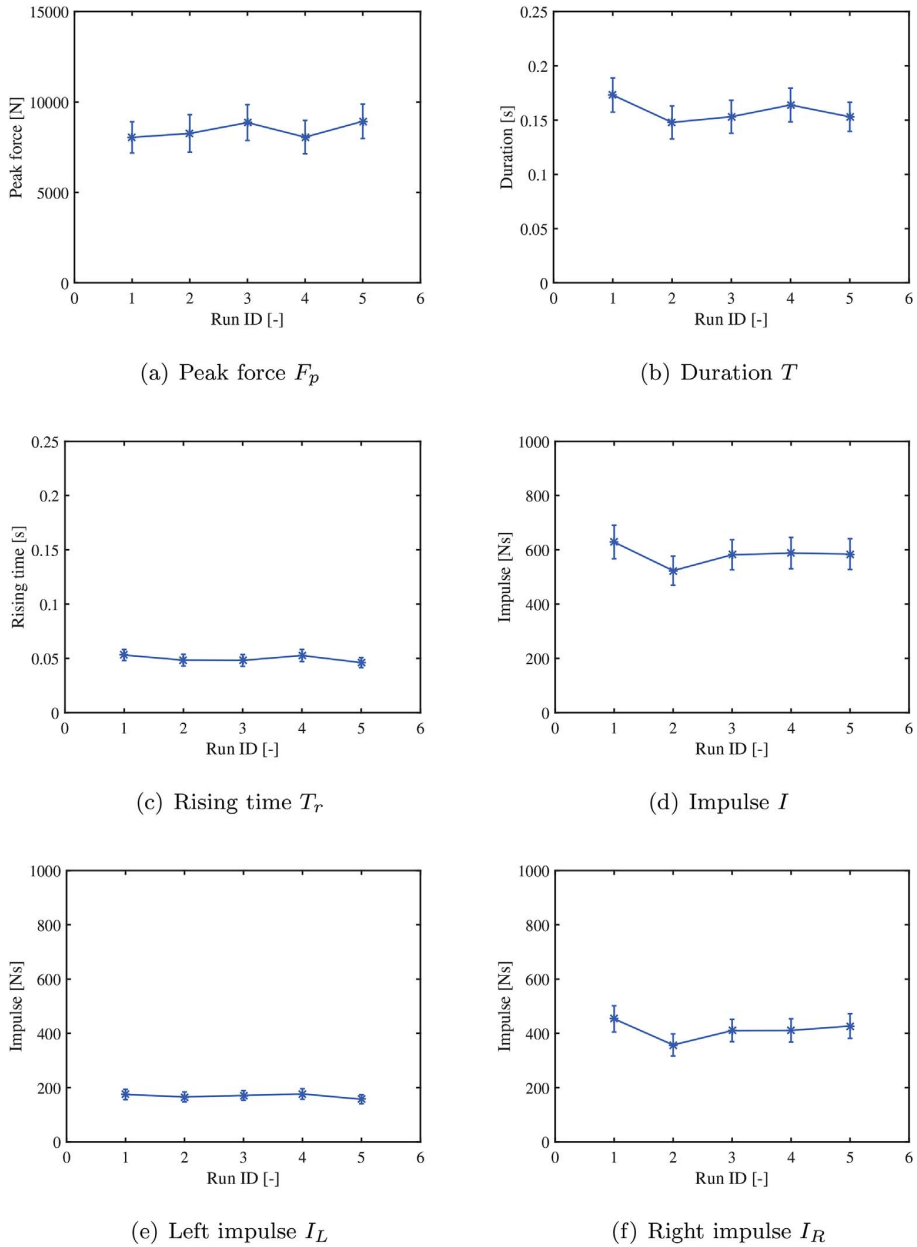


Fig. 15. Run variation of the six parameters representing the slaming force.

[21], the maximum wave slaming force on a cylinder is written as

$$F_s = \frac{1}{2} \rho_w C_s \lambda D \eta_b C_b^2 \tag{17}$$

where ρ_w is the water density, C_s the slaming coefficient, λ the curling factor, D the diameter of the cylinder, η_b the wave elevation and C_b the breaking wave celerity. When applying Eq. (17) on a jacket structure, D is interpreted as the width of the part that is exposed to the breaking wave. For the jacket structure considered in the WaveSlam project, D is estimated according to the geometry of the structure, as an expression of the diameter of the braces and the legs, $D = 2 \times (1 + 2.15) \times 0.14 \text{ m} = 0.88 \text{ m}$. Each inclined brace contributes $2.15 \times 0.14 \text{ m}$ to D , due to an inclined angle of 62° with respect to the vertical. The peak forces of the slaming force time series in the post-analysis level (see Section 4.1.2) are used as F_s for estimating the coefficient. The wave elevation η_b is taken as the

Table 4
Correlation matrix of the six parameters representing the slamming force.

| | F_p | T | T_r | I | I_L | I_R |
|-------|-------|-------|-------|------|-------|-------|
| F_p | 1.00 | -0.42 | -0.42 | 0.40 | 0.18 | 0.36 |
| T | -0.42 | 1.00 | 0.53 | 0.53 | 0.10 | 0.55 |
| T_r | -0.42 | 0.53 | 1.00 | 0.23 | 0.64 | -0.07 |
| I | 0.40 | 0.53 | 0.23 | 1.00 | 0.46 | 0.89 |
| I_L | 0.18 | 0.10 | 0.64 | 0.46 | 1.00 | 0.01 |
| I_R | 0.36 | 0.55 | -0.07 | 0.89 | 0.01 | 1.00 |

the mean is [0.506, 0.525], as indicated in Fig. 18. Taking the mean value of $C_s\lambda$ and a range plus or minus one standard deviation, the variation of slamming coefficient is plotted against the curling factor ranging from 0.1 to 0.5 in Fig. 19. At the maximum curling factor proposed by Goda et al. [21] for plunging breaking waves, $\lambda = 0.4$, the mean slamming coefficient is approximately $C_s = 1.29$. Taking one standard deviation around the mean into account due to the data uncertainties, the slamming coefficient C_s ranges from around 0.70 to 6.78 for the range of curling factor from 0.1 to 0.5.

It should be noted that in the above estimation of slamming coefficient, the assumption on the width D may cause some uncertainty in the estimation of slamming coefficient C_s . Depending on the wave impact location, the actual effective diameter D may be slightly smaller than the used one due to the local geometry at the joints. The geometry of the jacket is very different from that of a cylinder, so the effective impact area is also somewhat different.

6. Wave slamming force models

When performing a dynamic analysis of a structure subjected to slamming forces, the time history of the slamming forces is usually required as an input. Proper wave slamming force models, which can simulate the time history of wave slamming force, are thus desirable. Two models are proposed in this section, based on the representative time series of wave slamming force shown in Fig. 17 and the values of the six parameters.

6.1. Simplified model

A three-parameter triangular force model, denoted as simplified model, is proposed, considering the correlation among the studied parameters (see Section 4.3):

$$f(t) = \begin{cases} F_p \frac{(t - (t_p - T_r))}{T_r} & t_p - T_r < t \leq t_p \\ F_p \frac{(t_p - T_r + T - t)}{T - T_r} & t_p < t \leq t_p - T_r + T \\ 0 & \text{Otherwise} \end{cases} \tag{19}$$

where t_p denotes the instant of peak force; F_p , T_r and T are the peak force, rising time and duration of the slamming force, respectively. By applying the mean values of these parameters estimated in Section 4.4, the simplified model is obtained, as plotted in Fig. 20 by a red line. For a more conservative estimation, the mean plus one standard deviation values of the parameters are used in the model. The result is shown in the same figure by a yellow line.

To verify the simplified model, the left impulse, I_L , and the right impulse, I_R , are calculated for the representative time series and the simplified model. Here the I_L and I_R are calculated over the range of $[t_p - T_r, t_p]$ and $[t_p, t_p - T_r + T]$, respectively. The results are given in Table 6. It can be found that the simplified model greatly overestimates the I_L and I_R by approximately 50.02% and 36.61%, respectively. Hence, a more refined model is desirable to describe the time series of wave slamming force.

6.2. Refined model

As observed in Fig. 17, the wave slamming force seemingly ascends exponentially until it reaches the peak; after that, it descends also exponentially. Therefore, two exponential curves are used to model the data at both sides of the peak more precisely. This refined model is thus proposed as follows:

$$f(t) = \begin{cases} F_p \exp\left(\alpha_1 \frac{t - t_p}{T_r}\right) & t_p - T_r < t \leq t_p \\ F_p \exp\left(\alpha_2 \frac{t - t_p}{T - T_r}\right) & t_p < t \leq t_p - T_r + T \\ 0 & \text{Otherwise} \end{cases} \tag{20}$$

highest measured elevation of the corresponding wave. The breaking wave celerity is approximated by Ref. [22,23].

$$C_b = \sqrt{g(d + \eta_b)} \tag{18}$$

where g is the gravitational acceleration and d is the water depth. The curling factor λ is highly dependent on the wave properties and the type of structure, and it cannot be identified independently of C_s without further assumptions. Therefore, the slamming coefficient C_s is first estimated together with the curling factor, by using Eq. (17) with the estimated slamming forces.

For all used F_s , the product $C_s\lambda$ is estimated and its distribution is plotted in Fig. 18. The distribution is fit by a Gumbel distribution. The mean value of $C_s\lambda$ is about 0.515, and the corresponding 95% bootstrap confidence interval of

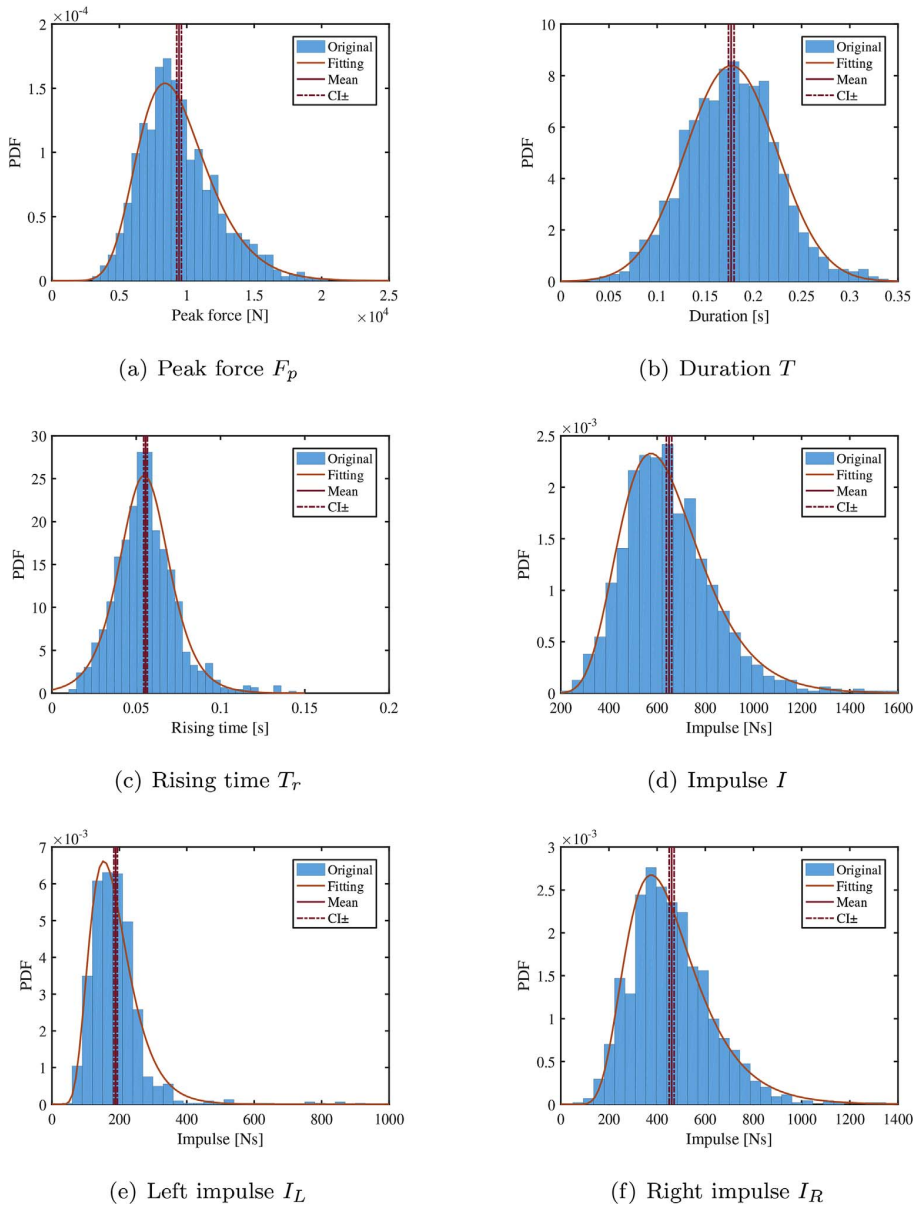


Fig. 16. Statistical properties of the six parameters representing the slamming force. Histogram, distribution, mean and confidence interval of mean are shown.

In addition to the three parameters, F_p , T_r and T , used in the simplified model, two coefficients α_1 and α_2 are introduced to indicate the rate of exponential decay on both sides of the peak. By using the mean values of the three parameters estimated in Section 4.4, the refined model is fit to the representative time series by employing a nonlinear least square curve fitting method. The results are demonstrated in Fig. 21 by a red line, and the fit coefficients are $\alpha_1 = 2.79$ and $\alpha_2 = -2.36$. The curve on the left side of the peak has a higher rate of decay than the curve on the right side, which is reflected by a higher absolute value of α_1 than α_2 . For a more conservative estimation, the mean plus one standard deviation values of the three parameters are used, while α_1 and α_2 are kept the same. The result is shown in the same figure by a yellow line.

Similarly, the left impulse, I_L , and the right impulse, I_R , are estimated to verify this refined model, as given in Table 6. The relative errors of I_L and I_R between the representative time series and the refined model are 0.89% and 4.50%, respectively, which implies that this refined model represents the wave slamming force time series fairly well.

The refined model has a more accurate match with the representative time series, while the simplified model leads to a more

Table 5
Mean, confidence interval of mean and distribution of the six parameters representing the slamming force.

| | F_p [N] | T [s] | T_r [s] | I [Ns] | I_L [Ns] | I_R [Ns] |
|---|---|-----------------------------------|-----------------------------------|-------------------------------------|-------------------------------------|-------------------------------------|
| Mean | 9425.2 | 0.177 | 0.056 | 649.4 | 189.0 | 460.3 |
| Confidence interval of the mean (lower limit) | 9273.9 | 0.174 | 0.054 | 638.5 | 184.1 | 449.8 |
| Confidence interval of the mean (upper limit) | 9618.3 | 0.180 | 0.057 | 661.6 | 194.9 | 470.7 |
| Fit distribution | Gumbel | Normal | Logistic | Log-normal | Log-normal | Log-normal |
| Distribution parameters* | $\sigma = 2395.7$ $\mu = 8196.9$ $k = -0.072$ | $\sigma = 0.048$ $\mu = 0.177$ | $\sigma = 0.010$ $\mu = 0.055$ | $\sigma_L = 0.29$ $\mu_L = 6.44$ | $\sigma_L = 0.37$ $\mu_L = 5.17$ | $\sigma_L = 0.37$ $\mu_L = 6.07$ |
| Log-likelihood of fitting | -9505.8 | 1659.5 | 2666.6 | -6734.9 | -5696.2 | -6622.2 |

* σ = scale factor, μ = location factor, k = shape factor, σ_L = log scale factor, μ_L = log location factor.

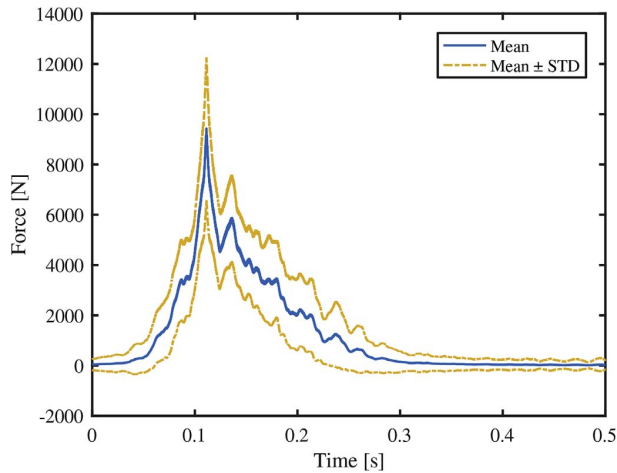


Fig. 17. Representative mean wave slamming force time series and its standard deviation.

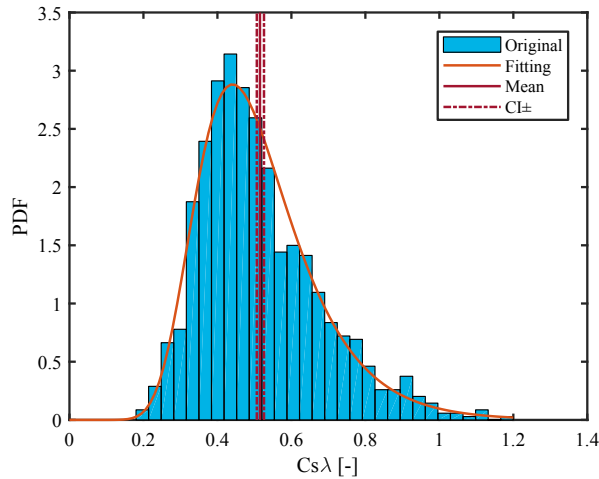


Fig. 18. Statistical properties of $C_s\lambda$, represented by histogram, Gumbel distribution fit, mean and confidence interval of the mean.

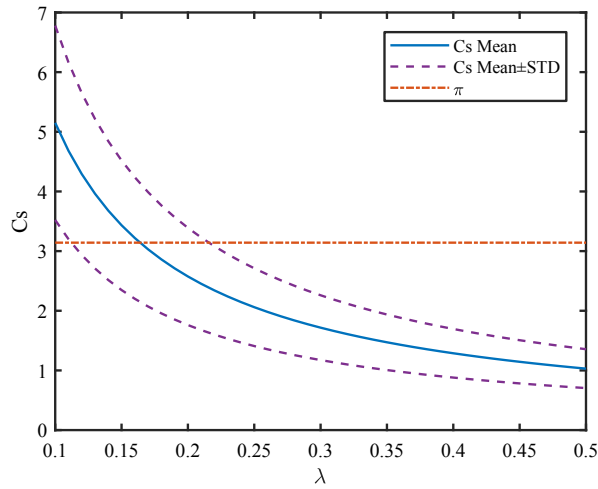


Fig. 19. C_s under different λ values.

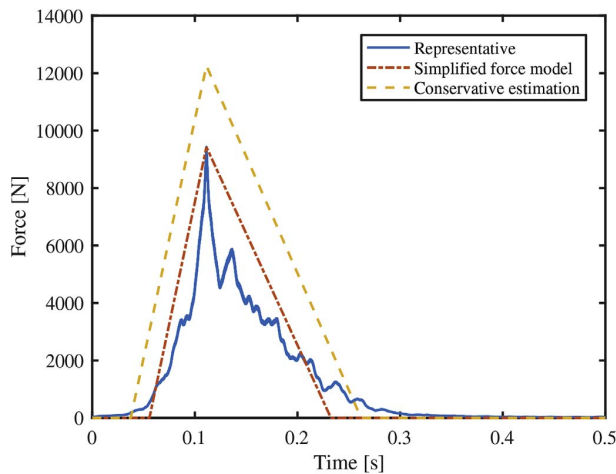


Fig. 20. Simplified force model for the representative wave slamming force time series.

conservative estimation of the impulse. On the other hand, the simplified model only requires three parameters. It is easier to be applied in practice, compared to the refined model, which requires two more parameters that are sensitive to the data.

7. Conclusions and outlook

This study aimed at investigating the global slamming forces due to plunging breaking waves on jacket structures, based on the statistical analysis of the experimental data from the WaveSlam project.

A total of 3910 time series of slamming forces were reconstructed based on the hammer test data and wave test data. To reveal the characteristics of the slamming force, six parameters were introduced to describe each force time series, including the peak force, duration, impulse, rising time, left impulse, and right impulse. The variation, correlation and distribution features of these parameters were investigated. High variability of these parameters is observed. Strong correlation is only found between the impulse and right impulse. A representative wave slamming time series was obtained by averaging all the reconstructed time series with respect to location, wave and run.

The statistical analysis serves as a basis for the estimation of slamming coefficient and the setup of force models. Taking one standard deviation around the mean into account due to the data uncertainties, the slamming coefficient C_s ranges from around 0.70 to 6.78 for the range of curling factor from 0.1 to 0.5. If the curling factor is set to 0.4, the mean C_s is approximately 1.29. Based on the representative slamming force time series, a 3-parameter triangular force model and a 5-parameter exponential force model were proposed to represent the time series of wave slamming force.

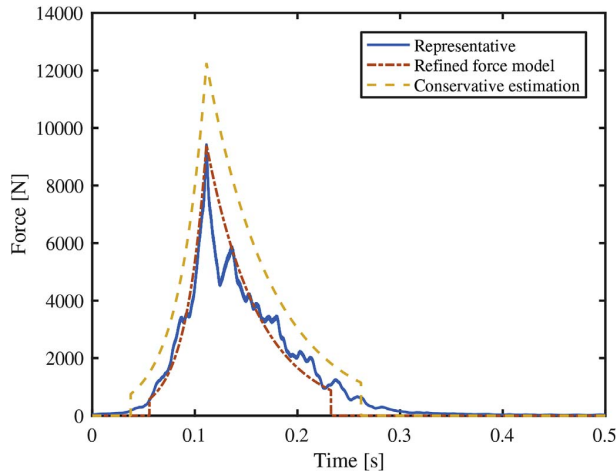


Fig. 21. Refined force model for the representative wave slamming force time series.

Table 6

The estimated impulse I_L and I_R by using the representative time series, simplified model and refined model.

| | Rep. time series | Simplified model | | Refined model | |
|-------|------------------|------------------|-----------|---------------|-----------|
| | Value [Ns] | Value [Ns] | Error [%] | Value [Ns] | Error [%] |
| I_L | 174.48 | 261.76 | 50.02 | 176.04 | 0.89 |
| I_R | 417.68 | 570.63 | 36.61 | 436.48 | 4.50 |

It should be noted that this paper statistically studied the global slamming forces on a jacket structure under one exemplary wave condition, more wave conditions should be investigated in the future to verify the slamming coefficient and the proposed wave models. The results in this study can also be verified by using a finite element model of the jacket structure, with careful consideration of the modeling strategies for various measurement devices and joints. For cylindrical structures, the slamming coefficient estimated from the Von Karman or Wagner theory is π or 2π and is not related to the curling factor. For the jacket structure considered in this paper, the slamming coefficient is dependent on the curling factor, because only the product $C_s \lambda$ is identified. The resulting slamming coefficient is therefore given as a range and different from that of cylindrical structures. Given a commonly used curling factor, $\lambda = 0.4$, the resulting C_s is significantly lower than the corresponding values for cylinders, because the breaking waves do not hit different parts of the jacket simultaneously. This result is important for the design of the structures, since it leads potentially to more economical jackets. Although only one jacket structure is considered in this paper, it is a typical jacket structure for offshore wind applications. The results are therefore valuable for slamming load considerations in the design of similar jacket structures.

For safe design of structures, the uncertainties of the external loads should be taken into account properly. The uncertainties of slamming loads not only result from the long term and short term wave statistics, but also arise from statistical variations under each wave condition. This study reveals the uncertainties of the slamming loads under one controlled wave condition in the laboratory. So far, this contribution to the uncertainties has mostly been neglected in the literature. Yet, as the present work shows, these variations are important. Using the slamming load distribution under one wave condition, together with the long term and short term distributions of wave conditions, it will be possible to determine a probability distribution of slamming loads. This could then be used to evaluate structural reliability and thereby serve as basis for probabilistic design of structures.

The challenges, of course, are the determination of the statistics of breaking wave conditions and slamming loads that occur in irregular wave conditions. The substructure geometry and bathymetry may also be different. Addressing the statistics of the slamming loads in such generality is very challenging, especially given the limitations of experimental data, where only a few of all possible parameters can be varied. Of course, the change from a single cylinder to a multi-element jacket structure – the topic of our study – results in effects that are also relevant for other multi-element structures. We therefore expect that the proposed model could also, with slight modifications, be used with other multi-element structures. Without further knowledge of the slamming loads under different wave conditions, one might use Eq. (17) with the identified $C_s \lambda$ values to obtain a first estimate of these loads. However, the suitability and accuracy of this approach still needs to be investigated. The biggest uncertainty when designing for breaking waves, however, still seems to be determining the long-term distribution of irregular breaking waves, i.e. which breaking waves are expected under a given irregular sea state, for a certain site and bathymetry. We hope that these issues will be addressed in the future.

Acknowledgment

This work has been supported by the European Community's Seventh Framework Programme through the grant to the budget of the Integrating Activity HYDRALAB IV within the Transnational Access Activities, Contract no. 261520.

Additional financial support from NOWITECH FME (Research Council of Norway, contract no. 193823) is gratefully acknowledged.

References

- [1] Hollowell S, Myers AT, Arwade SR. Variability of breaking wave characteristics and impact loads on offshore wind turbines supported by monopiles. *Wind Energy* 2016;19(2):301–12. <http://dx.doi.org/10.1002/we.2000>.
- [2] International Electrotechnical Commission (IEC). IEC 61400–61403, Wind turbines - part 3: design requirements for offshore wind turbines. 1.0 ed. 2009.
- [3] Det Norske Veritas (DNV). DNV-OS-J101, Offshore standard: design of offshore wind turbine structures. 2014.
- [4] GL Renewables Certification. Guideline for the certification of offshore wind turbines. 2012.
- [5] Faltinsen O. Sea loads on ships and offshore structures. Cambridge University Press; 1993.
- [6] Alagan Chella M, Tørum A, Myrhaug D. An overview of wave impact forces on offshore wind turbine substructures. *Energy Procedia* 2012;20:217–26. <http://dx.doi.org/10.1016/j.egypro.2012.03.022>.
- [7] Ridley JA. A study of some theoretical aspects of slamming. Technical Report. National Maritime Institute, UK: NMI R158; 1982.
- [8] Perlin M, Choi W, Tian Z. Breaking waves in deep and intermediate waters. *Annu Rev Fluid Mech* 2013;45:115–45. <http://dx.doi.org/10.1146/annurev-fluid-011212-140721>.
- [9] Wienke J, Oumeraci H. Breaking wave impact force on a vertical and inclined slender pile - theoretical and large-scale model investigation. *Coast Eng* 2005;52:435–62. <http://dx.doi.org/10.1016/j.coastaleng.2004.12.008>.
- [10] Irschik K, Sparboom U, Oumeraci H. Breaking wave loads on a slender pile in shallow water. Proceedings of 29th international conference on coastal engineering. Lisbon, Portugal. 2004.
- [11] Bredmose H, Slabiak P, Sahlberg-Nielsen L, Schlütter F. Dynamic excitation of monopiles by steep and breaking waves: experimental and numerical study. Proceedings of 32nd International Conference on Ocean, Offshore and Arctic Engineering. Nantes, France. 2013.
- [12] Rausa IE, Muskulus M, Arntsen ØA, Wåsjo K. Characterization of wave slamming forces for a truss structure within the framework of the WaveSlam project. *Energy Procedia* 2015;80:276–83. <http://dx.doi.org/10.1016/j.egypro.2015.11.431>.
- [13] Tu Y, Muskulus M, Arntsen ØA. Experimental analysis of slamming load characteristics for truss structures in offshore wind applications. *J Ocean Wind Energy* 2015;2(3):138–45. <http://dx.doi.org/10.17736/jowe.2015.jcr32>.
- [14] Jose J, Podrazka O, Obhrai C, Gudmestad OT, Cieslikiewicz W. Methods for analysing wave slamming loads on truss structures used in offshore wind applications based on experimental data. *Int J Offshore Polar Eng* 2016;26(2):100–8. <http://dx.doi.org/10.17736/ijope.2016.mkr05>.
- [15] Tu Y, Muskulus M, Grindstad TC. Two methods for the inverse estimation of local slamming loads on a jacket structure. Proceedings of 35th International Conference on Ocean, Offshore and Arctic Engineering. Busan, South Korea. 2016.
- [16] Arntsen Ø, Obhrai C, Gudmestad O. Data storage report: wave slamming forces on truss structures in shallow water. Technical Report, WaveSlam (HyIV-FZK-05). Norwegian University of Science and Technology; 2013.
- [17] Tørum A. Wave slamming forces on truss structures in shallow water. Technical Report Norwegian University of Science and Technology; 2011. Version 2011-10-03.
- [18] Aune L. Forces from plunging breaking waves on a truss structure Master thesis Norwegian University of Science and Technology; 2011
- [19] Cleveland WS. Robust locally weighted regression and smoothing scatterplots. *J Am Stat Assoc* 1979;74(368):829–36. <http://dx.doi.org/10.1080/01621459.1979.10481038>.
- [20] Efron B. Bootstrap methods: another look at the jackknife. *Ann Statistics* 1979;7(1):1–26. <http://dx.doi.org/10.1214/aos/1176344552>.
- [21] Goda Y, Haranaka S, Kitahata M. Study of impulsive breaking wave forces on piles. *Rep Port Harbour Tech Res Inst* 1966;6(5):1–30.
- [22] Tanimoto K, Takahashi S, Kaneko T, Shiota K. Impulsive breaking wave forces on an inclined pile exerted by random waves. *Coast Eng Proc* 1986;1(20):2288–302. <http://dx.doi.org/10.1061/9780872626003.168>.
- [23] Mei CC, Stiassnie M, Yue DK. Theory and applications of ocean surface waves: nonlinear aspects. World Scientific; 2005.

A.5 Paper 5

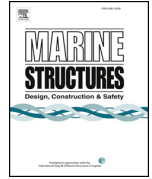
Paper 5:

Tu Y, Cheng Z, Muskulus M. A global slamming force model for off-shore wind jacket structures. *Marine Structures* 2018; **60**:201-217. <https://doi.org/10.1016/j.marstruc.2018.03.009>



Contents lists available at ScienceDirect

Marine Structures

journal homepage: www.elsevier.com/locate/marstruc

A global slamming force model for offshore wind jacket structures

Ying Tu^a, Zhengshun Cheng^{b,*}, Michael Muskulus^a^a Department of Civil and Environmental Engineering, Norwegian University of Science and Technology, Høgskoleringen 7A, 7491 Trondheim, Norway^b Department of Marine Technology, Centre for Autonomous Marine Operations and Systems, Norwegian University of Science and Technology, Otto Nielsens veg 10, 7491 Trondheim, Norway

ARTICLE INFO

Keywords:

Wave slamming force

Jacket structure

Experiment

Global force

Plunging breaking wave

ABSTRACT

Under certain harsh environmental conditions, jacket structures supporting offshore wind turbines might be exposed to plunging breaking waves, causing slamming forces that affect the structural integrity and fatigue life. The slamming forces should thus be properly considered during the design, but a suitable force model specifically for jacket structures is currently in absence. In this study, a five-parameter force model is developed for estimating global slamming forces due to plunging breaking waves on jacket structures, based on statistical analyses of experimental data from the WaveSlam project. The force model is developed by considering a total of 176 individual breaking waves, under six wave conditions. For each individual breaking wave, the time history of the slamming force is calculated based on hammer test data in addition to wave test data, and the wave parameters are acquired from a wave elevation measurement. The acquired time histories and wave parameters are then used to determine the parameters involved in the force model, including two exponential parameters (i.e. α_1 and α_2) and three dimensionless coefficients for the expressions of wave-dependent parameters (i.e. duration coefficient ζ_1 , rising time coefficient ζ_2 , and peak force coefficient ζ_3). It is found that α_1 , α_2 , ζ_1 and ζ_2 are approximately constant, and ζ_3 follows a lognormal distribution. The quantile that determines ζ_3 should be carefully selected so as to provide a conservative prediction. A quantile of 95% is suggested in this paper, and it is found to be conservative based on the verification of the developed force model. Therefore, for a given sea state, this force model can give a deterministic and conservative prediction of the slamming force time history, regardless of the randomness of slamming forces. Challenges for the application of the force model are also addressed.

1. Introduction

Currently, the development of offshore wind energy is mainly in shallow or intermediate water, where bottom-fixed substructures (e.g. monopiles and jacket structures) are mainly used. Under harsh environmental conditions at certain locations, these substructures are exposed to plunging breaking waves, which cause slamming forces. The slamming force features an extremely high impact force within a very short time. It can affect the integrity and fatigue life of the substructures of offshore wind turbines (OWTs). Therefore, slamming forces should be properly considered in the design of OWTs that are likely to be exposed to plunging breaking waves.

Slamming, violent impact on offshore structures, is a strongly nonlinear phenomenon involving the interaction among water, air and structure. Slamming forces are affected by various factors, such as compressibility of water, hydroelasticity of the structure, air bubbles entrapped, cavitation and ventilation etc. [1]. In the past decades, a large amount of effort has been made to investigate this

* Corresponding author.

E-mail address: zhengshun.cheng@ntnu.no (Z. Cheng).

Table 1
Comparison of different slamming force models for cylindrical structures (modified from Ref. [7]).

| Author | Theory | Maximum C_s | Slam duration, t_s | Time history of slamming coefficient, $C_s(t)$ |
|---------------------------|--|---------------|----------------------|--|
| Goda et al. [8] | von Karman | π | $\frac{D}{2C_b}$ | $\pi \left(1 - \frac{2C_b t}{D}\right)$ |
| Campbell and Weynberg [9] | Experimental study | 5.15 | $\frac{D}{C_b}$ | $5.15 \left(\frac{D}{D+19C_b t} + \frac{0.107C_b t}{D}\right)$ |
| Cointe and Armand [10] | Wagner and matched asymptotic expansions | 2π | $\frac{3D}{2C_b}$ | $2\pi - \left(4.72 - \ln\left(\frac{2C_b t}{D}\right)\right) \sqrt{\frac{2C_b t}{D}}$ |
| Wienke and Oumeraci [4] | Wagner | 2π | $\frac{13D}{64C_b}$ | $2\pi - 2\sqrt{\frac{2C_b t}{D}} \left(\tanh^{-1} \sqrt{1 - \frac{C_b t}{2D}}\right)$ (for $0 \leq t \leq \frac{D}{16C_b}$) $\pi \sqrt{\frac{1-D}{12 C_b t'}} - 4\sqrt{\frac{16 C_b t'}{3 D}} \tanh^{-1} \sqrt{1 - \frac{2C_b t'}{D}} \sqrt{\frac{12C_b t'}{D}}$ $t' = t - \frac{D}{64C_b}$ (for $\frac{D}{16C_b} \leq t \leq \frac{13D}{64C_b}$) |
| WiFi formulation [6] | Wagner | 2π | $\frac{13D}{64C_b}$ | a symmetric load shape |

Note that C_s is the slamming coefficient, D is the diameter of the cylinder, C_b is breaking wave celerity. In the WiFi formulation, the slamming force is assumed to be symmetric in time around the crest when the crest touches the structure surface.

complex phenomenon. The first work to study slamming forces theoretically was done by von Karman [2] on the estimation of forces on the floats of landing seaplanes. Later, Wagner [3] investigated the slamming forces on cylindrical structures, and in his study, the cylinder was approximated as a flat plate. The main difference between von Karman method and Wagner method is that the latter takes the local rise of free surface into account. This difference affects the duration and the magnitude of the calculated slamming force. Though the work by Wagner [3] was conducted 85 years ago, it is still widely used nowadays.

The von Karman method and Wagner method are usually used to determine the slamming coefficient of the slamming force for cylindrical structures, but the time history of the slamming force is also important when considering the effect of the slamming force. Several force models that can describe the time history of the slamming forces on cylindrical structures were thus developed, as given in Table 1. In these models, the slamming coefficients are time dependent. The Wienke and Oumeraci [4] model is recommended by the IEC 61400-3 standard [5] for designing OWT support structures. The WiFi formulation was newly developed in the WiFi JIP (Joint Industry Project Wave Impacts on Fixed turbines) in 2017 [6].

The models given in Table 1 were derived by using different approaches. The von Karman theory was implemented by Goda et al. [8], and Wagner theory was employed by Wienke and Oumeraci [4]. In addition to Wagner method, Cointe and Armand [10] also derived the asymptotic expressions for the inner domain and outer domain at the spray root during the impact and further solved the problem by matching the inner and outer asymptotic expressions. Campbell and Weynberg [9] determined the slamming coefficient by experimental study. The WiFi formulation was developed based on a combination of Wagner method and model tests at MARIN (Maritime Research Institute Netherlands) and at Deltares. It should be noted that these models were originally developed for a two dimensional (2D) slamming problem, hence the vertical distribution of slamming load was not taken into account. When applying these models to three dimensional (3D) problems, the vertical force distribution is usually assumed to be uniform or triangular.

The force models given in Table 1 were developed for cylindrical structures and can be used to estimate slamming forces on monopiles for OWTs. However, these force models might not be suitable for jacket structures, though they consist of several cylindrical legs and braces. One reason is that the water surface that approaches a leg or a brace is affected by other legs and braces, causing a more complicated slamming scenario than that for cylindrical structures.

The slamming forces acting on jacket structures are thus different from those on cylindrical structures. For jacket structures, wave slamming forces should be estimated both locally and globally. The local slamming forces are important for the design of e.g. individual legs, while the global slamming forces are essential for the design of e.g. foundation systems. Based on the experimental data from the WaveSlam project, Jose [11] discussed local versus global loads from breaking waves. Tu et al. [12] investigated the global slamming loads due to plunging breaking waves on jacket structures. A total of 3910 time series of slamming forces were reconstructed and statistically analyzed. The mean slamming coefficient was found to be about 1.30 at a curling factor of 0.4. In that study, two wave slamming load models were also proposed, i.e. a simplified force model and a refined force model, to represent the temporal development of global wave slamming loads on jacket structures. However, only one wave condition was considered in Ref. [12]. More wave conditions are thus required to further refine and verify the proposed force model.

In this study, six different wave conditions from the WaveSlam project are further analyzed to propose a more accurate global slamming force model for jacket structures for offshore wind applications. Under each wave condition, one or several wave test runs with a number of regular waves were carried out. Based on the experimental data, global slamming forces acting on a jacket structure model are inversely calculated by using the method developed by Tu et al. [13]. The parameters of the measured waves and the reconstructed slamming forces are then used to determine the parameters in the force model by statistical analysis. Verification and application of this developed force model are also addressed.

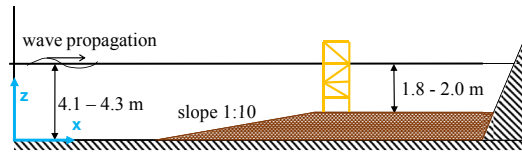


Fig. 1. Experimental setup and global coordinates [12]. The wave flume is about 300 m long, and the jacket is located at about 100 m before the end of the flume, with a much gentler slope than illustrated.

2. Experimental data

In this study, the experimental data from the WaveSlam project are used for the analyses. This project aims to improve the method for calculating slamming forces from plunging breaking waves on jacket structures through model tests on a large scale [14]. The project was conducted by a consortium headed by University of Stavanger (UiS) and Norwegian University of Science and Technology (NTNU) in 2012–2013. The experiment was conducted with a 1:8 scale model of a jacket structure, which is similar to the jacket designed by Reinertsen AS for the Thornton Bank offshore wind farm [15], using the Large Wave Flume facilities at the Coastal Research Centre (Forschungszentrum Küste, FZK)¹, Hannover, Germany. The experimental data have been released to the public since July 2015. The data used in this study are in model scale.

2.1. Experimental setup

The setup of the experiment is shown in Fig. 1. The wave flume is approximately 300 m long, 5 m wide and 7 m deep. The waves were generated by the wave board at the left end of the flume, went over a 1:10 slope, then reached the jacket model on a plateau. Since a water depth of 16 m was simulated, the water depth at the jacket model was set to 2.0 m for most cases. For some cases, the water depth was adjusted to 1.8 m. The diameter of the legs and the braces of the jacket model was 0.14 m.

A global coordinate system is defined as following: The origin is positioned at the middle position of the wave board ($x = 0$), at the bottom of the channel ($z = 0$) and at the south side of the flume, namely the right side when following the flow ($y = 0$). The x -axis is positive in the wave direction. The z -axis is positive upwards. The y -axis forms a right hand system with the other axes.

Wave gauges were installed at 15 different locations. Three Acoustic Doppler Velocity meters (ADV) were installed in the plane of the legs. The motion of the wave paddle was also recorded. The jacket was equipped with four total force transducers, ten local force transducers on the legs, twelve XY force transducers on the braces, and four one-directional accelerometers.

The measurements taken by the total force transducers and by the wave gauge at the plane of the front legs of the structure are used in this study. Other measurements are not used, thus not described in detail as in the original data report [14]. As shown in Fig. 2, there were two total force transducers installed at the top of the jacket model and two installed at the bottom of the jacket model. The structure was hung from the top and did not touch the ground during the tests. The measured forces are in global x direction and have a sampling frequency of 10 kHz. The details of the transducers are illustrated in the figure as well. The names and locations of the transducers are introduced in Table 2. The location of the wave gauge is also shown in the table.

2.2. Selected wave test cases

For a proper statistical analysis, as many wave test runs under different wave conditions as possible should be included. Therefore, all the test runs in the WaveSlam project were checked, and the test runs to be analyzed were selected according to four criteria:

- The waves should be breaking.
- The breaking locations should be close to the plane of the front legs.
- The waves in the runs should be regular.
- The water depth of all the selected runs should match that of the used hammer test runs.

The selected test runs are illustrated in Table 3. They are all regular runs with breaking waves and have 2 m water depth at the structure. Ideally, only those runs in which the waves were breaking exactly at the plane of the front legs of the jacket structure should be used. However, the available runs under such condition are limited in number in the WaveSlam project and not enough for statistical analysis. Therefore, run 5 and run 6 are also included. Although the waves in these two runs broke 1 m in front of the structure, their breaking points were closest to the desired location among the rest of the available data.

The selected test runs under the same preset wave conditions are categorized into one case. Each case is described by a wave height and a wave period. The wave height and the wave period represent the values preset at the wave board for wave generation. They are not the ones measured at the structure or at the breaking point.

There are five other test runs in the WaveSlam data that seem to fulfill the criteria at a first glance. However, they are not used due to issues with the data quality, such as measurement errors and no obvious breaking at the front legs.

¹ <https://www.fzk.uni-hannover.de/>; November 2017.

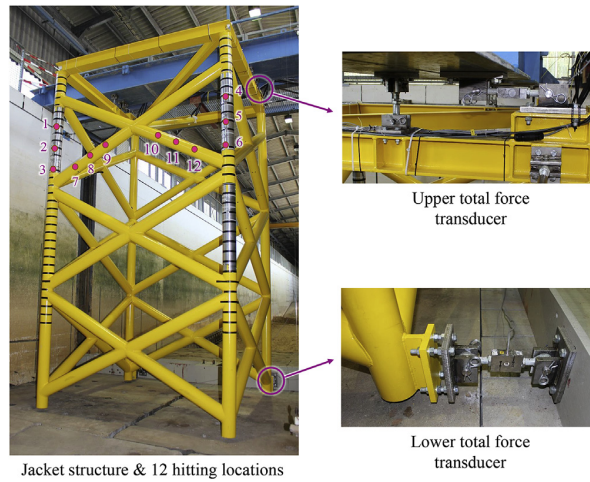


Fig. 2. Jacket structure, hammer hitting locations and total force transducers. Figures reprinted with permission from the WaveSlam project [12].

Table 2

The locations of total force transducers and wave gauge in global coordinates.

| Transducer | Description | x [m] | y [m] | z [m] |
|------------|-----------------------------|---------|-------|-------|
| FTTF01 | Total force bottom south | 200.961 | 1.405 | 2.465 |
| FTTF02 | Total force top south | 200.265 | 1.405 | 6.935 |
| FTTF03 | Total force bottom north | 200.961 | 3.655 | 2.465 |
| FTTF04 | Total force top north | 200.265 | 3.655 | 6.935 |
| WG S9 | Wave elevation at front leg | 198.37 | 0.60 | 7.00 |

Table 3

Selected wave test cases. The wave parameters as well as the rest of the data used in the study are in 1:8 model scale.

| Case number | Wave height [m] | Wave period [s] | Location of breaking | Run number | Run ID in WaveSlam | Number of waves in test run | Used waves in test run |
|-------------|-----------------|-----------------|---------------------------|------------|--------------------|-----------------------------|------------------------|
| 1 | 1.6 | 4.6 | at front leg | 1 | 20130614.04 | 20 | 2 to 20 |
| 2 | 1.65 | 4.6 | at front leg | 2 | 20130614.05 | 20 | 2 to 20 |
| 3 | 1.8 | 5.2 | at front leg | 3 | 20130618.03 | 10 | 2 to 6 and 8 to 10 |
| 4 | 1.7 | 5.55 | 1 m in front of structure | 4 | 20130618.04 | 10 | 2 to 6 and 9 to 10 |
| | | | | 5 | 20130614.24 | 20 | 2 to 20 |
| 5 | 1.7 | 5.2 | 1 m in front of structure | 6 | 20130617.09 | 20 | 2 to 20 |
| 6 | 1.5 | 4.9 | at front leg | 7 | 20130617.15 | 20 | 3 to 19 |
| | | | | 8 | 20130617.16 | 20 | 3 to 19 |
| | | | | 9 | 20130617.17 | 20 | 3 to 19 |
| | | | | 10 | 20130617.18 | 20 | 3 to 19 |
| | | | | 11 | 20130617.19 | 20 | 3 to 19 |

Even from the selected runs, not all the waves are used for analysis. The very first waves in each run are not breaking, so they are discarded. Some waves in the runs lead to a small peak in front of the two main peaks in the response data, which implies earlier breaking compared to the other waves. These waves are also discarded. The used waves in each test run are listed in the last column of Table 3.

2.3. Hammer test cases for force reconstruction

The measured total forces during the wave tests are to be used for slamming force reconstruction to be discussed in Section 3.2. Apart from the wave test data, hammer test data are also essential for the reconstruction. The selected hammer test cases are the same as in Ref. [12] and listed in Table 4. The hammer tests were carried out in 2 m deep water, the same as for the selected wave cases. The structure was hit by a 1.5 kg impulse hammer in the wave direction. The impulse hammer recorded the time series of the forces exerted on the structure with a sampling frequency of 9600 Hz, in addition to the total force measurements. The hammer hit at twelve

Table 4
Selected hammer test cases [12].

| Hit location number | Total hammer hits | ID of test run |
|---------------------|-------------------|------------------|
| 1 | 6 | 24062013.14 ~ 16 |
| 2 | 4 | 24062013.17 ~ 18 |
| 3 | 4 | 24062013.22 ~ 23 |
| 4 | 6 | 24062013.31 ~ 33 |
| 5 | 8 | 24062013.34 ~ 37 |
| 6 | 6 | 24062013.38 ~ 40 |
| 7 | 2 | 24062013.24 |
| 8 | 2 | 24062013.25 |
| 9 | 2 | 24062013.26 |
| 10 | 2 | 24062013.27 |
| 11 | 2 | 24062013.28 |
| 12 | 2 | 24062013.30 |

locations in the front plane of the structure, both on the braces and on the legs. These locations (see Fig. 2) are in or close to the expected wave slamming zone for the wave tests. Since the hammer impacts were exerted manually, the locations shown in the figure are approximate. The number of hits for each location is different as shown in Table 4.

3. Calculation of slamming forces

The total force measurements of the wave test cases described in Section 2.2 cannot be analyzed directly, since they are just the response of the structure due to the wave forces. These measurements were used together with the hammer test data to calculate the slamming forces under the corresponding wave conditions. It is the calculated time series of the slamming forces that are used in later sections for the analyses and model development. The method for the calculation has been described in detail in Ref. [12], so it is summarized briefly below.

3.1. Pre-processing of the data

The total force measurements of the wave tests and hammer tests were processed by the following steps to get the *wave response forces* and *hammer response forces* used for slamming force reconstruction. A bandpass filter was first used to eliminate the high frequency noise (above 300 Hz) in the total force measurements. Then, the forces measured by the four transducers (see Fig. 2) were summed to obtain the total forces. Finally, a time domain robust LOESS smoother [16] was used to estimate the quasi-static part from the total force, and the dynamic part remains. It was confirmed in Ref. [17] that this smoother does not overestimate the peak of the quasi-static part, and is effective to resolve the dynamic part.

The impulse hammer measurements were resampled to 10 kHz to match the total force measurements, and the resampled *hammer impact forces* were used for slamming force reconstruction.

3.2. Reconstruction of wave slamming forces

The wave response force due to each wave was paired with the hammer test data of each hit at each location to reconstruct the slamming forces. The reconstructed forces are “effective forces”, which means that the wave slam is assumed to occur only on the corresponding hammer impact location. For each wave-hammer data pair, a force reconstruction method based on linear regression [13] was used. This reconstruction method has been verified in Ref. [13] by a method-to-method comparison.

The following briefly summarizes the force reconstruction method. The wave slamming force is expressed in vector form as

$$\mathbf{f}_W = (f_{W_1} \ f_{W_2} \ f_{W_3} \ \cdots \ f_{W_n})^T \tag{1}$$

It can also be written as

$$\mathbf{f}_W = \mathbf{F}_H \boldsymbol{\beta} \tag{2}$$

where \mathbf{F}_H is a matrix composed of column vectors representing repeated and shifted hammer impact forces and is given by

$$\mathbf{F}_H = \begin{pmatrix} f_{H_1} & 0 & \dots & 0 \\ \vdots & \vdots & \ddots & \vdots \\ f_{H_\delta} & 0 & \ddots & 0 \\ f_{H_{\delta+1}} & f_{H_1} & \ddots & 0 \\ \vdots & \vdots & \ddots & \vdots \\ f_{H_{(p-1)\delta}} & f_{H_{(p-2)\delta}} & \ddots & 0 \\ f_{H_{(p-1)\delta+1}} & f_{H_{(p-2)\delta+1}} & \ddots & f_{H_1} \\ \vdots & \vdots & \ddots & \vdots \\ f_{H_n} & f_{H_{n-\delta}} & \dots & f_{H_{n-(p-1)\delta}} \end{pmatrix} \tag{3}$$

in which the symbol p denotes the total number of hypothetical hammer hits. The symbol δ denotes the interval between every two hammer hits, and is named *step factor*. The step factor is set to 5 for most cases, according to [13].

The parameter vector β represents the coefficients for scaling the hammer hits and is given as

$$\beta = (\beta_1 \ \beta_2 \ \beta_3 \ \dots \ \beta_p)^T \tag{4}$$

Similarly, the wave response force is written in vector form as

$$\mathbf{r}_W = (r_{W_1} \ r_{W_2} \ r_{W_3} \ \dots \ r_{W_n})^T \tag{5}$$

It can also be expressed as

$$\mathbf{r}_W = \mathbf{R}_H \beta + \mathbf{e} \tag{6}$$

where

$$\mathbf{R}_H = \begin{pmatrix} r_{H_1} & 0 & \dots & 0 \\ \vdots & \vdots & \ddots & \vdots \\ r_{H_\delta} & 0 & \ddots & 0 \\ r_{H_{\delta+1}} & r_{H_1} & \ddots & 0 \\ \vdots & \vdots & \ddots & \vdots \\ r_{H_{(p-1)\delta}} & r_{H_{(p-2)\delta}} & \ddots & 0 \\ r_{H_{(p-1)\delta+1}} & r_{H_{(p-2)\delta+1}} & \ddots & r_{H_1} \\ \vdots & \vdots & \ddots & \vdots \\ r_{H_n} & r_{H_{n-\delta}} & \dots & r_{H_{n-(p-1)\delta}} \end{pmatrix} \tag{7}$$

is composed of column vectors representing repeated and shifted hammer response forces, and

$$\mathbf{e} = (e_1 \ e_2 \ e_3 \ \dots \ e_n)^T \tag{8}$$

is an error term due to the noise in the measurements.

The parameter vector β can be solved by applying an ordinary least squares regression technique based on Eq. (6), when \mathbf{r}_W and \mathbf{R}_H are known. The estimated parameter vector is given by

$$\hat{\beta} = (\mathbf{R}_H^T \mathbf{R}_H)^{-1} \mathbf{R}_H^T \mathbf{r}_W \tag{9}$$

Knowing the hammer impact force and applying $\hat{\beta}$ to Eq. (2), the wave slamming force is estimated as

$$\hat{\mathbf{f}}_W = \mathbf{F}_H \hat{\beta} \tag{10}$$

3.3. Post-processing of the wave slamming forces

A reconstructed time series of slamming force contains two major peaks, corresponding to the wave impacts at the plane of the front legs and at the plane of the hind legs, respectively. Since the impact with larger force and impulse is of more importance in the design, only the first peak of the time series is considered in this study.

Four parameters were determined from each time series to describe the slamming forces, as illustrated in Fig. 3.

Since the wave response force due to each wave was paired with the hammer test data of each hit at each location to reconstruct the slamming forces, there are multiple force time series reconstructed for each wave impact. The slamming force due to each wave was obtained by averaging the reconstructed slamming forces. The averaging was performed in two steps and for both the time series and the parameters that describe the slamming force. When the time series were averaged, the peaks of them were aligned. We use symbol X to represent the time series or one of the parameters to be averaged. The subscripts h and l represent the indices of hit and location, respectively.

First, the values of different hits were averaged for each location of each wave.

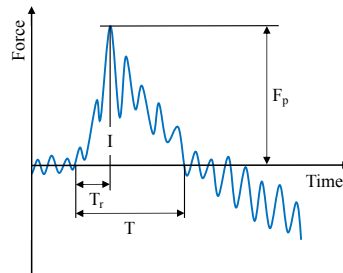


Fig. 3. Parameters to describe the force time series of one wave slamming event. The variation of the time series has been exaggerated for visualization purposes.

- F_p : Peak force, the maximum force in the time series.
- T : Duration, the time between the last zero-up-crossing before the peak and the first zero-down-crossing after the peak.
- T_r : Rising time, the time between the last zero-up-crossing before the peak and the peak itself.
- I : Impulse, the integral of the force over the duration.

$$\bar{X}_l = \frac{1}{N_h(l)} \sum_{h=1}^{N_h(l)} X_{l,h} \tag{11}$$

The number of hits $N_h(l)$ depends on the location (see Table 4).

Second, the averaged values of different locations were again averaged for each wave.

$$\bar{X} = \frac{1}{12} \sum_{l=1}^{12} \bar{X}_l \tag{12}$$

The purpose of the averaging is to obtain a single force time series that represents the wave hitting the front plane of the structure. Impacts at different locations result in slightly different responses (impulse response functions). The 12 locations for which hammer tests were performed sample the variability due to the impact location (studied in more detail in Ref. [12]). The average of the response from these 12 cases is considered the best available estimate of the response due to a wave hitting the front of the jacket at potentially different locations. In other words, what is averaged out is not noise or inherent randomness of the waves, but rather uncertainty regarding the exact positions on the structure where the wave hits (and in which sequence).

The resulting time series and parameters for all the waves described in Table 3 are used for the analyses in the next sections.

4. Model development

In Ref. [12], two parameterized models were proposed to describe the time series of the global slamming forces on jacket structures: a three-parameter simplified model and a five-parameter refined model. The refined model turned out to represent the force time series more accurately than the simplified one. Therefore, in this section, the refined model is further elaborated based on the slamming forces acquired by using the multiple wave cases in Table 3.

The original refined model is

$$f(t) = \begin{cases} F_p \exp\left(\alpha_1 \frac{t-t_p}{T_r}\right) & t_p - T_r < t \leq t_p \\ F_p \exp\left(\alpha_2 \frac{t-t_p}{T-T_r}\right) & t_p < t \leq t_p - T_r + T \\ 0 & \text{Otherwise} \end{cases} \tag{13}$$

where $f(t)$ is the time series of global slamming force; t_p denotes the moment of the peak in the time series; α_1 and α_2 are two parameters that determine the rate of exponential decay on both sides of the peak; peak force F_p , duration T and rising time T_r are three parameters determined by wave conditions.

Equation (13) can be transformed into

$$\ln\left(\frac{f(t)}{F_p}\right) = \begin{cases} \alpha_1 \frac{t-t_p}{T_r} & t_p - T_r < t \leq t_p \\ \alpha_2 \frac{t-t_p}{T-T_r} & t_p < t \leq t_p - T_r + T \\ 0 & \text{Otherwise} \end{cases} \tag{14}$$

The moment of peak t_p can be set to an arbitrary value. For simplification, it is set to zero, so Equation (14) becomes

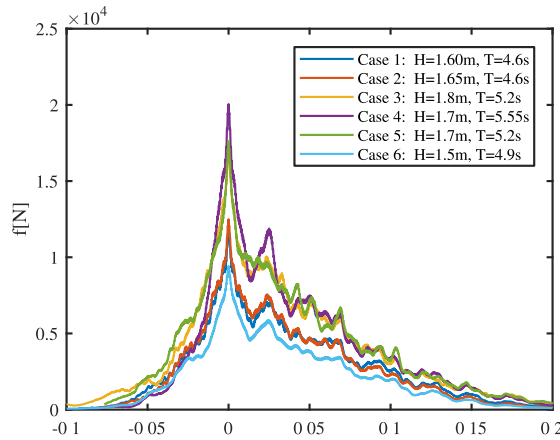


Fig. 4. Averaged force time series for six cases.

$$\ln\left(\frac{f(t)}{F_p}\right) = \begin{cases} \alpha_1 \frac{t}{T_r} & -T_r < t \leq 0 \\ \alpha_2 \frac{t}{T-T_r} & 0 < t \leq T-T_r \\ 0 & \text{Otherwise} \end{cases} \tag{15}$$

In order to apply the model in engineering practice, the five unknown parameters in the model have to be decided. They are discussed separately in two groups below, according to their features.

4.1. Determination of exponential parameters

The reconstructed time series of global slamming forces due to different waves in each case are averaged. The averaged force time series for the available six cases are plotted in Fig. 4. The peaks of the time series are aligned in the figure.

For all the six cases, the force seems to decay exponentially on both sides of the peak, which is in accordance with the proposed model.

The time series in Fig. 4 are then converted according to Equation (15) using the corresponding parameters F_p , T and T_r of each case. $\ln\left(\frac{f(t)}{F_p}\right)$ is plotted versus $\frac{t}{T_r}$ before the peak and versus $\frac{t}{T-T_r}$ after the peak in Fig. 5.

From the figure, $\ln\left(\frac{f(t)}{F_p}\right)$ is found to behave almost linearly with respect to $\frac{t}{T_r}$ before the peak and with respect to $\frac{t}{T-T_r}$ after the peak, which to some extent confirms the exponential behavior of the force time series.

To quantify this linear relationship between the horizontal axis value and the vertical axis value in Fig. 5, the mean $\mu(t)$ and

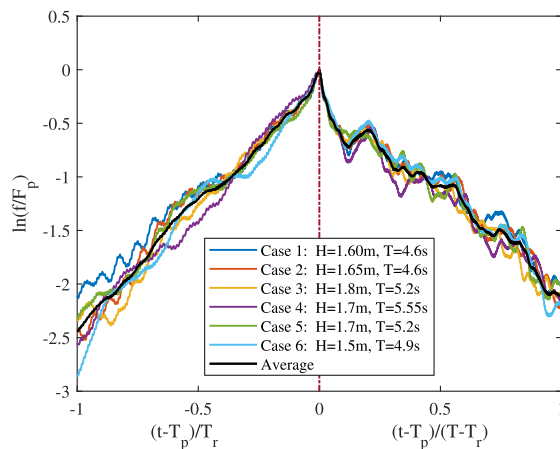


Fig. 5. Averaged force time series for six cases converted to Equation (15).

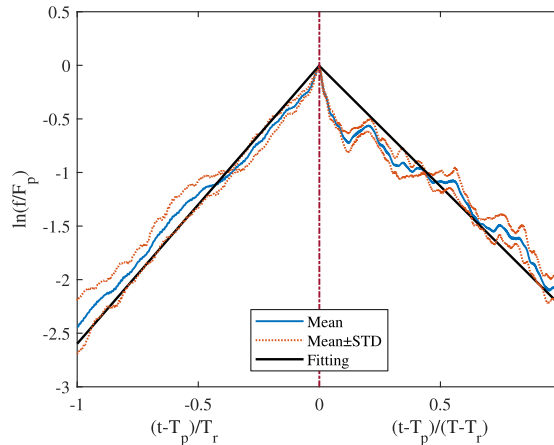


Fig. 6. Fitting of converted average force time series.

standard deviation $\sigma(t)$ of the six converted time series are estimated, as depicted in Fig. 6.

The standard deviation represents the variation of $\ln\left(\frac{f(t)}{F_p}\right)$ across the different wave conditions, and its value varies with the horizontal axis value. The variation of the slamming force time series due to the waves under the same preset condition (“Case” in this study) was discussed in detail in Ref. [12], and is thus not elaborated in the present study. However, the coefficient of variation (or relative standard deviation, $C_v(t) = \frac{\sigma(t)}{\mu(t)}$) varies only slightly with the horizontal axis value and has a low value of 0.08 on average. This implies that the variation among the time series are small, and it is plausible to use the mean curve to represent the six time series. It is found that the standard deviation in the vicinity of the peak is smaller than that far away from the peak. Since the force around the peak contributes the most to the impulse caused by a wave impact, it is important to estimate the force around the peak more accurately than the rest of the time series. Therefore, weighted linear regression [18] is applied to fit the mean time series on both sides of the peak. In weighted linear regression, the weighting coefficients are assumed to be inversely proportional to the variance (square of standard deviation), so a smaller standard deviation results in a larger weighting coefficient. This leads to higher weighting around the peak, where the standard deviation is lower. By using the fitting, the exponential parameters are determined: $\alpha_1 = 2.60$ and $\alpha_2 = -2.24$. The coefficients of determination, i.e. R^2 values, of the fitting are calculated using the same weighting scheme to be 0.9999 and 0.9992, respectively. This indicates that the exponential parameters α_1 and α_2 are determined with high confidence.

4.2. Determination of wave-dependent parameters

Given an arbitrary regular breaking wave condition, the other three parameters required by the model: duration T , rising time T_r and peak force F_p , are not known directly. However, they are wave-dependent parameters due to the physics, and can be determined by the given wave condition. In order to investigate the dependence of these parameters on the wave condition, three dimensionless coefficients are introduced.

The *duration coefficient* ζ_1 is defined as

$$\zeta_1 = \frac{T}{\frac{D_x}{C_b}} \tag{16}$$

where D_x is the equivalent width of the structure in the wave direction, the value of which depends on the structure geometry relative to the wave impact. Since the front legs and braces are all in a plane perpendicular to the wave direction and have the same diameter 0.14 m, this value is used for D_x . The breaking wave celerity C_b can be approximated by Equation (17), for shallow water waves with high steepness [19,20].

$$C_b = \sqrt{g(d + \eta_b)} \tag{17}$$

where g is the gravitational acceleration; d is the water depth; and η_b is the maximum elevation of the breaking wave, which can be obtained from the wave elevation measurement.

The *rising time coefficient* ζ_2 is defined as the ratio of rising time to duration.

$$\zeta_2 = \frac{T_r}{T} \tag{18}$$

The *peak force coefficient* ζ_3 is defined as

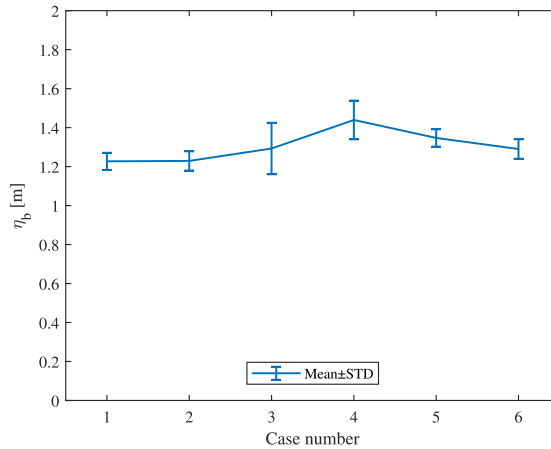


Fig. 7. Mean value and standard deviation of η_b in each case.

$$\zeta_3 = \frac{F_p}{\frac{1}{2}\rho D_y \eta_b C_b^2} = C_s \lambda \tag{19}$$

where ρ is the water density; D_y is the equivalent width of the structure in y-axis direction, the value of which depends on the structure geometry relative to the wave impact. For the investigated jacket, $D_y = 2 \times (1 + 2.15) \times 0.14 \text{ m} = 0.88 \text{ m}$. Two inclined braces contribute 2.15 times their diameter 0.14m each to D_y , due to an inclined angle of 62° with respect to the vertical, while two vertical legs contribute one diameter each to D_y .

A typical formulation of three dimensional slamming force includes two coefficients: slamming coefficient C_s and curling factor λ . In some other studies, e.g. Wienke and Oumeraci [4], C_s was first determined theoretically, then λ was calculated empirically based on the determined C_s . In this study, C_s and λ are treated together as one coefficient ζ_3 instead, since they are not independent.

The values of ζ_1 , ζ_2 and ζ_3 are calculated for each wave of the cases listed in Table 3. The η_b acquired from each single wave is the only essential wave parameter for the calculation. The mean and standard deviation of the input η_b values over each case are shown in Fig. 7. The variation of the calculated ζ_1 , ζ_2 and ζ_3 are demonstrated in Figs. 8–10. In the figures, the result variation over different waves in each case is illustrated by the blue bars representing means and standard deviations. The result variation over different cases is illustrated by the red lines. The continuous red line represents the mean value calculated by averaging the means of each case. The dashed red lines represent the standard deviation of the means of each case.

From Figs. 8 and 9, it can be noticed that the variation of ζ_1 and ζ_2 over different cases is much smaller than the variation over different waves inside each case. The coefficients of variation of ζ_1 for the six cases range from 0.17 to 0.31, while the value over the six cases is only 0.06. Similarly, the coefficients of variation of ζ_2 for the six cases range from 0.20 to 0.34, while the value over the six cases is only 0.09. Although there is variability of ζ_1 and ζ_2 within each case, the means of all the cases are similar. This implies that ζ_1 and ζ_2 are insensitive to wave condition, so they are treated as constants because their mean values can be assumed to be the same for

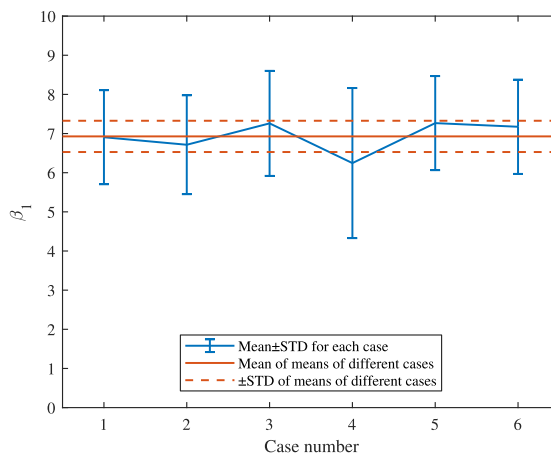


Fig. 8. Variation of ζ_1 in each case and over different cases.

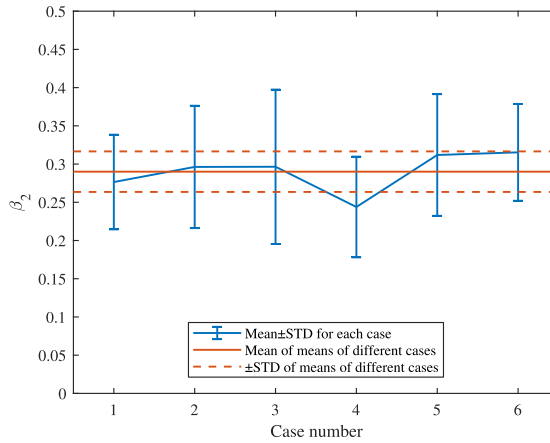


Fig. 9. Variation of ζ_2 in each case and over different cases.

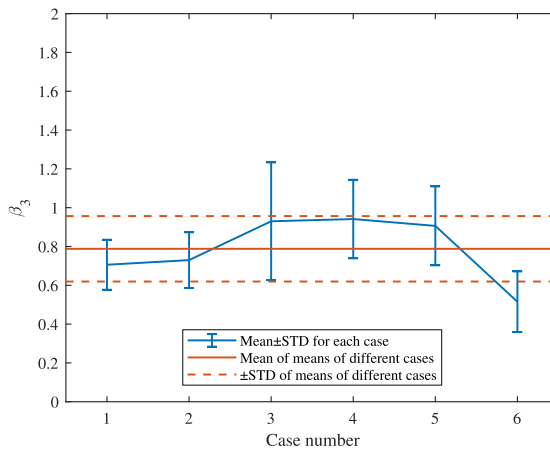


Fig. 10. Variation of ζ_3 in each case and over different cases.

different wave conditions.

The means and bootstrap 95% confidence intervals of ζ_1 and ζ_2 for each case are calculated and shown in Table 5. The confidence intervals are narrow compared to the mean values in general, so the means are representative for the cases. The duration coefficient and the rising time coefficient are therefore determined by averaging the means of each case, which leads to $\zeta_1 = 6.93$ with a 95% confidence interval of ± 0.32 and $\zeta_2 = 0.29$ with a 95% confidence interval of ± 0.02 .

From Fig. 10, it can be noticed that the variation of ζ_3 over different cases is comparable to the variation over different waves inside each case. The coefficients of variation of ζ_3 for the six cases range from 0.18 to 0.33, and the coefficient over the six cases is 0.21. The coefficients of variation of the nominator and denominator in Eq. (19) over the six cases are 0.087 and 0.276, respectively.

Table 5

Means and bootstrap 95% confidence intervals of ζ_1 and ζ_2 for each case.

| Case No. | ζ_1 | | | ζ_2 | | |
|----------|-----------|---------------------|------|-----------|---------------------|-------|
| | Mean | Confidence interval | | Mean | Confidence interval | |
| 1 | 6.91 | 6.43 | 7.50 | 0.277 | 0.249 | 0.304 |
| 2 | 6.71 | 6.12 | 7.21 | 0.296 | 0.269 | 0.339 |
| 3 | 7.26 | 6.63 | 7.94 | 0.296 | 0.250 | 0.345 |
| 4 | 6.25 | 5.46 | 7.15 | 0.244 | 0.216 | 0.273 |
| 5 | 7.27 | 6.76 | 7.80 | 0.312 | 0.281 | 0.356 |
| 6 | 7.17 | 6.90 | 7.41 | 0.315 | 0.303 | 0.329 |

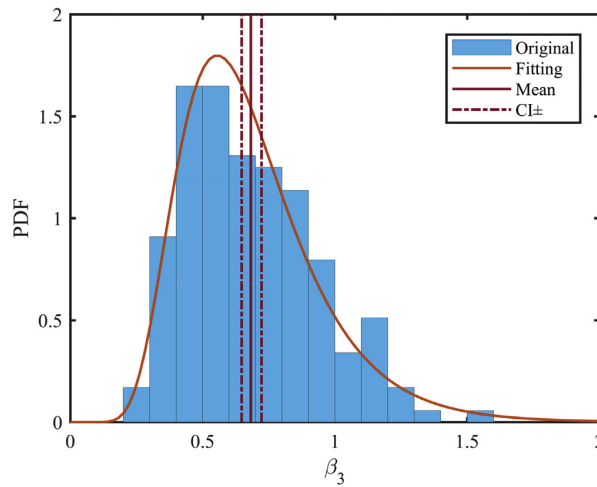


Fig. 11. Statistical properties of ζ_3 , represented by histogram, distribution fitting by lognormal function, mean and confidence interval of the mean. The log location and log scale parameters of the lognormal distribution are -0.4497 and 0.3727 , respectively.

So a constant value might not be representative enough for the peak force coefficient ζ_3 . Attempts have been made to figure out the relationship between ζ_3 and the wave parameters, such as wave height, wave elevation and deep water wave length, and their ratios. However, the values of ζ_3 are much more widely spread than the values of those parameters and ratios, which does not support an expression of ζ_3 in terms of the wave parameters. The reason for such widely spread ζ_3 values could be explained by the slightly shifted breaking point relative to the jacket structure at each wave impact. Although the location of breaking is given for each test run in Table 3, it is based on the visual estimation for the whole run, and it is not strictly controlled for each wave in such a shallow water breaking wave test with many nonlinearities involved. Even if a wave breaks just slightly before or after the plane of the front legs, the peak force reduces significantly, thus changing the value of ζ_3 also significantly.

Since peak force is a decisive parameter for an accurate estimation of the slamming force time series and the total impulse exerted by a wave on the structure, the peak force coefficient ζ_3 should be determined with a more reliable approach. The ζ_3 values of all the waves in all the test runs are sorted in a histogram in Fig. 11. The data are then fitted by various distributions, and a lognormal distribution function is found to give the best goodness of fit among the commonly used distribution functions. The lognormal distribution function is thus selected, and its expression is given by

$$f(\zeta_3|\mu_L, \sigma_L) = \frac{1}{\sqrt{2\pi}\sigma_L\zeta_3} \exp\left\{-\frac{(\ln\zeta_3 - \mu_L)^2}{2\sigma_L^2}\right\} \tag{20}$$

in which μ_L and σ_L are the log location and log scale parameters, respectively. The fitted values for these two parameters are $\mu_L = -0.4497$ and $\sigma_L = 0.3727$. The log-likelihood of the fitting is 3.6.

The cumulative distribution function of ζ_3 based on the original data is plotted together with the fitted lognormal distribution in Fig. 12. From this figure, we can see more clearly that the lognormal distribution fits the data very well in general, although slight overestimation and underestimation exist locally. Four representative quantiles of the cumulative distribution function and their corresponding ζ_3 values are marked in Fig. 12, and the ζ_3 values from the fitted distribution are compared to those from the original data in Table 6. Since the cumulative distribution function based on the original data is discrete, the smallest available value that is larger than the given quantile is used for the calculation of ζ_3 . In this way, ζ_3 can be well approximated when the number of data points at the quantile considered is very large; while for large quantile (e.g. 99%) where fewer data points are available, the approximated ζ_3 is likely to have a large uncertainty. Therefore, the relative difference between the two cumulative distribution functions is larger for the quantile of 99% than for the rest in the table. In this study, we use $\zeta_3 = 1.178$, which corresponds to the quantile of 95%, as a representative value for the peak force coefficient, because the quantile is relatively large, and the difference between the fitted distribution and the original data is relatively small for this quantile. In the application of the model, the peak force coefficient ζ_3 can be calculated from the lognormal distribution, according to the quantile needed for the design. Now that ζ_1 , ζ_2 and ζ_3 have been determined, the wave-dependent parameters T , T_r and F_p of the force model can be calculated with Equations (16), (18) and (19), for a given structure and given wave conditions.

4.3. Application of the model

Knowing the five parameters determined in Sections 4.1 and 4.2, the model of the slamming force time series is completely defined. Once the site conditions and the structure properties are known, time series of the slamming force can be calculated. A flow chart as shown in Fig. 13 summarizes the procedure to get the force time series by applying the model. Knowing site conditions, the

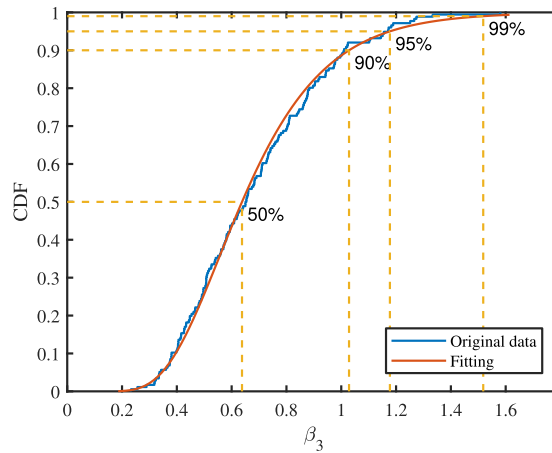


Fig. 12. Cumulative distribution function of ζ_3 based on the original data and the fitted lognormal distribution. Four representative quantiles and corresponding ζ_3 values are marked for the fitted distribution by the yellow lines. (For interpretation of the references to colour in this figure legend, the reader is referred to the Web version of this article.)

Table 6

Four representative quantiles and corresponding ζ_3 values estimated from the lognormal distribution and the original data.

| Quantile [%] | ζ_3 from fitted CDF | ζ_3 from original CDF | Relative difference [%] |
|--------------|---------------------------|-----------------------------|-------------------------|
| 50 | 0.638 | 0.651 | - 2.00 |
| 90 | 1.028 | 1.009 | 1.88 |
| 95 | 1.178 | 1.172 | 0.51 |
| 99 | 1.518 | 1.334 | 13.79 |

wave parameters for the potential breaking waves are determined. Knowing both site conditions and structural properties, water depth d at the structure and the equivalent widths of the structure D_x and D_y are determined. The wave parameters and water depth are then used with suitable wave theories and breaking criteria to derive breaking wave celerity C_b and the maximum elevation of the breaking wave η_b . The determination of wave parameters and η_b for a given site condition is further addressed in Section 6. Then, the parameters D_x , D_y , C_b and η_b are used together with the coefficients ζ_1 , ζ_2 and ζ_3 to calculate the wave-dependent parameters T , T_r and F_p . Finally, the wave-dependent parameters are used in the force model together with exponential parameters α_1 , α_2 to obtain the time series of the slamming force $f(t)$.

5. Model verification

In this section, the developed model is verified against the original reconstructed time history of slamming force. Since the peak force F_p , duration T and rising time T_r are wave-dependent, the verification is thus conducted with respect to each individual wave. For the six wave conditions considered in this study, there are in total 176 individual waves. In each individual wave, both the wave parameters (such as wave height, wave period, maximum elevation η_b , etc.) and reconstructed time history of slamming force are available. Knowing water depth d and η_b , breaking wave celerity C_b is determined according to equation (17). Then by using parameters D_x , D_y , C_b and η_b together with coefficients ζ_1 , ζ_2 and ζ_3 , the wave-dependent parameters T , T_r and F_p are achieved. The time history of slamming force can then be predicted according to equation (15). Here four representative quantiles (i.e. 50%, 90%, 95%, 99%) are used when determining the ζ_3 value. An exemplary comparison between the original reconstructed slamming force and the predicted slamming forces by the force model is shown in Fig. 14.

In the verification, both peak force and impulse are considered. The predicted value is compared to the original value. A ratio of the predicted value to the original value is introduced to quantify the comparison. If the ratio is larger than 1, it implies that the value is overpredicted. It should also be noted that for a given breaking wave and a given quantile, the predicted value is deterministic, while the actual value due to the breaking wave is very random, due to the inherent nature of slamming events [21]. As a result, the ratio of the predicted value to the original value is expected to vary in a certain range. However, if the ratio is more likely to be larger than 1 (i.e. predicted value overestimated), it indicates that such prediction is conservative, which is more desirable from the design point of view.

The ratio of the peak force from the predicted force time history to the peak force from the reconstructed force time history is calculated for each individual wave. The values of the ratio for all 176 waves are plotted in Fig. 15 for four different quantiles. The ratio points in the figure range from about 0.5 to about 6, with a concentration between 1 and 3. Depending on the selected quantile,

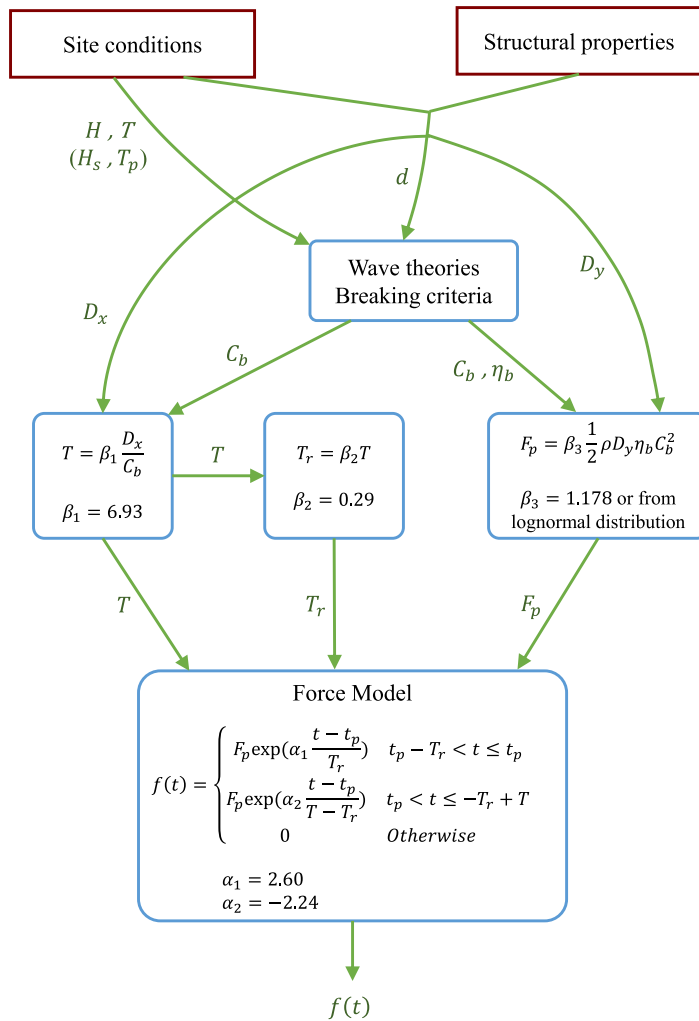


Fig. 13. Application flow chart of the slamming force time series model.

the points scatter around different values. The overestimation rates of peak force for the predicted slamming force with a quantile of 50%, 90%, 95% and 99% are approximately 0.5, 0.90, 0.96 and 0.99, respectively. The overestimation rate is fairly close to the corresponding quantile, this is because the predicted peak force is proportional to ζ_3 , which is determined based on the given quantile.

Total impulse (i.e. the integral of the force over time) is another important parameter that characterizes the slamming force. Similar to the peak force, the ratio of the impulse from the predicted force time history to the impulse from the reconstructed force time history is calculated for each individual wave. Fig. 16 depicts the values of the ratio for all 176 waves and for four different quantiles. The points of impulse ratio are distributed in a narrower range in the figure compared to the points of peak force ratio in Fig. 15, indicating that the impulse values tend to be overestimated to a less extent than the peak force values. However, the overestimation rates of impulse for the predicted slamming force with a quantile of 50%, 90%, 95%, and 99% are approximately 0.61, 0.94, 0.97 and 1.0, respectively. Therefore, for a given quantile (e.g. 95%), the impulse of more waves tend to be overestimated compared to the peak force.

It should be noted that in Figs. 15 and 16 wave IDs larger than about 90 correspond to case 6, which has 5 runs with the same preset condition. The other cases have only 1 or 2 runs, i.e., much fewer waves.

Considering the verification results for peak force and impulse above, the developed force model can give a conservative prediction of slamming force time histories, which can be used for engineering design purposes, provided that the ζ_3 value or the quantile is selected carefully to account for the inherent randomness of slamming forces. Such value should be large enough to ensure that the predicted slamming force is conservative enough to provide a safe design. A highly conservative prediction of slamming forces

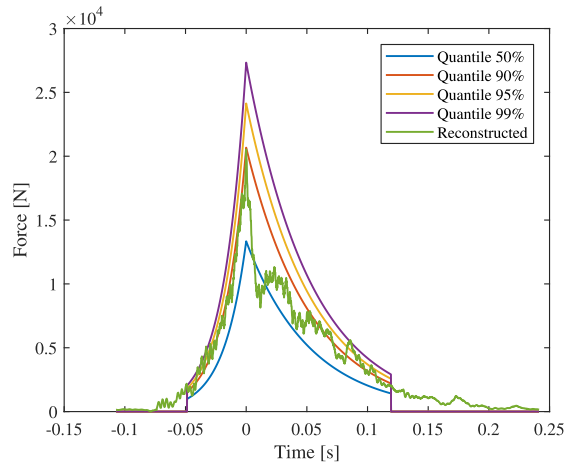


Fig. 14. An exemplary comparison between the original reconstructed slamming force and the predicted slamming forces. Time histories of the predicted slamming forces are estimated according to equation (15) with ζ_3 values corresponding to four quantiles.

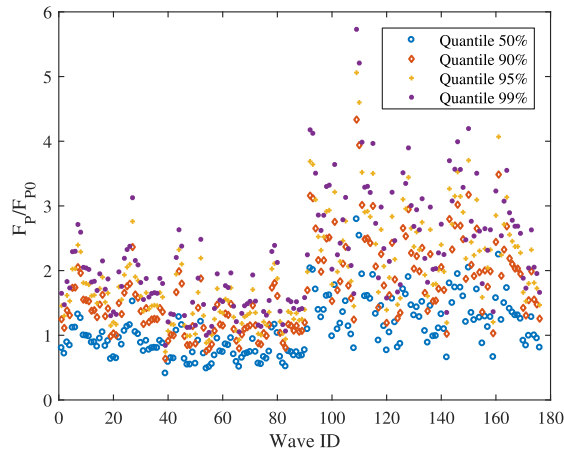


Fig. 15. The ratio of the peak force from the predicted slamming force, F_p , to that of the original reconstructed slamming force, F_{p0} . Four different quantiles are considered when estimating the predicted slamming force.

demands a much stronger structure, which increases its cost. Meanwhile, the value should not be too large, since the probability of waves breaking exactly at the structures is very low. Therefore, the quantile should be chosen based on the balance of structural safety and economy.

6. Discussion

The force model developed in Section 4 is based on the wave cases given in Table 3, in which several different combinations of wave height and wave period were considered. Hence the effect of variable wave conditions is included in the developed force model. The force model consists of five parameters that are independent of waves and structures, i.e. two exponential parameters (α_1, α_2) and three coefficients for calculating wave-dependent parameters (ζ_1, ζ_2 and ζ_3). These five parameters are dimensionless and were estimated at 1:8 scale, which is a relatively large scale compared to commonly used scaling ratios in wave basin model tests [6,22]. The scaling effect on these five parameters is expected to be small. Therefore, the force model can be considered applicable in full scale as well, though it was developed based on model scale data. Air bubbles affect the local pressure distribution significantly, and they might also affect global slamming forces. However, for a jacket structure, this effect is expected to be much less, due to the spatial and temporal averaging that occurs.

Though only one jacket structure was considered for the model development, it is a representative jacket structure for offshore wind applications. The developed force model is applicable to four-leg jackets with waves coming from 0° with respect to the jackets. The application of the model to other jacket types or for waves coming from other directions is not investigated this study. The force

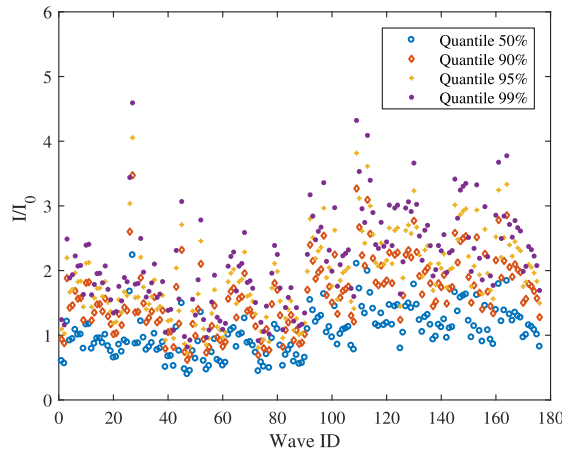


Fig. 16. The ratio of the impulse of the predicted slamming force, I , to that of the original reconstructed slamming force, I_0 . Four different quantiles are considered when estimating the predicted slamming force.

model is developed based on shallow water experimental data. The applicability of the model in intermediate water still needs to be studied in the future.

A time-resolved slamming force model as the developed one is essential for the analysis of a jacket structure, because a jacket structure is a multiple degree of freedom (MDOF) system. The slamming can excite modes of the jacket with natural periods that are comparable to the impact duration.

The developed force model has an evident rising time, which is quite different from most of the force models for cylindrical structures given in Table 1. It should be noted that most force models for cylindrical structures were originally developed for 2D slamming forces. When they were extended to 3D slamming problems, the steep fronts of breaking waves were assumed to act on the structures simultaneously, implying that the rising time is neglected. However, in the model tests of the WaveSlam project, it was clearly observed that the wave fronts impacted different parts of the front plane of the structure at different instants in a random manner [23]. Therefore, an exponential increase of the total slamming force before the peak, as observed in this study, can be expected. Actually, even for cylindrical structures, a rising time before the peak was observed in the experiment as well, such as in WiFi JIP project [6].

The fact that the steep fronts of breaking waves do not impact the structure at the same time causes a gradually increasing and then decreasing time history of the resulting slamming forces. Since the force model developed in this study is based on experimental data, such characteristics during the actual slamming events are thus more likely to be accounted for.

In the developed force model, an essential wave parameter is the maximum elevation of the breaking wave η_b . It is used to determine the breaking wave celerity C_b for shallow water, and it affects the values of duration T , rising time T_r , and peak force F_p . In the above model verification section, η_b was determined based on measured data. However, how to properly estimate η_b for a given sea state is very challenging. In addition, the total wave force consists of a quasi-static part and a dynamic part (i.e. slamming forces). The quasi-static load is estimated by the Morison equation, in which the wave kinematics, such as velocity and acceleration of the fluid, are required. These wave kinematics should also be properly estimated.

For a given sea state with a significant wave height H_s and peak period T_p , whether it is likely to include breaking waves should be first justified. During the model tests of the WiFi JIP, it was found that at steep sea states, some waves lead to impulse like impacts due to their steep fronts. The limiting sea state steepness above which such behavior was observed was found to be [6]

$$\frac{H_s}{L_p} > 0.04 \tag{21}$$

in which L_p is the peak wave length. It can be estimated by using the linear dispersion relationship based on known peak period T_p and water depth d . If the sea state is identified to potentially contain breaking waves, two approaches can be applied to determine η_b and the wave kinematics. One approach is to use a fully nonlinear numerical wave tank to generate the time series of wave elevation and wave kinematics. This approach is employed by Peeringa et al. [24] to generate stochastic nonlinear waves using the nonlinear potential flow solver OceanWave3D [25]. The other approach is to embed a stream function wave into a linear irregular wave realization. The extreme wave from an irregular wave time series is substituted with a stream function regular wave. This approach has been employed in engineering practice of offshore wind industry. Recent development of this approach includes a new method proposed by Pierella et al. [26] to embed a stream function wave based on the Hilbert transform.

For sea states containing breaking waves, the time series of the slamming forces on a structure can be determined for a specific percentile of ζ_3 . For these sea states, the target return period should account for the occurrence of the sea states, the occurrence of plunging breaking waves, and the percentile of ζ_3 . Therefore, the characteristic load with a target return period is not determined by

merely selecting a percentile of ζ_3 . Both the occurrence probability of the sea states and the occurrence probability of plunging breaking waves should be properly selected as well.

7. Conclusion

In this study, a force model was developed for estimating global slamming forces due to plunging breaking waves on jacket structures, based on statistical analyses of experimental data from the WaveSlam project. Given a sea state, this force model provides a deterministic and conservative prediction of the slamming force time history, which inherently has random features.

The force model was developed by refining a five-parameter model proposed by Tu et al. [12], using a total of 176 individual breaking waves, under six wave conditions. For each individual breaking wave, the time history of the resulting slamming force was reconstructed based on hammer test data and wave test data, and the wave parameters were acquired from a wave elevation measurement.

The parameters involved in the force model, including two exponential parameters and three wave-dependent parameters (i.e. duration T , rising time T_r and peak force F_p), were determined by using the acquired slamming force time histories and wave parameters. The two exponential parameters were found to be constant, by applying weighted linear regression to the slamming force time histories. The wave-dependent parameters were expressed by three dimensionless parameters (i.e. duration coefficient ζ_1 , rising time coefficient ζ_2 and peak force coefficient ζ_3), together with the acquired wave parameters and the structural dimensions. The dimensionless parameters were then determined in a statistical way. It was found that ζ_1 and ζ_2 are approximately constant, and ζ_3 follows a lognormal distribution. The value of ζ_3 is recommended to be determined by choosing a quantile that can give a conservative prediction.

The developed force model was verified against the original reconstructed force time histories. Since the model was developed based on regular wave cases, the applicability of the model to irregular waves should be validated against model test data or field measurements. It is also worthy of studying how to employ the slamming force model in probability-based design of jacket structures.

Acknowledgment

This work has been supported by the European Community's Seventh Framework Programme through the grant to the budget of the Integrating Activity HYDRALAB IV within the Transnational Access Activities, Contract no. 261520.

Additional financial support from NOWITECH FME (Research Council of Norway, contract no. 193823) is gratefully acknowledged.

References

- [1] Faltinsen O. *Sea loads on ships and offshore structures*. Cambridge University Press; 1993.
- [2] von Karman T. The impact on seaplane floats during landing Technical Note, NO. 321 National Advisory Committee on Aeronautics; 1929.
- [3] Wagner H. Über Stoß- und Gleitvorgänge an der Oberfläche von Flüssigkeiten. *ZAMM-J Appl Math Mech/Zeitschrift für Angewandte Mathematik und Mechanik* 1932;12(4):193–215.
- [4] Wienke J, Oumeraci H. Breaking wave impact force on a vertical and inclined slender pile - theoretical and large-scale model investigation. *Coastal Eng* 2005;52:435–62. <http://dx.doi.org/10.1016/j.coastaleng.2004.12.008>.
- [5] International Electrotechnical Commission (IEC). IEC 61400–61403, Wind turbines - part 3: design requirements for offshore wind turbines; 1.0. 2009.
- [6] Burmester S, de Ridder EJ, Wehmeyer C, Asp E, Gujer P. Comparing different approaches for calculating wave impacts on a monopile turbine foundation. ASME 2017 36th international conference on ocean, offshore and arctic engineering. American Society of Mechanical Engineers; 2017. V010T09A063.
- [7] Tu Y, Cheng Z, Muskulus M. A review of slamming load application to offshore wind turbines from an integrated perspective. *Energy Procedia* 2017;137:346–57.
- [8] Goda Y, Haranaka S, Kitahata M. Study of impulsive breaking wave forces on piles. Report of Port and Harbour Technical Research Institute. 5. 1966. p. 1–30. (6).
- [9] Campbell I, Weynberg P. Measurement of parameters affecting slamming. University of Southampton, Department of Aeronautics and Astronautics; 1980.
- [10] Cointe R, Armand JL. Hydrodynamic impact analysis of a cylinder. *J Offshore Mech Arctic Eng* 1987;109(3):237–43.
- [11] Jose J. Offshore structures exposed to large slamming wave loads. Norway: University of Stavanger; 2017.
- [12] Tu Y, Cheng Z, Muskulus M. Global slamming forces on jacket structures for offshore wind applications. *Mar Struct* 2018;58:53–72.
- [13] Tu Y, Grindstad TC, Muskulus M. Inverse estimation of local slamming loads on a jacket structure. *J Offshore Mech Arctic Eng* 2017;139(6). 061601.
- [14] Arntsen Ø, Ohnrai C, Gudmestad O. Data storage report: wave slamming forces on truss structures in shallow water Technical Report, WaveSlam (HyIV-FZK-05) Norwegian University of Science and Technology; 2013.
- [15] Tørum A. Wave slamming forces on truss structures in shallow water Technical Report, Version 2011-10-03 Department of Civil and Transport Engineering, Norwegian University of Science and Technology; 2011
- [16] Cleveland WS. Robust locally weighted regression and smoothing scatterplots. *J Am Stat Assoc* 1979;74(368):829–36. <http://dx.doi.org/10.1080/01621459.1979.10481038>.
- [17] Tu Y, Muskulus M. Statistical properties of local slamming forces on a jacket structure in offshore wind applications. In: Proceedings of 26th international ocean and polar engineering conference. vol.1. Rhodes, Greece: International Society of Offshore and Polar Engineers; 2016. p. 206–13.
- [18] Bevington PR, Robinson DK. Data reduction and error analysis for the physical sciences. McGraw-Hill; 2003.
- [19] Tanimoto K, Takahashi S, Kaneko T, Shiota K. Impulsive breaking wave forces on an inclined pile exerted by random waves. *Coast Eng Proc* 1986;1(20):2288–302. <http://dx.doi.org/10.1061/9780872626003.168>.
- [20] Mei CC, Stiassnie M, Yue DK. Theory and applications of ocean surface waves: nonlinear aspects. World Scientific; 2005.
- [21] Lian G, Haver SK. Estimating long-term extreme slamming from breaking waves. *J Offshore Mech Arctic Eng* 2016;138(5):051101.
- [22] Loukozeorgaki E, Lentsiou EN, Chatjigeorgiou IK, et al. Experimental investigation of slamming loading on a three-legged jacket support structure of offshore wind turbines. Proceedings of 26th international ocean and polar engineering conference. vol.1. Rhodes, Greece: International Society of Offshore and Polar Engineers; 2016. p. 192–8.
- [23] Tu Y, Muskulus M, Arntsen ØA. Experimental analysis of slamming load characteristics for truss structures in offshore wind applications. *J Ocean Wind Eng* 2015;2(3):138–45.
- [24] Peeringa JM, Hermans KW. Impact of new slamming wave design method on the structural dynamics of a classic, modern and future offshore wind turbine. ASME 2017 36th international conference on ocean, offshore and arctic engineering. American Society of Mechanical Engineers; 2017. p. V010T09A071.
- [25] Engsig-Karup AP, Bingham HB, Lindberg O. An efficient flexible-order model for 3D nonlinear water waves. *J Comput Phys* 2009;228(6):2100–18.
- [26] Pierella F, Stenbro R, Oggiano L, de Vaal J, Nygaard TA, Krokstad J, et al. Stream function wave embedment into linear irregular seas: a new method based on the hilbert transform. The 27th international ocean and polar engineering conference. International Society of Offshore and Polar Engineers; 2017.

A.6 Paper 6

Paper 6:

Tu Y, Cheng Z, Muskulus M. A review of slamming load application to offshore wind turbines from an integrated perspective. *Energy Procedia* 2017; **137**:346-357. <https://doi.org/10.1016/j.egypro.2017.10.359>



ELSEVIER

Available online at www.sciencedirect.com

SciVerse ScienceDirect

Energy Procedia 00 (2017) 000–000

Energy

Procedia

www.elsevier.com/locate/procedia

14th Deep Sea Offshore Wind R&D Conference, EERA DeepWind'2017, 18-20 January 2017, Trondheim, Norway

A review of slamming load application to offshore wind turbines from an integrated perspective

Ying Tu^{a,*}, Zhengshun Cheng^b, Michael Muskulus^a

^aDepartment of Civil and Environmental Engineering, Norwegian University of Science and Technology, Høgskoleringen 7A, 7491 Trondheim, Norway

^bDepartment of Marine Technology, Centre for Autonomous Marine Operations and Systems (AMOS), Norwegian University of Science and Technology, Otto Nielsens veg 10, 7491 Trondheim, Norway

Abstract

In harsh sea conditions, it is possible for offshore wind turbines (OWTs) to be exposed to slamming loads due to breaking waves, especially plunging breaking waves. These slamming loads lead to significant structural responses and can affect the ultimate limit state (ULS) design and the fatigue limit state (FLS) design of OWTs. However, detailed consideration of slamming loads is not a common practice in the design of primary structures in offshore wind industry. Studies on integrated dynamic analysis of OWTs with consideration of slamming loads are very limited. When applying slamming loads on OWTs, several aspects should be considered, such as the detection of breaking waves, the calculation of slamming loads, and the approaches to integrate the slamming loads in fully coupled analysis, etc. This paper provides an extensive review of key issues concerning these aspects, which can benefit the application of slamming loads on OWTs.

© 2017 The Authors. Published by Elsevier Ltd.
Peer-review under responsibility of SINTEF Energi AS.

Keywords: Breaking waves; slamming loads; integrated dynamic analysis; offshore wind turbine

1. Introduction

Slamming loads resulting from plunging breaking waves are dangerous for offshore wind turbines (OWTs) exposed to certain wave conditions. Although many studies have been carried out in the past decades about slamming loads and their application to OWT designs, detailed consideration of slamming loads is still not a common practice in the design of primary structures in offshore wind industry. The slamming load application involves many research topics in oceanography and ocean engineering, which have been elaborated separately in their respective fields. However, a state-of-the-art method that takes different aspects of the application problem into account is still in absence; accord-

* Corresponding author. Tel.: +47 735 94557 ; fax: +47 735 97021.
E-mail address: ying.tu@ntnu.no

ingly, the numerical tools used in offshore wind industry usually do not have a function to include slamming loads in the simulations. These limitations restrain the application of slamming loads in the design practice of OWTs.

This study starts from an general introduction of breaking waves and slamming loads. Then, how to include the slamming load in the integrated dynamic analysis of OWTs is thoroughly reviewed and discussed, including the detection of slamming events, the calculation of slamming loads and the integration of slamming loads in fully coupled analyses. The status and issues of slamming load applications are discussed and some improvement possibilities are proposed.

2. General slamming force characteristics

2.1. Breaking waves

A breaking wave is a wave whose amplitude reaches a critical level at which it becomes unstable and dissipates large amounts of wave energy into turbulent kinetic energy. It may occur at certain sites, depending on the local water depth, the breaker height, the local wave length, the wave steepness, the sea bed slope and probably some other parameters. Among different types of breaking waves, the plunging breaking wave is most relevant to slamming loads on the offshore wind turbine supporting structures. It features a relatively small dissipating area, a very high local pressure and a high impulsive load. In this paper, wave slamming loads due to plunging breaking waves are mainly reviewed and discussed.

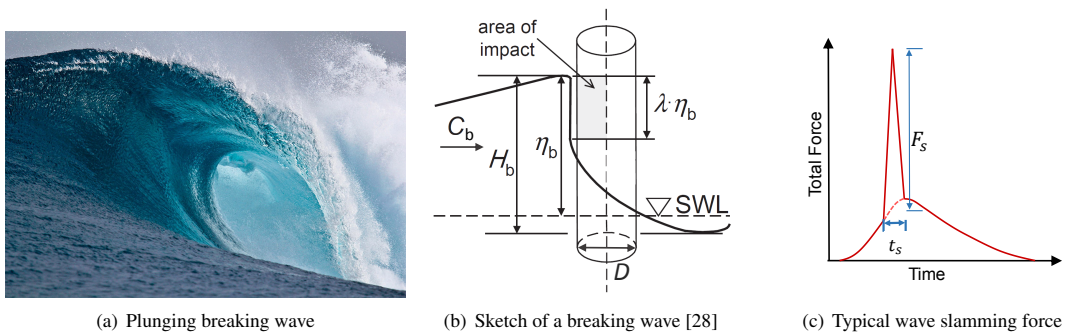


Fig. 1. Breaking wave and wave slamming force on a circular cylinder

2.2. Slamming load

The quasi-static wave force on a slender cylindrical structure is normally calculated by the Morison's equation as

$$F_{qs} = F_D + F_M \quad (1)$$

where F_D and F_M are the drag and inertia forces, respectively, and they are expressed as

$$F_M = \int_{-\eta_b}^{\eta_b} \rho \pi C_m \left(\frac{D}{2} \right)^2 a_x dz \quad (2)$$

$$F_D = 0.5 \int_{-\eta_b}^{\eta_b} \rho C_D D u |u| dz \quad (3)$$

in which ρ is the water density, η_b is the wave elevation at the breaking point, D is the diameter of the cylindrical structure, u and a_x are the velocity and acceleration of water particle. C_D and C_m are the drag and inertia coefficients, respectively, and they are dependent on Keulegan-Carpenter number, Reynolds number, roughness parameters and interaction parameters.

However, the Morison's equation is not sufficient to represent the wave force due to the plunging breaker on the structures. The force coefficients in the Morison's equation cannot describe the wave impact force of very short duration, typically of the order of milliseconds. A common engineering practice is to add an extra term F_S in Eq. 1 to represent the slamming load in the total wave force.

$$F = F_D + F_M + F_S \quad (4)$$

In the most general case, F_S is expressed as

$$F_S = \int_l C_s(z) \frac{1}{2} \rho U(z)^2 W(z) dz \quad (5)$$

where C_s is the slamming coefficient; U is the velocity of the water particles impacting the structure; and W is the effective width of the structure. The values of these three parameters depend on the height z . By integrating the line force at different z over the whole impact height l , the total slamming force is obtained.

There are many simplified expressions of Eq. 5, depending on the used slamming load model to be discussed in Section 3.2.3. For example, by using the model proposed by Wienke and Oumeraci [28], Eq. 5 for a cylinder is expressed as

$$F_S = C_s \frac{1}{2} \rho C_b^2 D \lambda \eta_b \quad (6)$$

The impact height range l is a portion of the breaking elevation $\lambda \eta_b$, where λ is the curling factor which indicates how much of the wave crest is active in the slamming load, as shown in Fig. 1. η_b is the wave elevation at the breaking point. The line force is considered to be constant over the impact height range. The water particle velocity U is approximated by the breaking wave celerity C_b , and the width W is the diameter of the cylinder D .

3. Slamming load application for offshore wind turbines

Three indispensable aspects should be considered for slamming load application on OWTs, i.e. how to detect a slamming event, how to calculate the slamming load and how to integrate it into fully coupled analysis. In each of the aspects, there are various issues that should be considered in more detail as shown in Fig. 2.

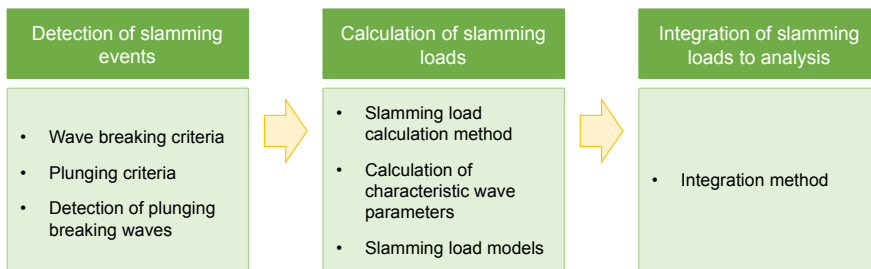


Fig. 2. Three aspects involved in slamming load application on OWTs

3.1. Detection of slamming events

The slamming load should only be considered when this event occurs in the vicinity of the structure. For a certain wave condition, a suitable breaking criterion should first be applied to judge whether a wave is broken or not. If the wave is broken, the plunging breaking criteria should then be applied, since plunging breaking waves are most relevant to slamming loads. These criteria are commonly developed for regular waves, however, OWTs are usually exposed to irregular waves, a suitable approach is then required to detect the incidence of plunging breaking waves from large amounts of irregular waves.

3.1.1. Wave breaking criteria

A large amount of effort has been made to identify the criteria for the inception of wave breaking. Robertson et al. [24] summarized the characteristic relationships of breaking waves theorized by different authors and their regions of applicability. Perlin et al. [23] reviewed the state-of-the-art progress of breaking waves in deep and intermediate waters, including the prediction of their geometry, breaking onset, and especially energy dissipation.

However, to find an intrinsic relation for a wave breaking in a general form is not easy. Liu et al. [15] extensively reviewed the existing formulas for the inception of wave breaking. By defining different breaking index, these formulas can be classified into four types, i.e. the McCowan [18] type, the Miche [19] type, the Goda [7] type, the Munk [20] type.

- The McCowan [18] type:

$$\frac{H_b}{h_b} = \gamma(s, \lambda_0) \quad (7)$$

- The Miche [19] type:

$$\frac{H_b}{L_b} = \alpha(s, \lambda_0) \tanh \left[\xi(s, \lambda_0) \frac{2\pi h_b}{L_0} \right] \quad (8)$$

- The Goda [7] type

$$\frac{H_b}{L_0} = \alpha'(s, \lambda_0) \left\{ 1 - \exp \left[-1.5 \xi'(s, \lambda_0) \frac{2\pi h_b}{L_0} \right] \right\} \quad (9)$$

- The Munk [20] type

$$\frac{H_b}{H_0} = \beta(s) \left(\frac{H_0}{L_0} \right)^m \quad (10)$$

where H_b , h_b , and L_b are the wave height, water depth, and wave length at the breaking point, H_0 and L_0 are the wave height and wave length in deep water. s is the bottom slope and $\lambda_0 = \frac{H_0}{L_0}$ is the wave steepness. γ , α , α' , ξ , ξ' are coefficients that are dependent on s and λ_0 . β is a coefficient as a function of s .

Within each type, several authors developed different formulas, The assumptions and regions of applicability for each formula should be aware of when the formula is employed. In addition, to compare the accuracy of these four types [15], one representative formula in each type was chosen and verified by a total number of 1193 experimental cases, covering a wide range of beach slope from 1/100 to 1/3. It was stated that the Goda's formula proposed in [8] is the best among the selected four criteria if excluding the data with the beach slopes larger than 1/10.

Liu et al. [15] also proposed a new predictive formula for the inception of regular wave breaking, by introducing a new breaking index, $\frac{gH_b}{C_b^2}$. By analyzing a large number of data, a breaking criterion was achieved. This criterion was claimed to be highly accurate for predicting the inception of regular wave breaking.

It should be noted that these wave breaking criteria are related to the bottom slope s , which implies breaking waves are more pronounced in the slope region. The above wave breaking criteria have been used in recent studies on slamming load application to OWTs. Marino [17] employed the Miche [19] type criterion, i.e. $\frac{H_b}{L_b} = 0.142 \tanh \left(\frac{2\pi h_b}{L_0} \right)$. Hollowell et al. [10] used four criteria, including the McCowan [18] wave limit $\frac{H_b}{h_b} = 0.78$, the Miche [19] wave limit $\frac{H_b}{L_b} = 0.142 \tanh \left(\frac{2\pi h_b}{L_0} \right)$, the Goda [7] wave limit $\frac{H_b}{L_0} = 0.17 \left\{ 1 - \exp \left[-1.5 \frac{\pi h_b}{L_0} \left(1 + 15s^{4/3} \right) \right] \right\}$, and the Battjes [11,13] wave limit $\frac{H_b}{h_b} = 0.78 \tanh \left(\frac{0.14g}{2\pi(0.78h_b)} T_z^2 \right)$. By comparing these criteria with breaking events measured, it was stated that the Goda limit identifies fewer false positives than Miche and Battjes limits [10].

3.1.2. Plunging criteria

Another important aspect for slamming event detection is plunging criteria. The breaking waves are usually classified into three types: spilling, plunging and surging [11] (or sometimes four types with an additional collapsing type). The wave profile of each type is different. The plunging breaking waves are the ones that cause the impulsive slamming loads. For slamming events to occur, the waves should not only fulfill the breaking criteria but also the plunging criteria.

The most common way to categorize the breaking waves is through surf similarity parameters [12].

$$\xi_o = \frac{\tan \alpha}{\sqrt{\frac{H_o}{L_o}}} \quad (11)$$

or

$$\xi_b = \frac{\tan \alpha}{\sqrt{\frac{H_b}{L_o}}} \quad (12)$$

in which α is the sea floor slope in radians.

According to IEC 2009 [11], the criteria for plunging breaker are

$$0.45 < \xi_o < 3.3 \quad (13)$$

or

$$0.4 < \xi_b < 2.0 \quad (14)$$

In fact, many studies have been carried out to discuss and correct the critical values for the criteria, and the results are different, depending on e.g. the bathymetry.

In order to apply the plunging criteria based on surf similarity parameters, the seabed slope has to be known, which is not always the case in reality. This limits the application of the criteria in practice. In another classification system, which is proposed recently by Yao et al. [29], a ratio of breaker depth to offshore wave height $\frac{h_b}{H_o}$ is used. The plunging breaker occurs if $\frac{h_b}{H_o} < 1.8$.

In the recent studies about slamming load application in OWTs, the plunging criteria are not used for slamming detection. Both Hallowell et al. [10] and Marino [17] assume that the slamming events occur as long as the breaking criteria are fulfilled regardless of the breaking type. This approach is reasonable, since the available research results on the plunging criteria and the available information about the site are not enough for detecting the plunging breakers. Nevertheless, it is essential to use proper plunging criteria in order to detect the slamming events more accurately, and further investigations on the criteria are therefore desired.

3.1.3. Detection of plunging breaking waves

The ideal approach to detect the breaking wave is based on the spatial evolution of wave breaking. Such kind of spatial evolution can be captured by computational fluid dynamics (CFD) methods, as those done by Christensen et al. [4], Corte and Grilli [6], Nielsen et al. [22], Bredmose and Jacobsen [2], Jose et al. [14] and Alagan Chella et al. [1]. However, the CFD methods are usually time consuming.

The detection of wave breaking can be simplified given the wave elevation. When performing the numerical simulations, it is possible to simulate the irregular wave field around the structure. At every time step in the time domain simulation, the spatial variation of the waves is acquired and can be analyzed by zero up- or down-crossing methods.

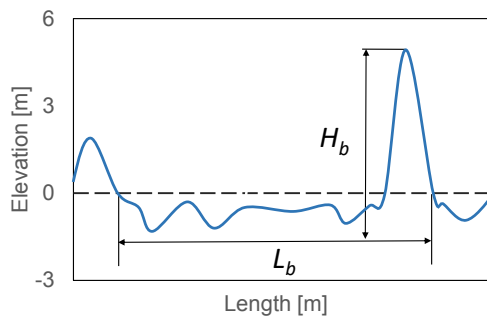


Fig. 3. Zero-crossing analysis of wave profile to get wave height H_b and wave length L_b

The zero-crossing analysis divides the sequential wave into a series of individual waves, and for each individual wave, the characteristic parameters, such as the wave height, wave length, wave period, etc. can be determined. Then, by applying a suitable breaking wave criterion and a plunging criterion, the individual breaking wave that is likely to break is identified. Such method is adopted by Marino [16,17] to identify the likely breaking waves. However, such method cannot capture the wave profile when it breaks.

When analyzing the measured data from an offshore site, the approach for breaking wave detection is quite different. Currently the wave elevation or sea surface data usually include measurements from a single point, which cannot capture the spatial evolution of wave breaking. Other indicators, such as the measured structural response, are therefore required to detect the slamming events. Hallowell et al. [10] employed the measured mudline bending moment as an indicator. If one peak in the measured moments is several times higher than the rest of time history, it implies that a wave has broken at or near the structure and it is a slamming event.

3.2. Calculation of slamming loads

3.2.1. Slamming load calculation method

In order to calculate and to include the slamming loads in the general wave loads, both an engineering approach and a numerical approach can be used. Based on the CFD, the numerical approach models the interaction of breaking waves with the structure. This approach costs tremendous simulation time and is therefore not suitable during the primary design phase of OWTs.

The engineering approach calculates the slamming load by employing a wave slamming load model. The slamming force model features a slamming coefficient and a certain force distribution pattern in space and in time. It also requires certain characteristic wave parameters, for instance the wave celerity in the model by Wienke and Oumeraci [28]. The engineering approach estimates the slamming load very quickly, hence it is a desirable way to integrate the slamming load into fully coupled analyses. However, this approach is highly dependent on the used wave slamming load model. In Sections 3.2.2 and 3.2.3, the characteristic wave parameters and wave slamming load models involved in the engineering approach are further discussed.

3.2.2. Calculation of characteristic wave parameters

During the detection of wave breaking by zero-crossing analysis of a wave field, the characteristic wave parameters can be acquired as well. However, as mentioned above, zero-crossing analyses can only detect likely breaking waves, but the characteristic parameters of the wave cannot be estimated very accurately. A possible way to improve the accuracy of the estimation is to use advanced methods to further simulate the evolution of likely breaking waves. Marino [16,17] used the domain decomposition technique to achieve this. The computational field was divided into two sub-domains. In the sub-domain without the structure, a potential flow theory was used. In the sub-domain containing the structure, a mixed-Eulerian-Lagrangian (MEL) method was used to further simulate the likely breaking waves. In this way, the wave profile at the breaking instance is simulated, so the accuracy of the characteristic breaking wave parameters is improved at a relatively small cost of computational time.

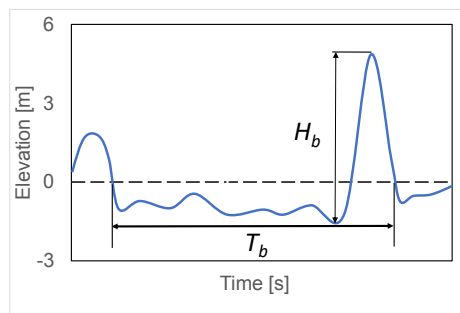


Fig. 4. Zero-crossing analysis of wave time history to get wave height H_b and wave period T_b

In the field measurements, these characteristic breaking wave parameters cannot be directly achieved. Assuming that the spatial evolution of waves can be approximated by their temporal evolution, these parameters can be calculated approximately. This is the method used by Hallowell et al. [10], which involves the following steps:

1. Data processing is carried out to remove any tidal or surge variance in the sea surface data, so as to obtain a zero-mean wave profile and identify individual waves and their associated parameters, such as height and period. The data are smoothed using a 1 s moving average to remove high-frequency noise from the wave measurements.
2. Down-crossing analysis is carried out to obtain individual wave characteristics, such as the height, the period and the depth. The structural response data recorded are synchronized with the wave profile data.
3. The slamming events are detected from the record of the structural response, and the wave parameters are determined for each of these events.

3.2.3. Slamming load models

Cylindrical structure

Wave slamming loads act on offshore substructures in a very short time and with a very high amplitude, as illustrated in Fig. 1. It is a strongly nonlinear phenomenon and is affected by various factors, such as compressibility of water, hydroelasticity of the structure, air bubbles entrapped, cavitation and ventilation etc.

One of the first attempts to theoretically investigate the wave slamming load was performed by von Karman [26]. The cylinder is approximated as a flat plate with a width equal to the immersed width of the cylinder. However, the local raise of the free surface during the impact is neglected, which affects the duration and magnitude of the slamming force. Later, Wagner [21,27] took the local raise into account. Currently there are several common wave slamming load models, as given in Table 1. Among them, the von Karman theory is implemented by Goda et al. [7], and Wagner theory is employed by Wienke and Oumeraci [28]. In addition to Wagner’s method, Cointe and Armand [5] also derived the asymptotic expressions for the inner domain and outer domain at the spray root during the impact and further solved the problem by matching the inner and outer asymptotic expressions. Experimental study is another approach to determine the slamming coefficient, as conducted by Campbell and Weynberg [3].

Table 1. Comparison of different wave slamming models for cylindrical structures and jacket structures (modified from [10])

| | Author | Theory | Maximum C_s | Slam duration, t_s | Time history, $C_s(t)$ |
|-----------------------|---------------------------|--|---------------|----------------------|---|
| Cylindrical structure | Goda et al. [9] | von Karman | π | $\frac{D}{2C_b}$ | $\pi \left(1 - \frac{2C_b}{D} t\right)$ |
| | Campbell and Weynberg [3] | Experimental study | 5.15 | $\frac{D}{C_b}$ | $5.15 \left(\frac{D}{D+19C_{st}} + \frac{0.107C_{st}}{D}\right)$ |
| | Cointe and Armand [5] | Wagner and matched asymptotic expansions | 2π | $\frac{3D}{2C_b}$ | $2\pi - \left(4.72 - \ln\left(\frac{2C_b}{D} t\right)\right) \sqrt{\frac{2C_b}{D}} t$ |
| | Wienke and Oumeraci [28] | Wagner | 2π | $\frac{13D}{64C_b}$ | $2\pi - 2\sqrt{\frac{2C_b}{D}} t \left(\tanh^{-1}\sqrt{1 - \frac{C_b}{2D} t}\right)$ (for $0 \leq t \leq \frac{D}{16C_b}$) $\pi \sqrt{\frac{D}{12} \frac{D}{C_b t'}} - \sqrt{\frac{16}{3} \frac{C_b}{D} t'} \tanh^{-1}\sqrt{1 - \frac{2C_b}{D} t'}$ (for $\frac{D}{16C_b} < t' \leq \frac{13D}{64C_b}$) $t' = t - \frac{D}{64C_b}$ (for $\frac{D}{16C_b} \leq t \leq \frac{13D}{64C_b}$) |
| Jacket structure | Tu et al. [25] Simplified | Experimental study | 2.05 | - | Triangular |
| | Tu et al. [25] Refined | Experimental study | 2.05 | - | Exponential |

These four wave slamming models provide time dependent slamming coefficient as well as the slamming duration, which are very helpful for slamming load application in the design practice. However, these four models are originally developed for a 2D slamming problem, hence the vertical distribution of slamming load is not taken into account. When applying these models, the vertical force distribution is usually assumed to be uniform or triangular. These models do not consider many factors that affect the wave slamming loads, such as nonlinear irregular waves, water particle velocities at free surface and the spatial variation of slamming loads. But laboratory experiments has shown that slamming loads approximated by these models are reasonable [28]. Additionally, the IEC 61400-3 standard [11] recommends the Wienke and Oumeraci [28] model for designing OWT support structures.

Jacket structure

Jacket structures are made of several cylindrical legs and braces. The waves approaching the aft legs and braces are affected by the front legs and braces. This will cause a more complicated slamming scenario than for a cylindrical

structure. Consequently, the global response of jacket structures subjected to wave slamming force is different. Based on the experimental data from the WaveSlam project, Tu et al. [25] investigated the global slamming loads due to plunging breaking waves on jacket structures. A total of 3910 time series were reconstructed and statistically analyzed. The mean slamming coefficient is found to be about 2.05 at a curling factor of 0.4. Tu et al. [25] also proposed two wave slamming load models, i.e. a 3-parameter triangular force model and a 5-parameter exponential force model, to represent the temporal development of global wave slamming load on jacket structures, as demonstrated in Figure 5.

However, these two models by Tu et al. [25] are proposed for breaking waves impacting the front legs of the jacket structure. They are not applicable to estimate the slamming load on the aft legs of the jacket structures. Actually, the waves acting on the hind legs are influenced by front legs, especially when the waves are broken.

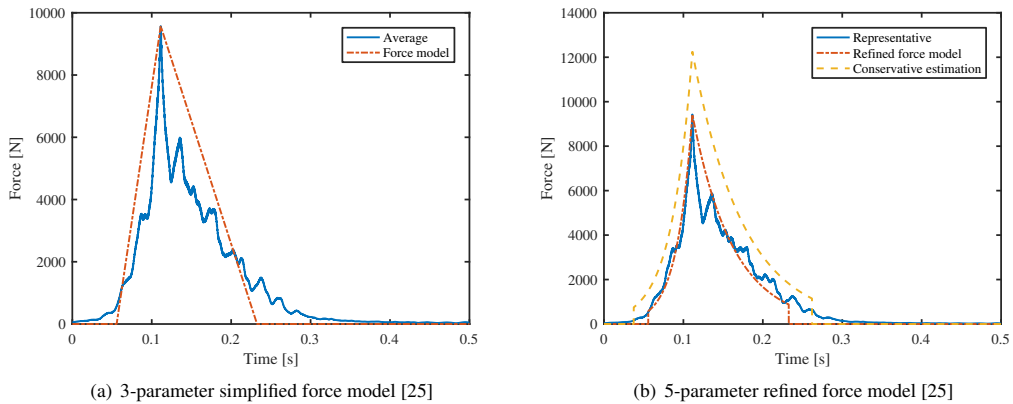


Fig. 5. Two models for the wave slamming loads on the front legs of jacket structures [25].

Comparison of the models

In order to compare the slamming force models described above, the models in Table 1 are applied to one study case, and the results are compared. The case is taken from a model scale wave test of the WaveSlam project. The vertical front side of a jacket model was exposed to shallow water breaking waves in the test. Two legs and two braces of the same diameter in this side were exposed to the plunging breakers. The model scale parameters of the wave case and the structure are given in Table 2.

In the application of the slamming force models for cylindrical structures, the wave is assumed to impact the four cylindrical legs and braces simultaneously. So the results are basically four times the slamming forces on one cylinder. The forces are assumed to be uniform along the axial length of cylinder, and calculated by Equation 6, where $C_b = \sqrt{g(d + \eta_b)}$. The results of the slamming force models for jacket structures are obtained directly from the analysis of the experimental data of the case.

Table 2. Parameters of the wave case and the structure.

| Parameter | Symbol | Value | Unit |
|--|-----------|-------|----------|
| Wave period | T | 4.9 | s |
| Wave height at the structure | H | 1.83 | m |
| Elevation at the breaking point | η_b | 1.28 | m |
| Water depth | d | 2 | m |
| Curling factor | λ | 0.4 | - |
| Gravitational acceleration | g | 9.81 | m/s^2 |
| Water density | ρ | 1000 | kg/m^3 |
| Diameter of braces and legs | D | 0.14 | m |
| Number of braces and legs exposed to the breaker | N | 4 | - |

The time series of the slamming forces calculated from different models are compared in Figure 6. The peak forces, durations and impulses derived from the time series are compared in Figure 7.

The peak forces are proportional to the maximum slamming coefficient of the models (see Table 1). Therefore, the slamming models for jacket structures, which have lower maximum slamming coefficients, lead to lower peak forces. In reality, the breaker does not impact different parts of the braces and legs simultaneously as we assumed. The impact is neither vertically nor horizontally uniform. So, it is reasonable to have lower maximum slamming loads on jacket structures than those calculated with simultaneousness assumption.

On the other hand, the duration obtained from the models for jacket structures are much higher than those from the models for cylindrical structures. The non-uniform impact of the breaker on different parts of the braces and legs is again partly the reason for this difference. Moreover, the breaking locations were decided by human observation during the experiment, whose data were used for developing the slamming models for jacket structures. The waves might have broken slight before or after the front side of the structure, so the durations calculated from those models can be longer than the ones from the idealized models. It also worth noticing that the models for cylindrical structures are mainly or partly based on theory, and they do not match the whole time series of the experimental data which were used for developing the models very well. The agreement is best inside the peak force region and less accurate outside of it. So, the estimated durations from these models can be shorter than in reality.

The impulses obtained from the models for jacket structures are also higher than those from the models for cylindrical structures. This difference results from the different peak forces, durations and the shape of the time series.

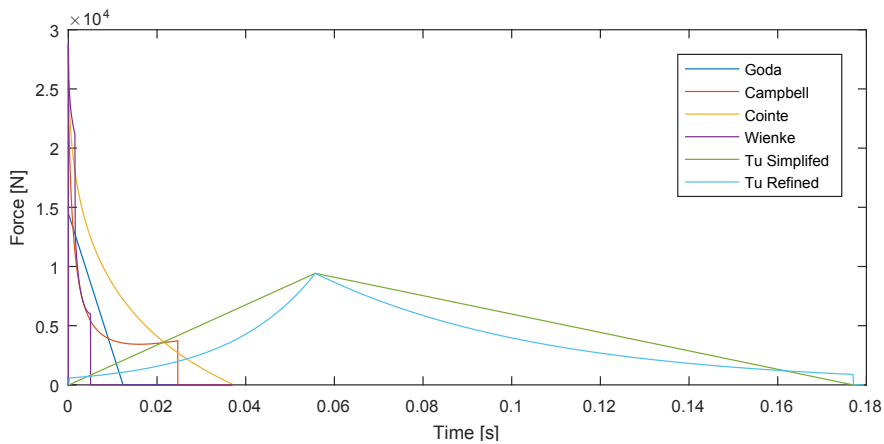


Fig. 6. Time series comparison among different slamming force models for one jacket structure and one wave case.

3.3. Integration of slamming loads in fully coupled analysis

In the design practice of OWTs, the effect of slamming loads should be assessed by integrated dynamic analysis, which is commonly based on the engineering approach. The slamming loads can be estimated directly according to Eqs. 5 or 6, given the slamming coefficient, wave celerity, impact area and vertical force distribution pattern. However, most fully coupled simulation tools for OWTs, such as FAST, SIMO-RIFLEX-AeroDyn, BLADED, do not have the option to directly include the slamming loads. A possible way to consider the slamming loads in the existing tools without modifying the codes is to add the slamming load as an additional inertial or drag term in the Morison's equation.

Including slamming loads as an additional inertial term has been used in several publications, such as Hallowell et al. [10] and Marino [16]. This is achieved by modifying the acceleration in Eq. 2 as

$$a_x^{new} = a_x + a'_x \quad (15)$$

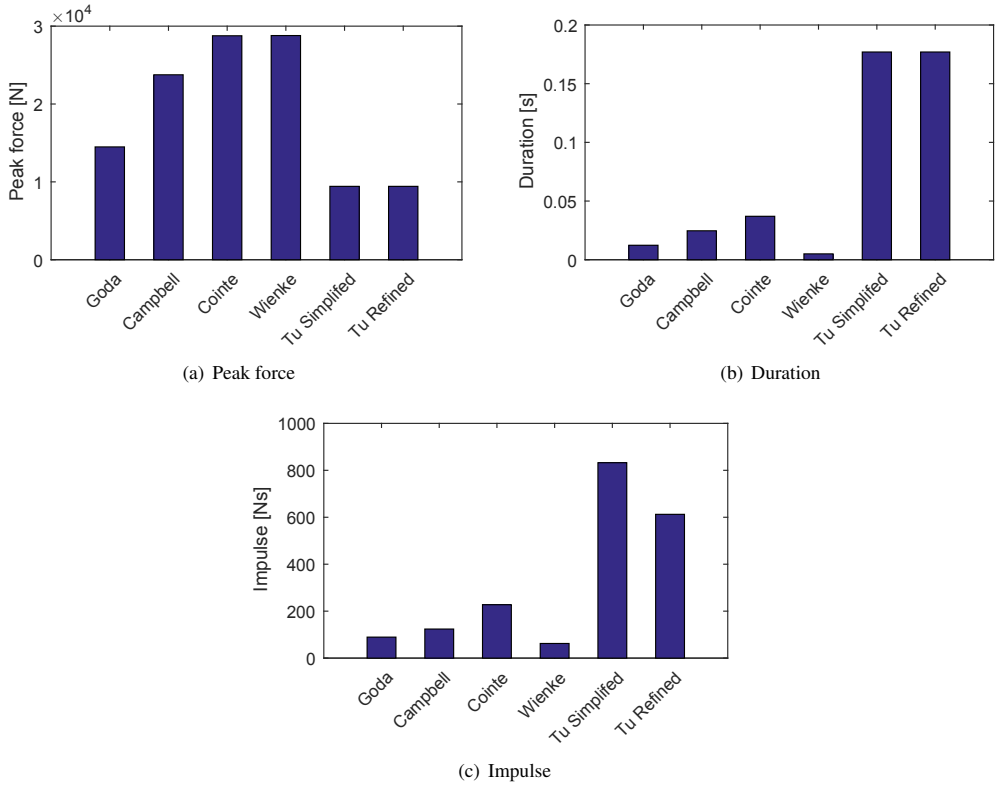


Fig. 7. Parameter comparison among different slamming force models for one jacket structure and one wave case.

where a'_x is due to the slamming load and is estimated by

$$a'_x = 2 \frac{C_s}{C_m} \frac{C_b^2}{D\pi} \tag{16}$$

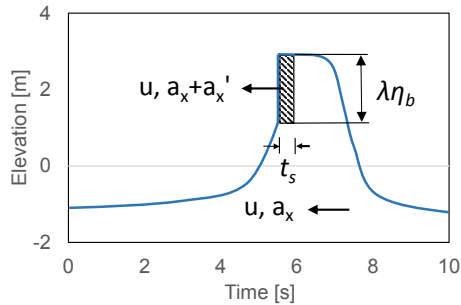


Fig. 8. Illustration of modified wave kinematics for wave slamming load application through Morison’s equation.

4. Conclusions

Aiming at facilitating the application of slamming loads in the design practice of offshore wind turbines (OWTs), this paper reviewed the three most important aspects: the detection of slamming events, the calculation of slamming loads, and the integration of slamming loads into analysis.

There are some critical issues worth highlighting in these aspects. The first issue is about slamming detection. When identifying the breaking wave through zero-crossing analysis, it is assumed that the presence of the structure does not affect wave evolution, even in the vicinity of the structure. In realistic ocean conditions, wave breaking is significantly affected by local bathymetry, currents, wind-wave interaction, and other parameters. Therefore, using a suitable wave breaking criterion and plunging criterion is of significant importance. The second issue is about identifying the parameters that are required in the wave slamming load models. The parameters can be estimated by using, for instance, stream function method. But since the detected breaking waves are irregular and strongly nonlinear, it is challenging to have an estimation that is accurate enough. By using advanced methods, e.g. the MEL method, the detection of likely breaking waves and associated parameters can be circumvented. However, these methods are usually very time consuming. The third issue is about selecting a reliable wave slamming load model, including the slamming coefficient, impact area, vertical force distribution pattern and temporal development pattern, etc. The existing wave slamming load models present much difference in these factors. The issues discussed above affect the critical structural responses in the integrated dynamic analysis of OWTs, and have an impact on the ultimate limit state (ULS) and fatigue limit state (FLS) design of OWTs. They should be carefully taken into account in the design practice.

Acknowledgements

This work has been supported by the European Community's Seventh Framework Programme through the grant to the budget of the Integrating Activity HYDRALAB IV within the Transnational Access Activities, Contract no. 261520.

Financial support from NOWITECH FME (Research Council of Norway, contract no. 193823) is gratefully acknowledged.

References

- [1] Alagan Chella, M., Collados, X. R., Bihs, H., Myrhaug, D., Arntsen, Ø. A., 2016. Numerical and experimental investigation of breaking wave interaction with a vertical slender cylinder. *Energy Procedia* 94, 443–451.
- [2] Bredmose, H., Jacobsen, N. G., 2011. Vertical wave impacts on offshore wind turbine inspection platforms. In: *ASME 2011 30th International Conference on Ocean, Offshore and Arctic Engineering*. American Society of Mechanical Engineers, pp. 645–654.
- [3] Campbell, I., Weynberg, P., 1980. Measurement of parameters affecting slamming. University of Southampton, Department of Aeronautics and Astronautics.
- [4] Christensen, E. D., Bredmose, H., Hansen, E. A., 2005. Extreme wave forces and wave run-up on offshore wind turbine foundations. *Proceedings of Copenhagen Offshore Wind*, 1–10.
- [5] Cointe, R., Armand, J.-L., 1987. Hydrodynamic impact analysis of a cylinder. *Journal of offshore mechanics and Arctic engineering* 109 (3), 237–243.
- [6] Corte, C., Grilli, S. T., et al., 2006. Numerical modeling of extreme wave slamming on cylindrical offshore support structures. In: *The Sixteenth International Offshore and Polar Engineering Conference*. International Society of Offshore and Polar Engineers.
- [7] Goda, Y., 1975. Irregular wave deformation in the surf zone. *Coastal Engineering in Japan* 18, 13–25.
- [8] Goda, Y., 2010. Reanalysis of regular and random breaking wave statistics. *Coastal Engineering Journal* 52 (01), 71–106.
- [9] Goda, Y., Haranaka, S., Kitahata, M., 1966. Study on impulsive breaking wave forces on piles. *Report Port and Harbour Technical Research Institute* 6 (5), 1–30.
- [10] Hallowell, S., Myers, A., Arwade, S., 2016. Variability of breaking wave characteristics and impact loads on offshore wind turbines supported by monopiles. *Wind Energy* 19 (2), 301–312.
- [11] IEC, 2009. International standard 61400-3, wind turbines, part 3: Design requirements for offshore wind turbines.
- [12] Iribarren Cavanilles, R., Casto Nogales, M., 1949. Protection des ports. 17th Int. Navigation Congress 2, 31–80.
- [13] Jensen, M. S., 2004. Breaking of waves over a steep bottom slope. Ph.D. thesis, Aalborg University, Department of Civil Engineering.
- [14] Jose, J., Choi, S.-J., Lee, K.-H., Gudmestad, O. T., et al., 2016. Breaking wave forces on an offshore wind turbine foundation (jacket type) in the shallow water. In: *The 26th International Ocean and Polar Engineering Conference*. International Society of Offshore and Polar Engineers.
- [15] Liu, Y., Niu, X., Yu, X., 2011. A new predictive formula for inception of regular wave breaking. *Coastal Engineering* 58 (9), 877–889.

- [16] Marino, E., 2011. An integrated nonlinear wind-waves model for offshore wind turbines. Ph.D. thesis, University of Florence, Firenze, Italy.
- [17] Marino, E., Borri, C., Peil, U., 2011. A fully nonlinear wave model to account for breaking wave impact loads on offshore wind turbines. *Journal of Wind Engineering and Industrial Aerodynamics* 99 (4), 483–490.
- [18] McCowan, J., 1894. On the highest wave of permanent type. *Philosophical Magazine Series 5* 38 (233), 351–358.
- [19] Miche, A., 1944. Mouvements ondulatoires de la mer en profondeur croissante ou décroissante. *Annales des Ponts et Chaussées* 114, 42–78.
- [20] Munk, W. H., 1949. The solitary wave theory and its application to surf problems. *Annals of the New York Academy of Sciences* 51 (3), 376–424.
- [21] Newman, J. N., 1977. *Marine hydrodynamics*. MIT press.
- [22] Nielsen, A. W., Mortensen, S. B., Jacobsen, V., Christensen, E. D., 2008. Numerical modelling of wave run-up on a wind turbine foundation. In: *ASME 2008 27th International Conference on Offshore Mechanics and Arctic Engineering*. American Society of Mechanical Engineers, pp. 597–603.
- [23] Perlin, M., Choi, W., Tian, Z., 2013. Breaking waves in deep and intermediate waters. *Annual review of fluid mechanics* 45, 115–145.
- [24] Robertson, B., Hall, K., Zytner, R., Nistor, I., 2013. Breaking waves: Review of characteristic relationships. *Coastal Engineering Journal* 55 (01), 1350002.
- [25] Tu, Y., Cheng, Z., Muskulus, M., 2017. Global slamming forces of jacket structures for offshore wind applications. *Marine Structures* (under review).
- [26] Von Karman, T., 1929. The impact on seaplane floats during landing. *National Advisory Committee on Aeronautics*.
- [27] Wagner, H., 1925. Über die entstehung des dynamischen auftriebes von tragflügeln. *ZAMM-Journal of Applied Mathematics and Mechanics/Zeitschrift für Angewandte Mathematik und Mechanik* 5 (1), 17–35.
- [28] Wienke, J., Oumeraci, H., 2005. Breaking Wave Impact Force on a Vertical and Inclined Slender Pile - Theoretical and Large-Scale Model Investigation. *Coastal Engineering* 52, 435–462.
- [29] Yao, Y., Huang, Z., Monismith, S. G., Lo, E. Y., 2012. Characteristics of monochromatic waves breaking over fringing reefs. *Journal of Coastal Research* 29 (1), 94–104.

A.7 Paper 7

Paper 7:

Tu Y, Cheng Z, Muskulus M. Detection of plunging breaking waves based on machine learning. *ASME 2018 37th International Conference on Ocean, Offshore and Arctic Engineering*, American Society of Mechanical Engineers, 2018.

Is not included due to copyright

